RICE UNIVERSITY

Development of a Biomimetic Hydrogel Scaffold as an Artificial Niche to Investigate and Direct Neural Stem Cell Behavior

by

Christy Lynn Franco

A THESIS SUBMITTED
IN PARTIAL FULFILLMENT OF THE
REQUIREMENTS FOR THE DEGREE

Doctor of Philosophy

APPROVED, THESIS COMMITTEE:

Jennifer L. West, Chair
Isabel C. Cameron Professor, Bioengineering

Junghae Suh, Ph.D.
Assistant Professor, Bioengineering

Peter Lwigale, Ph.D.
Assistant Professor, Biochemistry and Cell Biology

HOUSTON, TEXAS
SEPTEMBER 2011

ABSTRACT

Development of a Biomimetic Hydrogel Scaffold as an Artificial Niche to Investigate and Direct Neural Stem Cell Behavior

by

Christy Lynn Franco

The mature central nervous system has a very limited capacity for self-renewal and repair following injury. Neural stem cells (NSCs), however, provide a promising new therapeutic option and can be readily expanded *in vitro.* Towards the development of an effective therapy, greater understanding and control is needed over the mechanisms regulating the differentiation of these cells into function-restoring neurons. *In vivo,* the neural stem cell niche plays a critical role in directing stem cell self-renewal and differentiation. By understanding and harnessing the power of this niche, a tissue engineered system with encapsulated neural stem cells could be designed to encourage neuronal differentiation and ultimately regeneration of damaged neural tissue. Poly(ethylene glycol)-based hydrogels were used here as a platform for isolating and investigating the response of neural stem cells to various matrix, soluble, and cellular components of the niche. When covalently modified with a cyclic RGD peptide, the synthetic scaffold was demonstrated to support attachment and proliferation of a human NSC line under conditions permissive to cell growth. Under differentiating conditions, the scaffold maintained appropriate lineage potential of the cells by

permitting the development of both neuronal and glial populations. Expansion and differentiation of NSCs was also observed in a more biomimetic, three dimensional environment following encapsulation within a degradable hydrogel material. To simulate the soluble signals in the niche, fibroblast growth factor and nerve growth factor were tethered to the hydrogel and shown to direct NSC proliferation and neuronal differentiation respectively. Finally, as an example of the cell-cell interactions in the niche, the pro-angiogenic capacity of encapsulated neural stem cells was evaluated both *in vitro* and *in vivo*. Ideally, the optimal scaffold design will be applied to guide NSCs in a therapeutic application. Toward this goal, a novel method was developed for encapsulation of the cells within injectable hydrogel microspheres. This technique was optimized for high cell viability and microsphere yield and was demonstrated with successful microencapsulation and delivery of neural stem cells in rodent model of ischemic stroke.

ACKNOWLEDGMENTS

Thank you Jennifer for your guidance and mentorship throughout my doctoral research. It has been an honor to work with you.

Thank you Dr. Suh and Dr. Lwigale, my thesis committee members, for your continued advice and assistance.

Thank you to my funding sources, Rice Institute of Biosciences and Bioengineering Training Grant (NIH Grant No.5T32 GM008362) and the National Institutes of Health Quantum Grant (NIH Grant No. 1P20B007076)

Thank you to my fellow West Lab Members, past and present, and to my dedicated undergraduates, Georgia and Matt, for so much of your time, advice, and energy.

Thank you to my collaborators in the Hirschi, Dickinson, Price, and Modo Labs.

Thank you to my husband, John, for all your love and support.

Thank you to my brother, Ryan, for your encouragement and guidance.

This thesis is dedicated to my parents, John and Judy Steger.
Thank you Mom and Dad for everything.

CONTENTS

LIST OF FIGURES

1 Introduction and Background

Cerebrovascular disease is the third leading cause of death and the leading cause of serious, long term disability.[1] In addition, neurodegenerative diseases such as Alzheimer's and Multiple Sclerosis collectively affect over 6 million people.[1] For all of these conditions, a lack of intrinsic repair mechanisms and scarcity of clinical treatments beyond physical therapy leaves few options for affected individuals. Recent research has shown, however, that stem and progenitor cells may be a source for repairing and regenerating those tissues of the body that are incapable of doing so on their own.

1.1 Stem Cells in the Central Nervous System

The basic definition of a stem cell requires two key characteristics to be present: the ability to self-renew, and the ability to differentiate into more specialized cell types.[2] Stem cells can be further classified based on their potential. Totipotent stem cells have the capacity to completely regenerate a whole organism if introduced into the uterus.[3] A pluripotent stem cell, also known as an embryonic stem (ES) cell, is capable of producing all tissue types except that of the placenta.[3-5] As an organism develops, the cells become more restricted to the specific tissue that they make up. Nearly all stem cells found in an adult organism are classified as multipotent, or able to differentiate along a few, but not all, lineages.[3] Although the hematopoietic stem cell of the bone marrow was the first to be discovered and studied, it is now known that many adult tissues harbor their own stem cell populations.[2] For example, crypt stem cells are found within pits in the intestinal lining, and epidermal stem cells can be found near the base of the hair folicules.[4,5] Owing to their significant regenerative potential, each of these cell populations presents new possibilities for repairing and engineering tissues.

1.1.1 Neural Progenitors

For many centuries it was believed that neurogenesis did not occur in the fully developed central nervous system.[3,6,7] In 1983, however, Goldman and Nottebohm proved that active replacement of neurons occurred in the brains of adult canaries as they learned new songs.[8] By the 1990's several researchers showed that neural stem cells exist in the mammalian brain and can proliferate and migrate to replenish olfactory bulb neurons in rodents.[3,6,9] Further evidence of a neural stem cell was provided when Reynolds and Weiss showed that cells isolated from highly proliferative zones in the adult mammalian brain could be cultured *in vitro* as non-adherent cell clusters termed neurospheres, and could be induced to differentiate along both neural and glial lineages.[2,5,10] The neurosphere assay has since become a common tool for the characterization of neural stem cells *in vitro*.[11]

1.1.2 Neural Stem Cell Lineage

Identification and characterization of neural stem cell populations *in vivo* has proven to be significantly more challenging. The transcription factor SOX2 as well as the intermediary filament nestin are common antigenic markers used in the literature to identify NSC populations.[7,12,13] Additional characterization methods must be used, however, since neither marker is entirely unique to NSCs.[3,4,11] For example, nestin in particular has been reported in a wide variety of healthy and injured adult tissues.[14] In addition to immunostaining, the use of S-phase labeling and *in vitro* neurosphere-forming assays have been the primary methods used to identify NSCs since they allow observation of the two key traits: self-renewal and differentiation.[3,9,10,15] The exact nature of these tests, however, may vary widely between labs in everything from the harvesting technique to the cell culture methods, leading to changes in the resulting cell populations being studied.[2,3] Additional differences in harvested stem cell

characteristics have been reported based on the age of the animal and the location in the brain from which they are derived.[2,16] As a result of all these complications, the precise nature and origin of the neural stem cell has yet to be determined and is widely debated in the literature.[3] For example Johansson *et al.* showed evidence that ependymal cells lining the ventricle walls have some stem cell characteristics.[3,7,17] Other researchers have identified a population of cells with an astrocyte phenotype that were capable of self-renewal and differentiation into both neurons and glia.[3,7,18] A comprehensive theory to explain the variety of NSCs was presented by Alvarez-Bullya *et al.* in 2001 and 2006 and is diagramed in Figure 1.[19,20] This theory proposes that neuroepithelial cells give rise to radial glia and then astrocyte stem cells, all of which have the capacity to form neurons and glia.[19,20] In the adult brain, the astrocyte stem cell is the quiescent population which upon stimulation can give rise to transit amplifying cells that then become lineage restricted progenitors and ultimately mature neurons or glial cells.[18-20] The ependymal cells themselves are also suggested to be derived from the radial glia of this lineage, explaining some of their stem cell-like features.[20] Within only the last few years, a significant body of research has been published providing further support and clarification of this theory.[21] For example, adult astrocyte stem cells are now known to extend a single primary cilium into the ventricular space on one end, and alternately long processes which connect with the pial microvasculature on the other.[22,23] This morphology is strikingly similar to that of their proposed precursors, the radial glia, which stretch between the ventricular and pial surfaces of the embryo.[22-24] Lineage mapping of labeled radial glia has provided additional validation that they give rise to stem and non-stem astrocytes as well as the ependymal cell layer in the adult.[25] Overall, generating an accurate picture of NSC development allows a better understanding of their ultimate potential to regenerate the cells and tissues of the central nervous system.

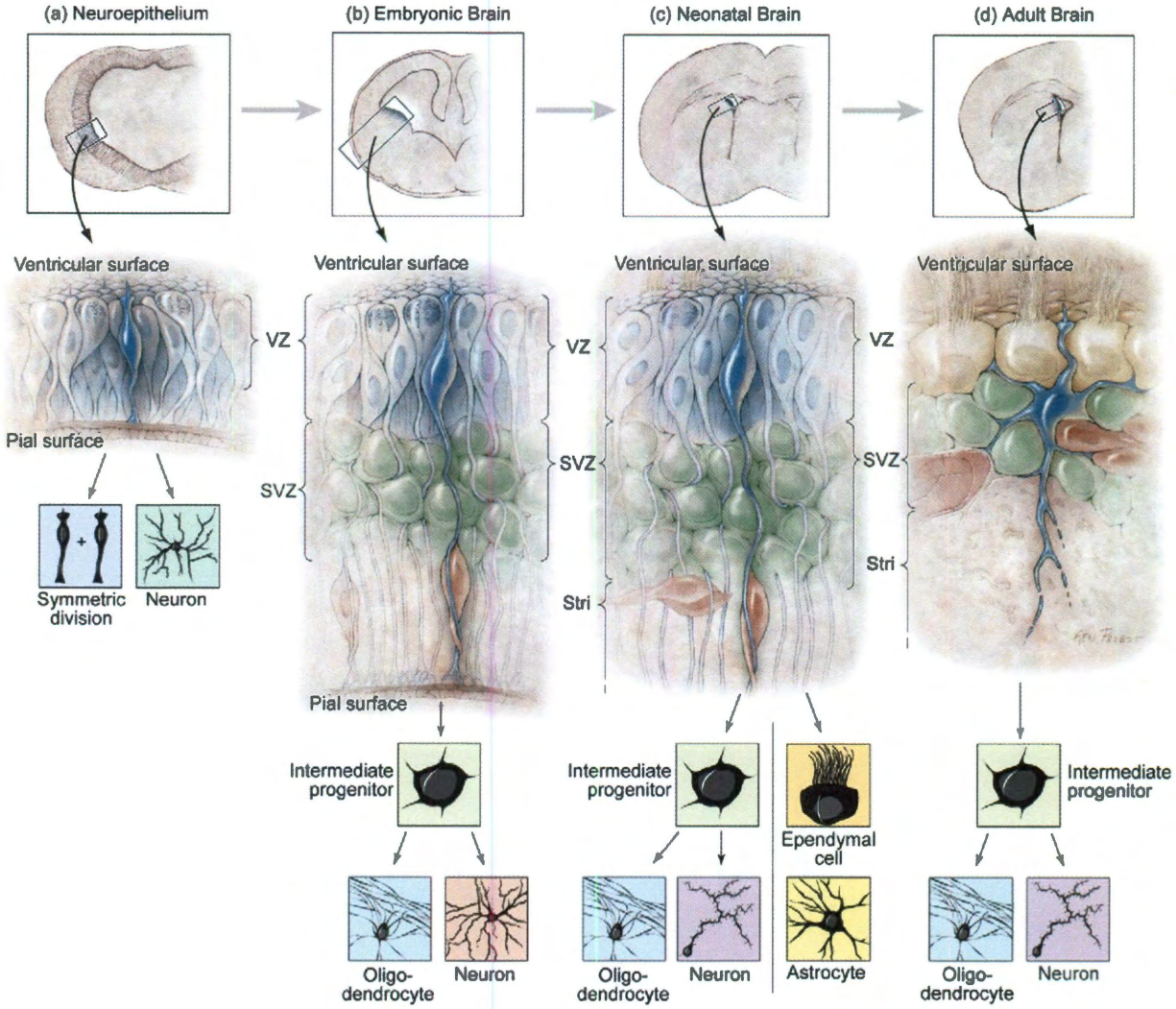

Figure 1. Unified theory on the origin of the adult neural stem cell.[20] Neuroepithelial cells (blue) line the pial surface of the neural tube (a). In the embryonic brain (b), neuro-epithelial cells become radial glia (blue), which line the walls of the forming ventricles. In the neonatal brain (c) the radial glia transition into the mature, ciliated ependymal cells lining the ventricle walls (tan). A few of these radial glia retain stem cell characteristics in the adult brain (d) as astrocyte stem cells (blue) which extend a single cilia into the ventricular space. When stimulated, the astrocyte stem cells proliferate as transit amplifying cells (green) and differentiate into neurons and glia.[20] Figure from Merkle *et al.* 2005.

1.1.3 Potential for Cell-Based Therapies

Due to their regenerative capacity, neural stem cells are promising candidates for the treatment of a wide variety of neurological diseases and injuries.[10,26,27] Activation of the endogenous niche through delivery of neurotrophic factors as well as implantation of allogenic or autologous cells have both been investigated as therapeutic strategies (Figure 2).[21,28] Since they are already

somewhat restricted, NSCs do not carry the same risk for the formation of teratoma, a scrambled mass of tissue types generated by uncontrolled proliferation and differentiation of implanted embryonic stem cells.[26,27,29] Several central nervous system impairments have already shown promise as targets for stem cell therapy. These fall into two main categories: acute injury such as from stroke or spinal cord damage, or more gradual onset resulting from progressive, neurodegenerative disease.[27,30,31] In the case of Parkinson's disease, the gradual loss of dopaminergic neurons is the primary pathology.[27,32] Transplanted neurons from fetal tissue have been shown to engraft and provide some improvement in clinical trials, however there are serious moral concerns and a limited a supply of fetal tissue to use this as common treatment modality.[27,32] A more recent trial for Parkinson's treatment avoids this controversy since autologous cells were harvested from patient biopsies and expanded *in vitro* prior to implantation.[33] Another solution for cell sourcing is through the development of a bank of neural stem cells that have been validated for stable karyotype and phenotype.[34] In one

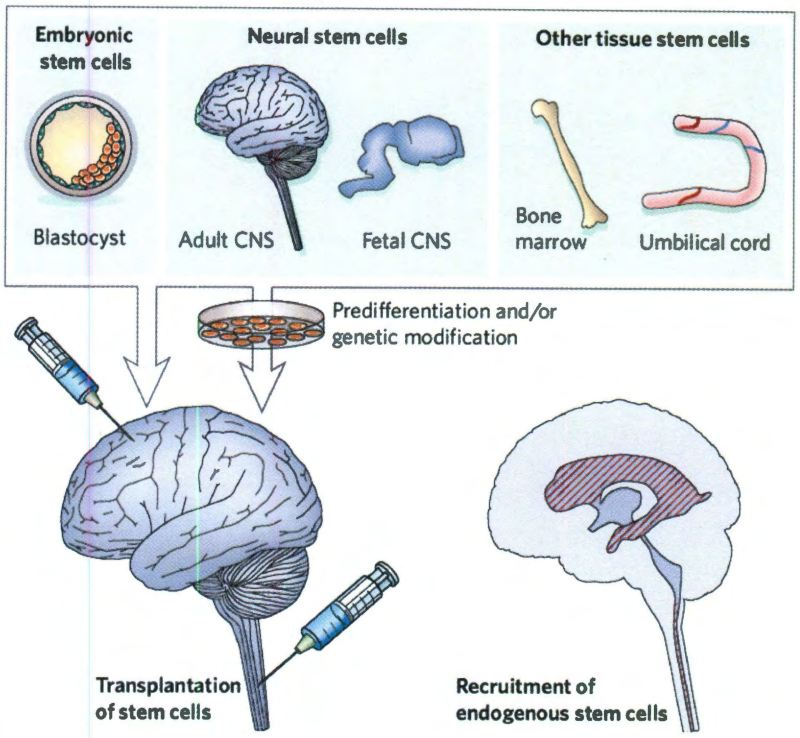

Figure 2. Approaches for neural stem cell-based therapies.[27] Exogenous stem cell sources could be expanded and/or differentiated *in vitro* towards the desired phenotype prior to delivery. Alternatively, a therapy could focus on recruiting endogenous neural stem cells.[27] Figure from Lindvall *et al.* 2006.

example, a fetal-derived NSC line has been expanded and conditionally immortalized for use in human clinical trials to treat ischemic stroke.[33,35] Other indications currently undergoing clinical trials include spinal cord injury, ALS (Lou Gehrig's Disease), and lysozomal storage disorders such as Batten's Disease.[33,36,37] Preclinical studies are additionally investigating treatment of multiple sclerosis, Alzheimer's disease, Huntington's disease, and traumatic brain injury to name a few.[21,27,32,37-39]

Despite the growing body of research and a surge in clinical trials in recent years, a continued challenge to improving the therapeutic outcome is the largely unknown mode-of-action for many of these cell-based therapies.[40] Tracking of cell fate following NSC implantation in animal models has shown rapid clearance and minimal engraftment with host tissue, supporting a hypothesis of neuro- or immunoprotective effects rather than cell or tissue regeneration.[27,40,41] Low persistence times may be one factor behind marginal patient improvements thus far observed in human trials.[33] In the case of stroke, the implant environment can be characterized by necrosis, hypoxia, and glial scar formation, all of which may contribute to low transplant survival.[32] Direct cell delivery to the site of tissue damage may not be necessary, however. Using a stroke model in the rat brain, neural stem cells engrafted in the parenchyma were shown by Modo *et al.* to migrate to the infarct region and provide improved functional recovery in the animals based on behavioral testing.[27,42,43] Additional strategies to enhance survival and neuronal differentiation of engrafted cells may be one approach to further improve results and patient outcomes.[27,31]

Recently, the highly motile property of implanted NSCs has also been utilized in cancer therapy. Transfection of NSCs with oncolytic-genes coupled with their intrinsic capacity to home in on cancerous cells in the brain has shown to reduce tumor volume in rodent models.[30,39] Due to the

highly invasive nature and lack of treatment options for malignant brain tumors such as glioblastoma, finding a targeted therapy to "search and destroy" rogue tumor cells could prove to be a promising approach.[39,42,44]

1.2 The Neural Stem Cell Niche

To maintain self-renewal and prevent nonspecific differentiation, stem cells in the body require a complex combination of signals and interactions.[5,30,45-47] Within their respective tissue, therefore, the adult stem cell is restricted to specific regions which provide the necessary microenvironment to maintain stemness.[5,6,48] These regions have been termed in the literature as the stem cell niche, and are unique for each type of multipotent stem cell.[5,30,47] Figure 3 shows the different forms of interactions which may be present in the niche and play a role in controlling stem cell behavior.[48] Such interactions can be classified as physical signals from the extracellular matrix, soluble signals such as growth factors and cytokines, and direct interaction with neighboring cells.[49] Evidence has shown that signals from the surrounding environment may play an even greater role in defining stem cell behavior

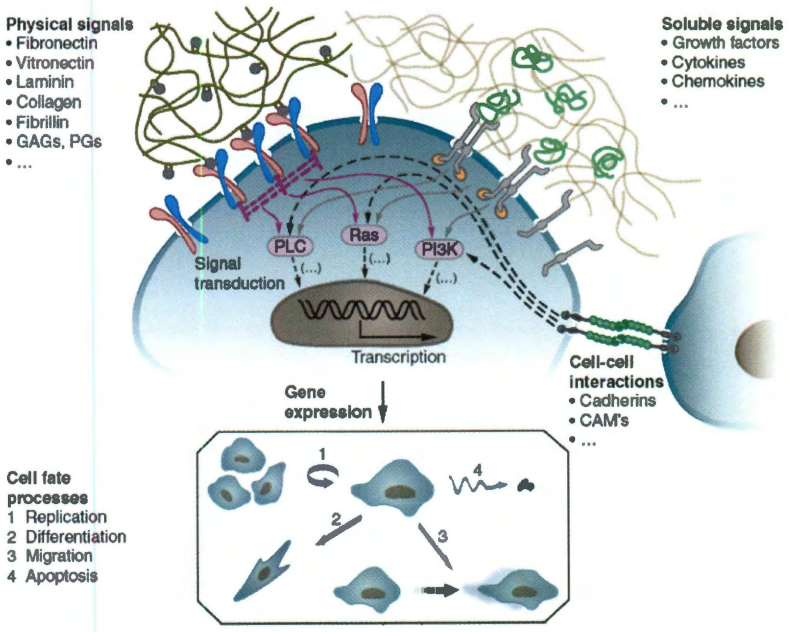

Figure 3. Niche interactions affecting NSC fate.[49] These can include physical signals from adhesion to the matrix, interaction with soluble signals, and direct contact with neighboring cells. All can lead to changes in gene expression and therefore cell response.[49] Figure from Lutolf *et al.* 2005.

and fate than its origin.[3,6] For example, *in vitro* protocols have been developed that use soluble signals added to the media to coax mesenchymal stem cells to differentiate along neuronal lineages.[50]

Since their discovery it has been determined that NSCs are concentrated in two distinct niches in the rodent and human CNS.[3,5,15,48] The subventricular or subependymal zone (SEZ) defines a region of stem cells directly adjacent to the ependymal cells that line the lateral ventricle walls.[3,18,48] Alternatively, the subgranular zone (SGZ) involves a region of the hippocampus with a high concentration of cells shown to proliferate and form new neurons in the dentate gyrus.[3,7,48] In both regions, the stem cells are shown to be of an astrocyte phenotype based on morphology and antigen presentation.[18,19,48] This evidence supports one theory that glial lineages are the default differentiation pathway for neural stem cells.[18,48] Some researchers even hypothesize that populations of astrocytes outside the niche, which were typically regarded as merely support cells, retain the capacity for neurogenesis.[18,48] Of the two characterized niches, the SEZ has been the focus of greater study since the NSCs in this region appear to be less committed and have a wider range of potential.[19] Although there is some debate, SGZ stem cells show signs of being restricted to the formation of new granular neurons.[5,19,48]

Histological analysis of the adult rodent SEZ has revealed several distinguishing characteristics which are summarized in Figure 4.[48,51] Slowly dividing, astrocyte stem cells, termed Type B cells, are located directly adjacent to ciliated ependymal cells lining the ventricle walls.[20,22,23,48] These stem cells give rise to transient amplifying cells which divide rapidly and progress on to committed neural or glial progenitors.[20] The principal function of the SEZ in mammals is the generation of new neurons to replenish those in the olfactory bulb.[23] As such, the transit

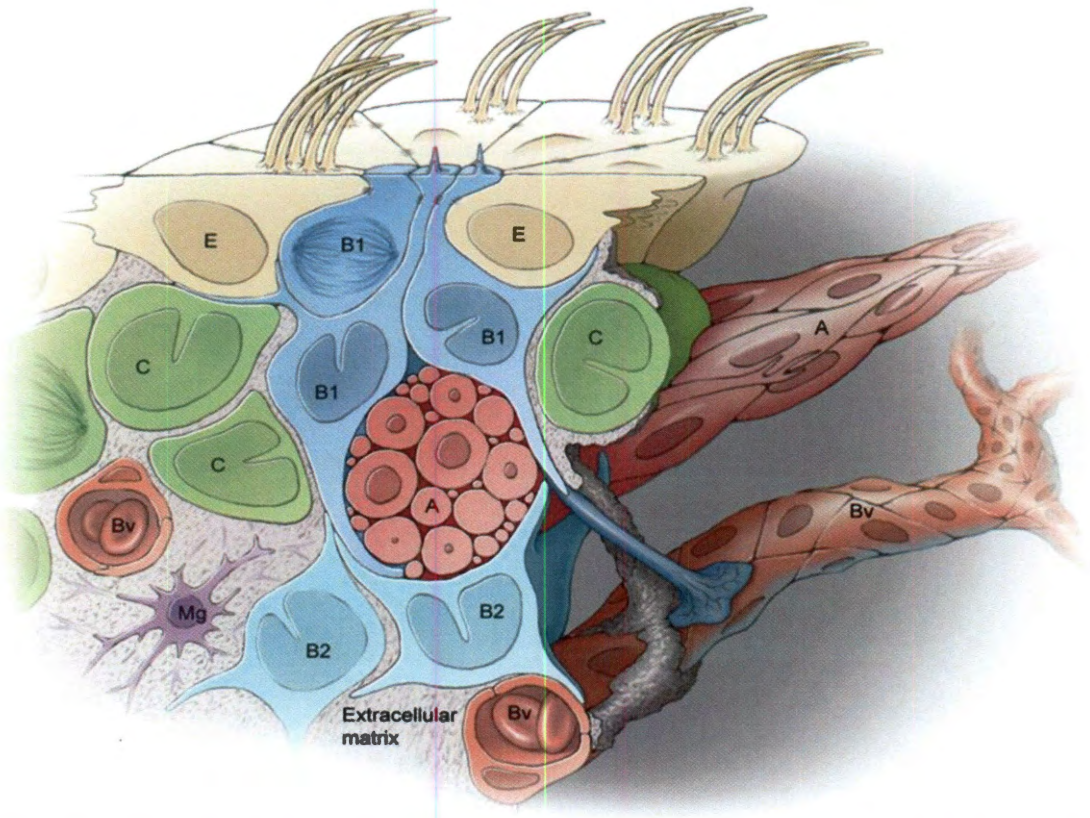

Figure 4. The subependymal neural stem cell niche.[23] Slow-dividing astrocyte-like neural stem cells (Type B cells) are localized at the center of pinwheel arrangements of ciliated ependymal cells (Type E cells). These type B stem cells interact with and receive signals from multiple aspects of the niche including fast-dividing transit amplifying cells (Type C cells), neuroblasts (Type A cells), specialized basal lamina and extracellular matrix (grey), microglia (Mg), and endothelial cells of the microvasculature (Bv).[23] Figure from Ihrie *et al*. 2011.

amplifying cells largely differentiate into highly motile neuroblasts which travel en masse and parallel to the SEZ to ultimately form the rostral migratory stream.[48]

Due to its complexity and variety of cellular components, the overarching spatial organization of the SEZ had for some time remained ambiguous. In 2008, however, Mirzadeh *et al.* employed a unique method for whole-mount, *en face* dissection of the lateral ventricle wall and subependymal tissue of the rodent brain.[22] This perspective of the intact ventricular surface and underlying niche revealed that type B NSCs were localized at the center of pinwheel-shaped arrangements of ciliated ependymal cells as shown in Figure 5. They additionally found that the

type B cells extended a single, non-functioning cilia into the ventricular space and retained a long basal process with specialized endfeet terminating directly on blood vessels. Subsequently, these highly extended cells may be capable of receiving information directly from both the cerebral spinal fluid and microvasculature.[22]

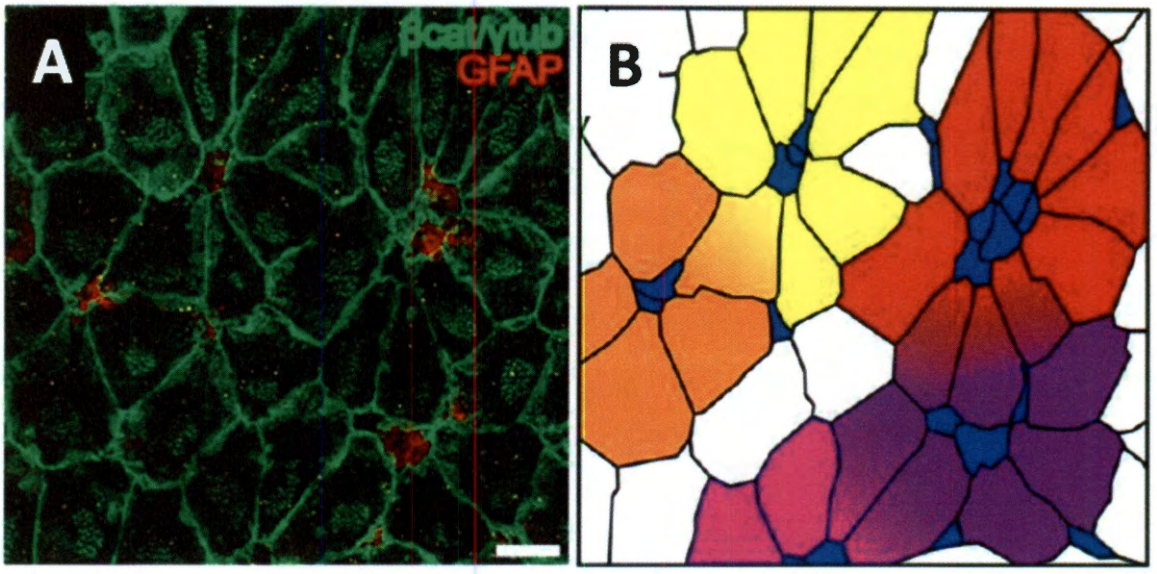

Figure 5. Pinwheel organization on the lateral ventricle surface.[22] Immunostaining (A) shows β-catenin at the cell borders and punctate γ-tubulin at the basal bodies of the cilia. Type B neural stem cells are distinguished by the astrocyte marker, glial fibrillary acidic protein (GFAP). Graphical representation of the same field of view (B) in which pinwheel arrangements are highlighted by color-coded ependymal cells and Type B stem cells are identified in blue.[22] Scale bar, 10 μm. Figure from Mirzadeh *et al.* 2008.

Observation of physical proximity provides minimal insight into the functional relationships between the various elements of the NSC microenvironment. In fact, all of the components of the niche including soluble factors, extracellular matrix, and surrounding cell types may play a role in controlling the behavior of the primitive neural stem cell.[5,48] *In vivo* investigations of which components are the primary regulators can provide some mechanistic insight. One common approach has been infusion of a particular factor of interest into the CSF of the ventricles where it is likely to diffuse directly into the subependymal zone.[23] EGF and FGF infusion, for example, both lead to an increase in type B cells and reduction of neurogenesis,

supporting their role in promoting NSC self-renewal.[52] Knocking down the expression of a particular component is another way to study its particular role in the niche. Tenascin C (TNC) is an extracellular matrix protein observed at high concentrations in the NSC niche.[53] Investigation of TNC null mice found that the absence of this glycoprotein lead to delayed expression of EGF receptor during development and a shift in NSC differentiation towards the neuronal linage.[53] To accurately interpret this result, however, *in vitro* studies are required since gene knockdown rarely affects a singular component of the complex living system.

1.3 Approaches in Neural Tissue Engineering

A method to isolate and individually study cell response to particular components of the niche *in vitro* can significantly aid in understanding the regulators of neural stem cell fate. Ideally, such a system would present low intrinsic bioactivity to avoid confounding influence from substrate bioactivity. Furthermore it should allow a wide range of modifications in order to mimic the physical, soluble, and cellular signals found *in vivo*. A biomaterial that is additionally suitable for implantation would be preferred. Potentially, once *in vitro* studies have defined the optimal scaffold properties, this matrix could be utilized as a delivery mechanism to support implanted NSCs for therapeutic applications.

1.3.1 Biomaterials for Tissue Engineering

In vitro systems are an ideal way to scale down the complexity of this niche so that the significance of individual interactions can be determined.[54] Within the literature there are several examples where a specific aspect of the niche such as an ECM molecule or soluble factor was introduced to NSCs under controlled conditions.[54] These experiments often involve a biomaterial substrate in place of tissue culture polystyrene (TCPS), since it can be more easily

modified to simulate the natural microenvironment.[49] The materials used for *in vitro* experiments may or may not be applicable subsequent, *in vivo* work.[54]

Biomaterials fall into two basic classes: natural and synthetic.[49] Often, natural biomaterials are composed of whole ECM proteins isolated from animal tissues.[55] These materials can closely recreate the complex environment that cells experience within normal tissue, and they are typically degradable by cellular proteases allowing cell migration and remodeling.[49,54] Common examples used in tissue engineering include collagen, Matrigel (reconstituted basement membrane), laminin, and fibronectin.[56] Due to difficulties in isolation and purification, however, naturally derived materials are frequently expensive and can experience batch to batch variability, making results more complicated to interpret.[49] The alternative approach attempts to incorporate features of the native ECM proteins into a man-made, polymeric constructs.[49] Examples include poly(lactic acid) (PLA), poly(glycolic acid) (PGA), poly(caprolactone), and poly(ethylene glycol).[56] With these synthetic materials, the polymer chemistry and mechanical properties can be finely tuned and regulated, improving consistency.[49] The ECM structures presented to the cells can also be more highly controlled, for example a specific cell adhesion site can be used instead of the entire fibronectin protein chain.[49] A number of methods have been developed for the incorporation of bioactivity and are specific to the material being used. A final consideration is whether the system will eventually be tested *in vivo.* If so, immunocompatibility and mechanisms for degradation should be essential features.[49,54]

1.3.2 Hydrogel Scaffolds for Neural Tissue Engineering

Poly(ethylene glycol) or PEG, is a hydrophilic material that may be particularly useful for neural tissue engineering both *in vitro* and *in vivo*.[49,57] When combined with an photoinitiator and activating light source, acrylated PEG molecules can be cross-linked into a solid, hydrogel matrix.

This process can be controlled such that it is sufficiently mild to allow encapsulation of cells into the bulk of the material for three dimensional studies.[58] Fully hydrated, the cross-linked polymer is composed primarily of water and has diffusional and mechanical properties close to that of soft tissue in the body.[59] The material is also FDA approved, highly biocompatible even following implantation into the brain[57], and a strong inhibitor of nonspecific protein adsorption.[60]

Well developed chemistries have been established to incorporate bioactivity into PEG materials.[61,62] A common strategy involves attachment of a bifunctional PEG spacer molecule to the free amine or carboxyl group of the peptide or protein to be investigated.[61] The other end of the PEG spacer is then covalently attached to the surface or throughout the bulk of a PEG hydrogel. Figure 6 shows the possibilities for bioactive modification of PEG-based scaffolds.

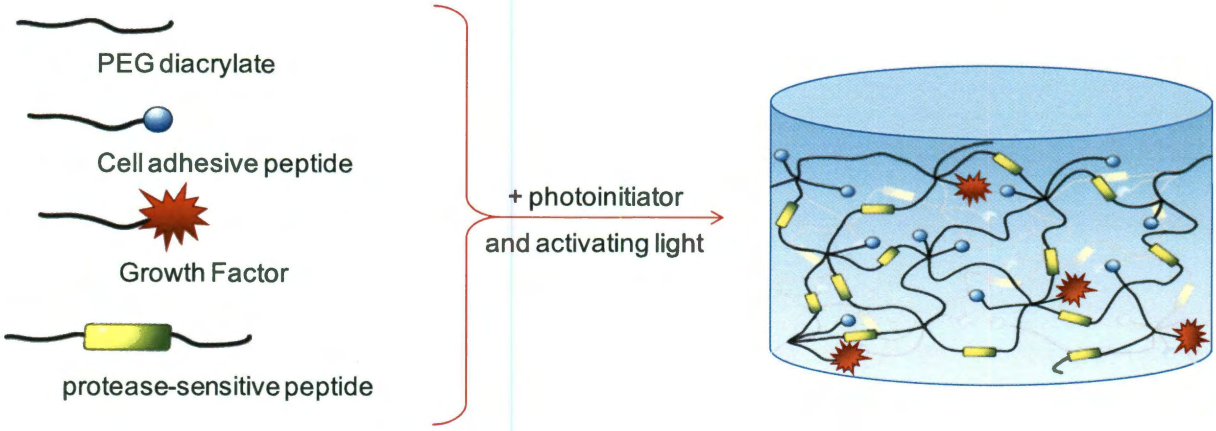

Figure 6. Bioactive modification of poly(ethylene glycol)-based hydrogels. When combined with a photoinitiator and activating light, several bioactive molecules can be incorporated in the hydrogel matrix. The gelation process is mild such that cells can additionally be included in the liquid polymer solution and encapsulated in the bulk of the material.

In the simplest application of this method, bioactive oligopeptides (sequences known to interact with cell surface receptors) are attached to the hydrogel and the response of surface seeded cells is evaluated.[63] Examples of peptides that have been studied in this way include RGDS, YIGSR, and IKVAV.[63-65] The chemistry used to attach the PEG spacer can also be performed in

aqueous solutions so that proteins can be incorporated without altering their folded structure.[61,62] Previous studies have demonstrated immobilization of epidermal growth factor, vascular endothelial growth factor, and fibroblast growth factor.[66-68] Since attachment is often initiated by exposure to light, these bioactive components can additionally be patterned with a photomask into gradients or distinct regions to spatially control cell behavior.[67]

For encapsulated cell studies and *in vivo* applications, any scaffold used should be able to degrade and allow cell migration and organization. One type of degradable hydrogel reported in the literature employed a block co-polymer of PEG and hydrolytically sensitive PLA. Primary neural tissue was observed to proliferate and migrate when encapsulated within this material as shown in Figure 7.[58]

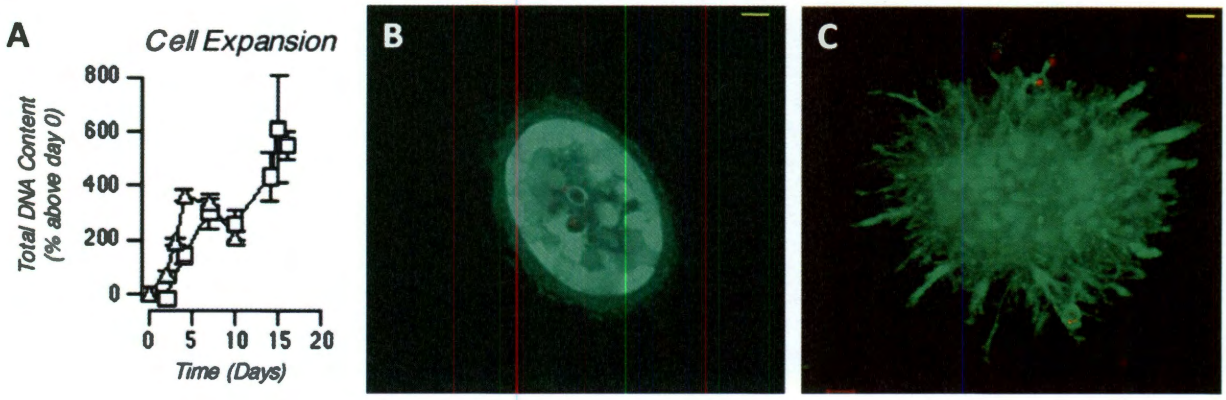

Figure 7. NSC culture in three dimensional PEG-PLA hydrogels.[58] Proliferation (A) is observed for an encapsulation of primary neural tissue. Morphology of the encapsulated cell clusters at 10 days (B) and 14 days (C) post-encapsulation show spreading and migration of the cells within the synthetic scaffold.[58] Scale bar, 20 μm. Figure from Mahoney *et al.* 2006.

A similar chemistry as used for the tethering of adhesive peptides can be adapted to embed a peptide sequence in the center of the polymer backbone.[69] By specifically selecting sequences that are known substrates for cellular proteases, the hydrogel material can be tuned to degrade by secreted cellular enzymes such as plasmin or collagenase.[69,70] In one published study, it was

found that a collagenase sensitive hydrogel modified with the RGD adhesive peptide supported self-organization of an angiogenic co-culture (Figure 8).[71] Over a period of six days, the co-encapsulated mural and endothelial cells developed into a primitive vascular plexus with similar characteristics as the *in vivo* microvasculature.[71]

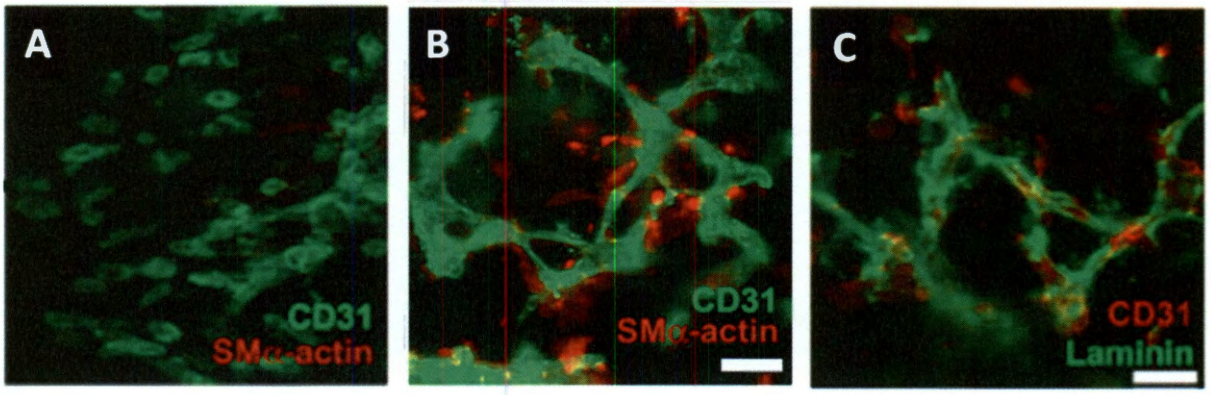

Figure 8. Cell-adhesive and collagenase-degradable hydrogel supports organization of co-encapsulated smooth muscle progenitors (SMα-actin positive) and endothelial cells (CD31 positive) into a primitive vascular network.[71] Immunostaining at day 1 (A) and day 6 (B) shows progression of cellular reorganization. Encapsulated cells also secrete extracellular matrix proteins such as laminin (C) within the synthetic microenvironment.[71] Scale bar, 50 μm. Figure from Moon *et al.* 2010.

Overall the PEG-based hydrogel system is extremely customizable for a variety of applications. High biocompatibility coupled with the capacity for precise control over the physical and chemical characteristics of the cellular microenvironment make the material valuable for both *in vitro* and *in vivo* applications. As such, PEG hydrogels have been chosen as the core substrate for the research presented herein.

1.4 Overview of Thesis

The neural stem cell niche is a unique environment, specialized for maintaining neural stem cells and capable of directing their differentiation. In this thesis work, a modified poly(ethylene glycol) hydrogel with specific matrix, soluble, and cellular niche components independently incorporated was studied *in vitro* to determine the influence of these factors on cell fate under permissive (growth) as well as differentiating media conditions. This artificial niche was furthermore synthesized in the form of injectable hydrogel microspheres and demonstrated to support therapeutic delivery of encapsulated NSCs in a rodent model of ischemic stroke.

Influence of the ECM: It has been reported that a unique arrangement of basal lamina exists in the subependymal zone and may play a role in controlling stem cell behavior. To investigate this hypothesis, cell-adhesive peptides from fibronectin were studied within a PEG hydrogel system for their effect on the behavior of a human neural stem cell line. Specifically, the ability of the material to support attachment, spreading, and proliferation of undifferentiated neural stem cells was first demonstrated and found to be comparable to standard culture on laminin coated TCPS. The influence of the synthetic matrix on NSC lineage commitment was additionally evaluated under differentiating conditions by flow cytometry of the resulting cell populations. Finally, both growth and differentiated cell phenotype was characterized within the 3D hydrogel microenvironment.

Influence of Soluble Factors: Growth factors are well known to influence stem cell behavior and are commonly used in the isolation and expansion of primary neural stem cells. The hydrogel environment was demonstrated here as a platform for presenting immobilized growth factors to surface seeded NSCs. Two factors in particular, FGF-2 and NGF, were chosen for their contrasting effects on proliferation and differentiation. Successful PEG conjugation was

determined for both factors by western blot analysis and the effect of the PEG linkage on bioactivity was assessed. Finally, the PEG-FGF and PEG-NGF conjugates were shown to influence NSC proliferation and neuronal differentiation respectively when immobilized within the bulk of a hydrogel matrix.

Influence on the Microvasculature: *In vivo,* neural stem cells directly contact the microvasculature though the specialized endfeet on their extended basal process. It is theorized that signaling between NSCs and endothelial cells coordinates both angiogenesis and neurogenesis within the niche. The bioactive hydrogel was used as a platform to observe the angiogenic potential of neural stem cells in an *in vivo* cornea micropocket assay as well as *in vitro* through co-culture with brain microvascular endothelial cells. Cells were observed to stimulate an angiogenic response *in vivo,* and furthermore promoted close interaction and self-organization within an endothelial co-culture system.

Microencapsulation and *In Vivo* Delivery: Neural stem cell delivery to treat brain injury or neurodegenerative disease is a promising new therapeutic approach that has already progressed into clinical trials. Significant room for improvement still exists, however, as cell survival following implantation is often poor. It is theorized that encapsulation of the cell therapy within a protective and supportive matrix will improve cell viability, persistence, and ultimately the therapeutic effect. A novel method was developed to synthesize hydrogels in an injectable microsphere form. Several parameters of this technique were optimized to improve particle gelation, yield, and size distribution and to maintain compatibility of the microencapsulation protocol across multiple cell lines. Finally, the constructs were demonstrated to support long-term *in vitro* culture as well as successful *in vivo* delivery of encapsulated neural stem cells.

2 ECM Mimetic Scaffold for Investigation of NSC Behavior *In Vitro*

2.1 Introduction

2.1.1 Extracellular Matrix Interactions in the NSC Niche

The extracellular matrix (ECM) most notably forms a structural scaffold to physically support the cells that make up a tissue.[72] These molecules, however, also provide attachment points for cells, sequester growth factors and cytokines, and transmit mechanical signals.[48,72] Cellular attachment to the ECM often occurs through integrin binding.[48,73] Far from a passive attachment, these integrins are connected to the cytoskeleton within the cell and can trigger intercellular signaling cascades leading to changes in cell behavior such as promotion of cell survival or increased proliferation.[48,73] Integrins are dimeric transmembrane proteins formed from a combination of alpha and beta subunits.[73] As shown in Figure 9, different ECM molecules can have binding sites that are specific for particular subunit pairs, and can lead to unique downstream signaling effects within the cell.[73] The composition and arrangement of ECM in a region of tissue could therefore play a direct role in influencing cell behavior.[48,72,73]

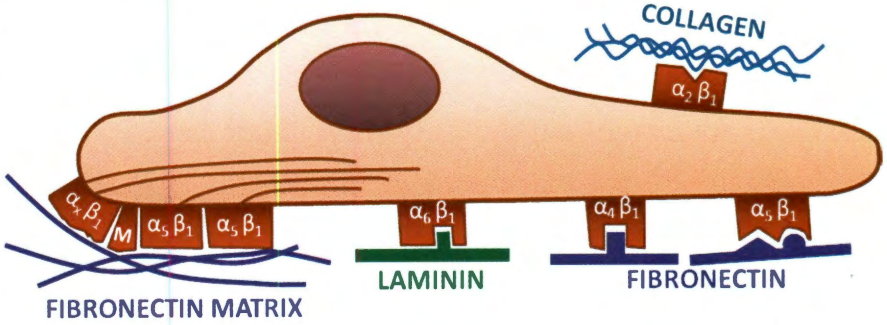

Figure 9. Integrin adhesion to the extracellular matrix.[73] Cell attachment to ECM molecules such as laminin or fibronectin occurs through integrins. Specificity of cell attachment and response is achieved by unique binding site affinity for different integrin subunit pairings.[73] Figure adapted from Yamada *et al.* 2001.

Within the SEZ of both humans and rodents, a particularly unique arrangement of the ECM has been observed to be intimately associated with the neural stem cells.[48,72,74] In most tissues, the

basal lamina is a thin, two dimensional sheet of specialized ECM that wraps around blood vessels or lines the back of epithelial cell layers.[51] Basement membranes are known to play a key role during development by affecting cell proliferation, polarization, and morphogenesis.[72] In contrast to the normal arrangement, the basal lamina of the SEZ microvasculature extends out past the capillary tips, ending in clusters just beneath the ependymal cell layer.[48,51] Referred to as a fractone, this extravascular basal lamina has a highly branched, three dimensional structure and therefore connects between many different cell types in the vicinity.[51,74] Figure 10 provides a graphical representation of the typical fractone arrangement in the SEZ.[51]

A single fractone starts from a perivascular macrophage and may interact with several NSCs, transit amplifying cells, and macrophages before reaching the ependymal layer.[51] It is made up of many classic basal lamina components such as laminin β1 and γ1, collagen I and IV, nidogen, and perlecan.[51,74] A more unusual ECM component associated with some of the fractones is N-sulfate heparin sulfate proteoglycan (N-sulfate HSPG), which was shown by Kerever *et al.* to sequester and activate growth factors, in particular basic fibroblast growth factor, or FGF-2.[74] Taken together, observations of the unique composition and arrangement of the ECM in the niche as well as the close association of the NSCs with these structures suggest a key role for ECM in directing NSC behavior.[48,51]

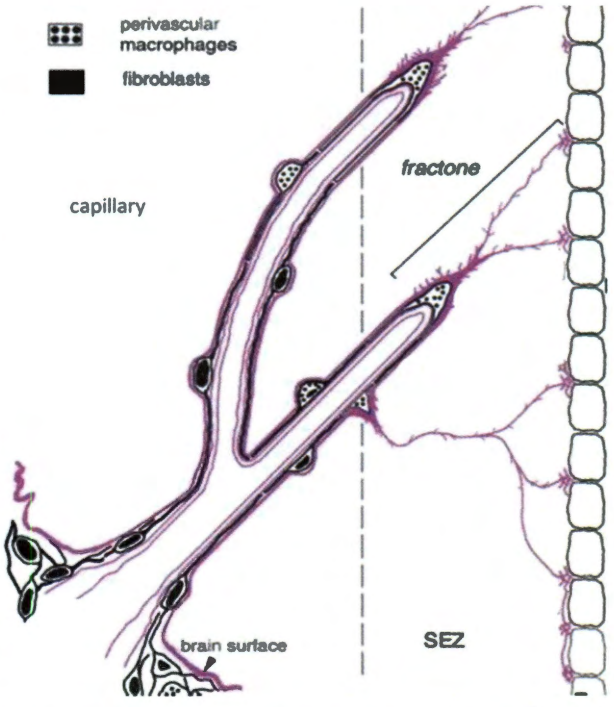

Figure 10. Fractone structure in the NSC niche.[51] Basal lamina in the subependymal zone is arranged in a unique branching structure referred to as a fractone (shown in purple).[51] Figure from Mercier *et al.* 2002.

2.1.2 Investigating ECM Interactions In Hydrogel Scaffolds

Both synthetic and natural biomaterials have been used in conjunction with neural stem cells.[54] Thornhoff *et al.* investigated multiple commercially available products including Matrigel and PuraMatrix (peptide-based hydrogel), and found that they had different effects on NSC proliferation, migration, and differentiation.[55] A more specialized collagen/hyaluronan matrix was shown by Brannville *et al.* to allow thermoresponsive encapsulation and 3D culture of NSCs.[75] Recently, a laminin-functionalized PuraMatrix was shown to allow improved 3D growth and differentiation of a human neural progenitor line.[76] All of these materials, however, can be relatively expensive to generate. These studies are also difficult to interpret due to intrinsic and variable bioactivity from the scaffold proteins.[49]

Within the literature the use of synthetic materials appears to be more common and to provide greater versatility. One study compared common polymers used for tissue engineering including poly(lactic-co-glycolic acid), poly(L-lactide-co-ε-caprolactone), and poly(L-lactic acid) and concluded that there were significant differences in proliferation and neuronal differentiation of an embryonic rat hippocampal stem cell line, designated HiB5.[77] The variation in cell response was attributed to differences in protein adsorption on the surface of the three scaffolds.[77] In a separate study, a unique synthetic material developed primarily for *in vitro* work involved a biomimetic, interfacial interpenetrating network of polymers (IPN).[78] The interpenetrating network was used to immobilize peptides containing known, cell-adhesive sequences (RGD sequence from fibronectin or IKVAV sequence from laminin) at varying concentrations. Their results showed that only RGD supported attachment and survival of primary adult hippocampal neural stem cells.[78] Other groups, in contrast, have shown that laminin derived peptides such as IKVAV can actually promote neuronal attachment and differentiation, for example when

covalently linked to a PEG hydrogel surface (Figure 11).[65,79] For this work by Ranieri *et al.*, however, a more committed neural progenitor line, PC-12, was used. The conflicting data on NSC adhesion to these materials indicates that we are only beginning to understand the interactions between NSCs and their physical environment. Significant work remains to identify appropriate platforms for studying the cellular response across a variety of experimental conditions.

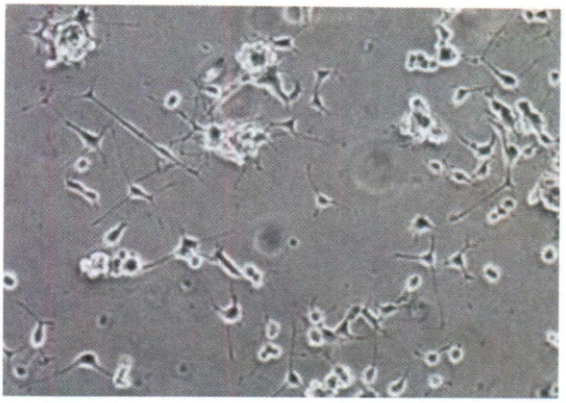

Figure 11. Neural progenitor cell adhesion to IKVAV-modified hydrogels.[65] Phase contrast image shows attachment and neurite extension of PC-12 cells. Figure from Gunn *et al.* 2005.

In some cases, conflicting cell behavior may be caused by differences in the cell type or cell line used in the research. Primary cells can be particularly variable due to the lack of standard harvesting techniques. Cell lines can provide greater homogeneity, however may not be as representative of *in vivo* cell behavior. The human neural stem cell line CTX0E03, was developed for therapeutic implantation to treat ischemic stroke in humans.[80] As such, this cell line is clinically relevant, provides a readily expandable and homogeneous source for *in vitro* studies, and has no known tendencies for tumor formation *in vivo*.[35] Furthermore, the cell line is conditionally immortalized with the *c*-mycER^{TAM} transgene to allow undifferentiated expansion in the presence of the synthetic drug, 4-hydroxy-tamoxifen (4-OHT) and rapid activation of differentiation pathways on implantation or removal of 4-OHT from the media.[80] The combination of clinical relevance and standard expansion / differentiation protocols make the CTX0E03 cell line an excellent model to study the mechanisms regulating neural stem cell proliferation and differentiation. For these reasons, CTX0E03 has been chosen as the primary cell line for developing and testing the synthetic hydrogel scaffold presented herein.

2.3 Materials and Methods

All materials were purchased from Sigma unless otherwise noted.

2.3.1 Cell Culture

Conditionally immortalized human cortical neural stem cells (CTX0E03 line, passage 10 to 20)[80,86,87] were generously donated from the lab of Dr. Jack Price. The cells were cultured on laminin coated TCPS flasks, which were prepared by applying 0.07 ml per cm^2 of a 20 μg/ml solution of laminin in Hank's balanced salt solution (HBSS, Invitrogen) to the surface for 4 h at room temperature (RT). Cells were cultured a 1:1 mixture of Dulbecco's Modified Eagle's Medium and Ham's F12 (DMEM/F12, Invitrogen) supplemented with 0.03% human albumin (SeraCare), 100 μg/ml apo-transferrin, 16.2 μg/ml putrescine dihydrochloride, 5 μg/ml recombinant human insulin, 60 ng/ml progesterone, 2 mM $_L$-Glutamine, 40 ng/ml sodium selenite, 10 ng/ml human basic fibroblast growth factor (FGF, Peprotech), 20 ng/ml epidermal growth factor (EGF, Peprotech), and 100 nM 4-hydroxy-tamoxifen (4-OHT). The cells were incubated at 37 °C in a 5% CO_2 environment and passaged 1: 8 every 5 to 7 days with Accutase solution. For select studies, spontaneous differentiation along neural and glial lineages was induced by culturing cells in media lacking FGF, EGF, and 4-OHT.

2.3.2 Characterization of Cellular Integrin Expression

Integrin expression by the neural stem cells was evaluated with an α/β Integrin-Mediated Cell Adhesion Array Kit (Millipore) using manufacturer's protocol. Briefly, microwell strips from the alpha integrin array plate (containing immobilized antibodies against α_1, α_2, α_3, α_4, α_5, α_V, and $\alpha_V\beta_3$) and from the beta integrin array plate (containing immobilized antibodies against β_1, β_2, β_3, β_4, β_6, $\alpha_V\beta_5$, and $\alpha_5\beta_1$) were soaked in HBSS at RT for 1 h to rehydrate. CTX0E03 cells were

Although the CTX0E03 cell line is expanded on laminin coated surfaces, previous investigations of laminin derived peptide sequences such as YIGSR and IKVAV have reported inconsistent responses from the different neural progenitor sources.[65,78,79] Only the fibronectin-derived RGD peptide sequence has been found to consistently promote neural stem cell adhesion on synthetic substrates.[65,78,81,82] The RGD motif is arguably one of the most ubiquitous and well characterized adhesive peptide sequences and may be bound by a number of integrin pairs including $\alpha_v\beta_3$, $\alpha_v\beta_5$, and $\alpha_5\beta_1$.[83] For this work a linear RGD- containing peptide, RGDS, was investigated in addition to a cyclicized RGD peptide, c(RGDfK), which has been reported to present a more natural conformation, have greater integrin binding strength and specificity, and to be more resistant to proteolysis (30-fold more stable at pH 7.0).[84,85]

2.2 Objectives

Current platforms for investigation of neural stem cells have primarily been limited to 2D studies on modified surfaces such as TCPS, or 3D studies within complex and difficult to control naturally-derived matrices. In order to begin to isolate the effects of the physical environment on stem cell fate, a highly controlled substrate with potential for both 2D and 3D investigations is needed. For this work, a tunable PEG-based scaffold is proposed as a superior platform for studying CTX0E03 cell behavior *in vitro*. Cell adhesion and spreading on the scaffold was evaluated for hydrogels modified with the well characterized RGD motif in both a linear and cyclic form. Furthermore, cell behavior under growth and differentiating conditions was compared between laminin-coated TCPS and the synthetic scaffold. Finally, these investigations were repeated under more biomimetic, 3D encapsulation conditions using a matrix metalloproteinase (MMP)-degradable polymer scaffold.

passaged with Versene chelating solution (Invitrogen) and seeded at $2x10^5$ cells/cm^2 on the assay plate. After 16 h incubation, the cells were rinsed with phosphate buffered saline (PBS, Cellgro) and stained with the provided crystal violet cell stain solution for 10 min at RT. After two additional PBS rinses, wells were allowed to air dry before addition of 100 µl/well of the provided extraction buffer. Gentle rocking of the samples at RT in the extraction buffer was conducted for 10 minutes to allow complete disruption of the cells and dissolution of the crystal violet stain. Sample absorbance was read at 570 nm on a microplate reader (Bio-Tek ELx800) and compared to negative control wells with immobilized anti-mouse IgG.

2.3.3 Synthesis of Poly(ethylene glycol) Diacrylate

Poly(ethylene glycol) diacrylate (PEGDA) was synthesized by reacting 10 kDa PEG with 3 molar excess of acryloyl chloride and 1 molar excess triethylamine (TEA) in anhydrous dichloromethane (DCM) under argon overnight. The reacted mixture was transferred to a separatory funnel where 2 M K_2CO_3 was added at a 5 molar excess to the PEG (Figure 12). After mixing well, the solution was allowed to separate and the organic phase was collected, dried with magnesium sulfate and filtered. The final, clear liquid was precipitated in cold diethyl ether, filtered, and dried under vacuum.

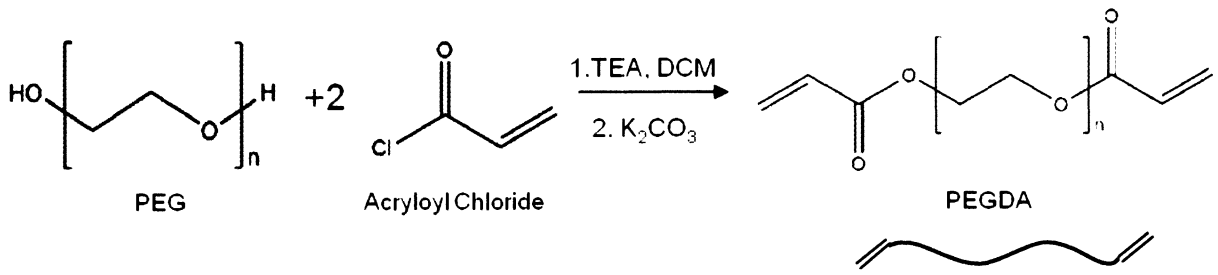

Figure 12. Chemical synthesis of poly(ethylene glycol) diacrylate by reaction of poly(ethylene glycol) with acryloyl chloride in DCM. Acrylate end groups permit crosslinking of a liquid PEGDA solution of into a solid hydrogel matrix in the presence of photoinitiator and activating light.

2.3.4 Synthesis of PEG-peptide Conjugates

Monoacrylate PEG-peptide conjugates were synthesized by reacting acrylate-PEG-succinimidyl carboxymethyl (acrylate-PEG-SCM MW 3400 Da, Laysan Bio) with a 0.2 molar excess of peptide and a 1 molar excess N,N-diisopropylethylamine (DIPEA) in anhydrous dimethyl sulfoxide (DMSO) on a rocker plate at RT overnight. The reacted mixture was then dialyzed to remove unreacted peptide, lyophilized, and characterized by gel permeation chromatography (GPC, Varian Inc.). Peptide sequences investigated here include linear RGDS (American Peptide), a lysine-containing, cyclic form of RGD (c(RGDfK), Creative Peptide), and a tryptophan containing RGD peptide, GGGWGGRGDS (referred to as WRGDS), which was synthesized by Melissa McHale with a solid phase peptide synthesizer (Aapptec) using standard Fmoc chemistry. See Figure 13 for a diagram of the reaction scheme.

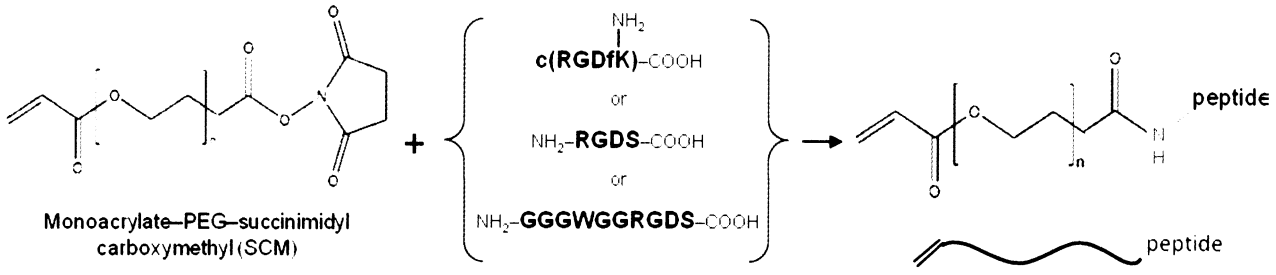

Figure 13. Chemical synthesis of PEG-peptide conjugates. Reaction of PEG-SCM with the primary amine of a cell adhesive peptide forms an acryl-PEG-peptide conjugate that can be covalently linked to the hydrogel matrix. Cyclic, linear, and tryptophan-containing RGD motifs were prepared for investigation within the hydrogel.

2.3.5 Synthesis of Degradable PEG-PQ-PEG

The MMP-sensitive peptide GGGPQGIWGQGK (abbreviated as PQ)[68,71,88] was similarly synthesized with a solid phase peptide synthesizer (Aapptec) using standard Fmoc chemistry. The product was analyzed with matrix-assisted laser desorption ionization time-of-flight mass spectrometry (MALDI-ToF, Bruker Daltonics). Enzyme degradable PEG-PQ-PEG was synthesized

by reacting PQ peptide with a 1 molar excess of acrylate-PEG-SCM and a 3 molar excess DIPEA in anhydrous DMSO on a rocker plate at RT overnight. The product was then dialyzed, lyophilized, and characterized by GPC to determine coupling efficiency.

2.3.6 Characterization of PEG-PQ-PEG Enzymatic Degradation

Sensitivity of the PEG-PQ-PEG hydrogel material to enzyme-mediated degradation was determined by exposing cross-linked gels to a collagenase containing buffer. Since the PQ peptide contains a tryptophan in the sequence, the degradation of a hydrogel can be monitored by measuring the tryptophan absorbance peak (280 nm) in the surrounding solution over time.[71] To produce the gels, a hydrogel precursor solution was formed by mixing 10% by weight PEG-PQ-PEG or 10 kDa PEGDA in 10 mM HEPES buffered saline (HBS, pH 8.5) containing 3.4 µl/ml N-vinylpyrrolidone (NVP), 10 µM eosin Y photoinitiator, and 1.5% v/v triethanolamine (TEOA, Fluka BioChemika). The polymer solution was then sterilized via filtration through a 0.2 µm membrane (Whatman). Droplets of this precursor solution (5 µl volume) were pipetted into the bottom of ethanol sterilized 200 µl cuvettes, cross-linked by exposure to 60 s of white light (Fiber-Lite, Dolan Jenner), and then incubated in 200 µl sterile degradation buffer (PBS containing 3.6 mM $CaCl_2$ and 0.2 mg/ml NaN_3, pH 7.4) overnight. The solution was then exchanged with 200 µl fresh degradation buffer with or without 100 µg/ml collagenase (≥125 CDU/mg, Type IV from *Clostridium histolyticum*) and absorbance measurements at 280 nm were taken between 0 and 72 h with a UV spectrophotometer (Carey 5000, Varian). Degradation buffer without collagenase or hydrogel was used as reference blank.

2.3.7 Formation of Coverglass-Immobilized hydrogels

Hydrogels were formed as disks immobilized against acrylated glass coverslips to improve handling of the constructs and to stabilize the gel at the bottom of the well plate during surface

seeding of cells. First, 12 mm diameter glass coverslips (TedPella) were cleaned with piranha solution (3:1 ratio of sulfuric acid and hydrogen peroxide, 30% soln.) for 2 h at RT. The glass was rinsed with MilliQ H_20 and then incubated for 3 days in acrylating solution (2% w/v trimethylsilylpropyl acrylate (TMPSA) in 95% Ethanol, pH 4.5) on a rocker at RT. Finally the slides were cleaned with 95% ethanol and baked overnight at 100 °C. To produce the gel disks, a hydrogel precursor solution was formed by mixing 10% by weight PEGDA in 10 mM HBS containing 3.4 µl/ml NVP, 10 µM eosin Y photoinitiator, and 1.5% v/v TEOA. A 10 µl volume of precursor solution was placed between an acrylated coverslip and clean glass slide separated by 380 µm thick polydimethylsiloxane (PDMS) spacers before crosslinking by exposure to white light (Fiber-lite 180 Illuminator) for 1 min. Handling only the coverglass portion with tweezers, the immobilized gels were transferred to a 24 well plate and soaked in 1 ml HBSS for a minimum of 24 h prior to cell seeding. A complete diagram of this process is provided in Figure 14.

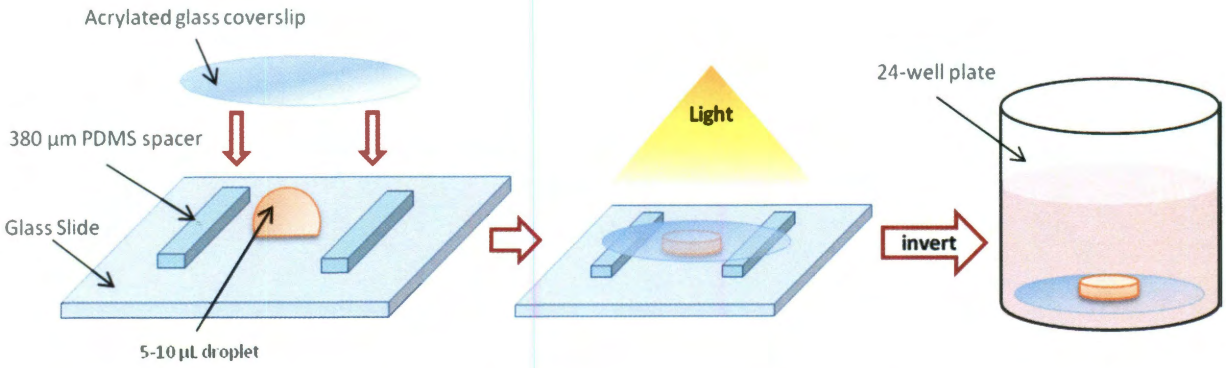

Figure 14. Technique for generating coverglass-immobilized hydrogels. Droplet of polymer precursor solution is sandwiched between acrylated coverslip and glass slide before crosslinking as a hydrogel disk.

2.3.8 Characterization of PEG-peptide Incorporation

The tryptophan-containing peptide, WRGDS, was used to evaluate incorporation efficiency in crosslinked hydrogels. Sterile 10% hydrogel precursor solution (10% 10 kDa PEGDA in HBS with

1.5% TEOA, 3.4 µl/ml NVP, and 10 µM eosin Y) was prepared both with and without 3 mM PEG-WRGDS. The UV absorbance at 280 nm was evaluated for these solutions and compared to a serial dilution of PEG-WRGDS (0.0156 to 0.5 mM in HBS with 1.5% TEOA). Disk-shaped hydrogels (10 µl volume) were then formed with 35 s or 1 min exposure as described in section 2.3.7 with the exception that a non-acrylated coverslip was used. The gels were transferred to a 24 well plate and soaked in HBSS with 1.5% TEOA for 48 h. At 24 and 48 h, 500 µl of soak solution was temporarily removed and absorbance read at 280 nm with a UV spectrophotometer. Additionally at the 48 h time point, the gels were removed, dried of excess moisture, and placed on a quartz coverglass (TedPella) for direct measurement of 280 nm absorbance in the UV spectrophotometer. Finally, each gel was manually sectioned and imaged on a dissecting scope affixed with a ProgRes C5 CCD camera to determine thickness and final volume.

2.3.9 Investigation of NSC Adhesion and Spreading

Neural stem cell adhesion to the hydrogel matrix was investigated by seeding cells on the surface of immobilized hydrogel disks. Polymer precursor solution was prepared as 10% 10 kDa PEGDA in HBS with 1.5% TEOA, 3.4 µl/ml NVP, and 10 µM eosin Y. Linear PEG-RGDS or cyclic PEG-c(RGDfK) were added to separate aliquots of the precursor solution and serially diluted to create a range of concentrations from 0.375 to 6 mM. The solutions were filter-sterilized and used to prepare immobilized 380 µm thick, 10 µl volume disk gels with three gels per test condition as described in section 2.3.7. Coverglass with attached hydrogel was placed in a 24-well plate and soaked at RT for 24 h in 1 ml of HBSS. CTX0E03 cells were then passaged with Accutase and seeded at 10,000 cells/cm^2 in complete growth media. After 16 h incubation, samples were visualized with nuclear and actin staining. Briefly, the cells were fixed for 1 h in 4% paraformaldehyde (PFA), permeabilized for 15 min with 0.5% Triton X-100, blocked overnight at

4 °C with 5% bovine serum albumin (BSA), and finally stained for 2 h in PBS with 5 U/ml rhodamine-phalloidin (Invitrogen) and 2 μM DAPI to label actin and nuclei respectively. All steps were performed at RT (unless otherwise noted) with reagents diluted in PBS and three PBS rinses following each step. Finally, the samples were imaged by phase contrast and fluorescence microscopy (Zeiss Axiovert 135) and analyzed in ImageJ (NIH) to quantify cell adhesion (count of DAPI positive nuclei per cm^2) and cell spreading (actin signal area divided by cell number based on DAPI count). To identify the lower limit of cell adhesion and spreading on the cyclic RGD modified surface, the study was repeated in a similar manner with 0.003 to 0.3 mM PEG-c(RGDfK) and with an incubation time of 3 h.

A final study was performed to identify the integrins primarily involved in NSC interaction with the c(RGDfK) modified hydrogel. Immobilized hydrogel disks (10% 10 kDa PEGDA with 0.3 mM PEG-c(RGDfK)) were prepared as described in section 2.3.7. Cells were passaged with Versene to preserve surface integrins and resuspended in media at approximately $5x10^4$ cells/ml. Cells were then incubated for 40 min at RT with either $\alpha_v\beta_3$ integrin blocking antibody (1:100, Millipore), β_1 integrin blocking antibody (1:100, Millipore), or no blocking antibody and seeded onto the hydrogels at 20,000 cells/cm^2. After 4 h, all samples were fixed and stained with DAPI and rhodamine-phalloidin.

2.3.10 Hydrogel substrates for Expansion of NSCs

CyQyuant Proliferation Assay: Neural stem cell behavior was first compared between the hydrogel and laminin-coated TCPS under non-differentiating culture conditions. To assay rate of proliferation, hydrogel disks containing 0.3 mM PEG-c(RGDfK) were prepared as described in section 2.3.7 with non-acrylated coverglass. After swelling for 24 h in HBSS, 6 mm diameter punches were made from the disks and transferred to the wells of a 96 well plate. Other wells

for TCPS conditions and standard curve generation were coated with laminin as described in section 2.3.1. Cells were passaged and seeded at 10,000 cells/cm^2 for test conditions or at 0 to 100,000 cells/cm^2 for a standard curve. After allowing cells to adhere for 12 h, the 0 time point (with standard curve) was acquired by aspirating the media and storing the dry samples at -80 °C. Remaining samples were similarly collected at 24, 48, and 72 h time points with a minimum of 4 samples per condition and per time point. After all samples had been collected, cell number was determined with the CyQuant Cell Proliferation Assay (Invitrogen) according to manufacturer's instructions. In this assay, the CyQuant GR dye becomes highly fluorescent upon binding to cellular DNA. Briefly, the provided cell-lysis buffer stock solution was diluted 20-fold in MilliQ water and supplemented with CyQuant GR dye at 400-fold dilution to produce 1X working solution. To each well of the thawed samples, 200 µl of working solution was added and allowed to incubate for 10 min with gentle rocking protected from light. Finally, 180 µl from each well was transferred to a black-bottom 96-well plate and read on a fluorescent microplate reader (SPEX FluoroLog-3 Spectrofluorometer) with excitation set at 480 nm and emission set at 520 nm.

Ki-67 Expression Analysis: Proliferative response to growth conditions was also assayed via immunohistochemical staining of cellular markers. Cells were seeded at 10,000 cells/cm^2 on immobilized hydrogel disks or laminin-coated TCPS and cultured for 3 days. A standard protocol for immunostaining was used for all samples. The cells were fixed for 1 h in 4% PFA, permeabilized for 15 min with 0.5% Triton X-100, and blocked overnight at 4°C with 5% BSA. Primary antibodies were added in PBS containing 0.5% BSA and incubated overnight at 4 °C followed by 4, 1 h PBS rinses at RT. Secondary antibodies (Alexa Fluor conjugated, Invitrogen) were all used at 1:500 dilution and incubated on the sample at 4°C overnight in PBS with 0.5%

BSA. Finally, samples were rinsed with PBS and stained for 1 h at RT in 2 μM DAPI working solution. To quantify actively proliferating cells, samples were stained according to protocol with rabbit anti Ki-67 primary antibody (1:200, Vector Labs) and donkey anti-rabbit AlexaFluor 488 secondary antibody. Images were quantified in ImageJ by determining percent of total DAPI positive nuclei that were positive for the Ki-67 marker.

Undifferentiated NSC Marker Analysis: Recognized markers for undifferentiated neural stem cells (nestin and SOX2) were also assessed to determine if the hydrogel-cultured cells retained their proper NSC phenotype. Samples were stained with rabbit anti-nestin (1:200, Sigma) and mouse anti-SOX2 (1:200, R&D Systems) primary antibodies in combination with donkey anti-rabbit Alexa Fluor 488 and donkey anti-mouse Alexa Fluor 555 secondary antibodies (1:500, Invitrogen). Images were acquired by fluorescence microscopy (Zeiss Axiovert 135) or confocal microscopy (Zeiss Live5 DuoScan) and analyzed in ImageJ to determine percent of nestin and SOX2 positive cells relative to DAPI positive nuclei count.

2.3.11 Hydrogel Substrates for the Study of NSC Differentiation

To determine if the substrate on which the CTX0E03 cells were cultured would affect lineage specification, cells were seeded at 40,000 cells/cm^2 on 0.3 mM PEG-c(RGDfK) modified hydrogel disks or laminin-coated TCPS controls in differentiating media lacking EGF, bFGF, and 4-OHT. After 2 weeks in culture, the cells were fixed and immunostained for lineage markers according to the protocol in section 2.3.10. Rabbit anti-βIII Tubulin (1:1000, Abcam) and mouse anti-GFAP (1:200, Invitrogen) primary antibodies were used to label neuronal and glial lineage committed cells respectively. Secondary antibodies used included donkey anti-rabbit Alexa Fluor 488 and anti-mouse Alexa Fluor 555. Samples were imaged by fluorescence (Zeiss Axiovert 135) and confocal (Zeiss Live5 DuoScan) microscopy.

2.3.12 Analysis of Encapsulated Cell Viability

In preparation for 3D encapsulation studies, the effect of encapsulation conditions on neural stem cell viability was determined. First, a hydrogel precursor solution was prepared as 5% 10 kDa PEGDA in HBS with 1.5% TEOA, 3.4 µl/ml NVP, and 10 µM eosin Y and filter-sterilized through a 0.2 µm filter. CTX0E03 cells were passaged, counted by hemacytometer, pelleted at 600 xg, and resuspended in the polymer solution at $10x10^6$ cells/ml. Cells were encapsulated within immobilized hydrogel disks of 10 µl volume with 35, 45, or 60 s exposure to crosslinking light. A control group of cells that had been resuspended in polymer solution but not crosslinked was also generated. Gels and control cells were transferred to a 24 well plate and incubated at 37 °C in 1 ml growth media for 2 h prior to staining. To observe viability and distribution of encapsulated cells, samples were incubated for 30 min at RT in PBS containing 2 µM calcein AM and 4 µM ethidium homodimer (Live/Dead Kit, Invitrogen) and imaged by fluorescence microscopy (Zeiss Axiovert 135). Calcein AM exhibits green fluorescence when metabolized within living cells. Ethidium homodimer penetrates the compromised cell membrane of dead cells and fluoresces red upon binding to cellular DNA. Three gels were generated for each set of conditions and images were analyzed in ImageJ to quantify viable cells as a percent of total.

2.3.13 NSC Encapsulation and Three Dimensional Culture

Neural stem cell response to growth and differentiating conditions was additionally evaluated for three dimensional encapsulated cultures. Polymer solution was prepared with degradable PEG-PQ-PEG in place of PEGDA (5% PEG-PQ-PEG in HBS with 0.3 mM PEG-c(RGDfK), 1.5% TEOA, 3.4 µl/ml NVP, and 5 µM eosin Y) and filter-sterilized through a 0.2 µm filter. CTX0E03 cells were passaged, counted by hemacytometer, pelleted at 600 xg, and resuspended in the polymer solution at $30x10^6$ cells/ml. Immobilized hydrogels with the encapsulated cells (5 µl volume

each) were prepared as described in section 2.3.7 with a 60 s exposure to white light. Gels were transferred to a 24 well plate and incubated in 1 ml growth or differentiation media. After 1 week for growth or 2 weeks for differentiating conditions, gels were fixed for 1 h in 4% PFA and immunostained against phenotypic markers: SOX2 and nestin for growth condition gels or βIII Tubulin and GFAP for differentiated samples) according to the same protocol as described for surface seeded cultures (section 2.3.10). Samples were then imaged by confocal microscopy (Zeiss Live5 DuoScan).

2.3.14 Flow Cytometry for Analysis of Cellular Populations

Flow cytometry was used to characterize cell populations under growth, differentiating, and encapsulated conditions. For growth conditions on TCPS, CTX0E03 cells were seeded at 20,000 cells/cm^2 and grown for 1 week on laminin-coated TCPS with complete growth media. For differentiating conditions on TCPS, cells were seeded at 40,000 cells/cm^2 and cultured for 2 weeks on laminin-coated TCPS with differentiation media lacking FGF, EGF, and 4-OHT. For surface-seeded samples, 25 mm diameter hydrogel disks were prepared from sterile-filtered polymer precursor solution (10% 10 kDa PEGDA in HBS with 0.3 mM PEG-c(RGDfK), 1.5% TEOA, 3.4 µl/ml NVP, and 10 µM eosin Y) using a slightly modified protocol from section 2.3.7 in which 25 mm diameter coverglass and a 200 µl volume per gel disk was used in place of 12 mm diameter coverglass and 10 µl volume. Similar to the TCPS samples, cells were seeded at 20,000 cells/cm^2 for growth conditions or 40,000 cells/cm^2 for differentiating conditions on the gels in 6-well plates and cultured for either 1 week in growth media or 2 weeks in differentiating media. For encapsulated cultures, cells were resuspended at 30x10^6 cells/ml in 5% PEG-PQ-PEG with 0.3 mM PEG-c(RGDfK), encapsulated in immobilized hydrogels (protocol in section 2.3.7), and cultured for either 1 week in growth media or 2 weeks in differentiating media. To collect

samples for flow cytometry, cells were dissociated in Accutase solution (supplemented with 0.25 μg/ml proteinase K for encapsulated samples) for 30 min at 37 °C, rinsed two times with sterile PBS, fixed for 20 min at RT in 4% PFA, rinsed twice with sterile PBS, and finally resuspended at 10^6 cells/ml in ice cold 90% MeOH for storage at -20 °C. On the day of FACS analysis, samples were rinsed two times in staining buffer (sterile-filtered PBS with 1% BSA and 0.1% sodium azide) and labeled for 1 h at RT in staining buffer with 1:20 dilution of fluorescently-tagged primary antibiodies (mouse anti-class III β Tubulin – Alexa Fluor 488, mouse anti-nestin – PE, mouse anti-SOX2 – PerCP-Cy5.5, mouse anti-GFAP – Alexa Fluor 647; BD Biosciences). Finally, samples were rinsed twice in staining buffer and analyzed with a BD FACSCanto II Flow Cytometer with compensation controls established using BD Anti-Mouse IgG CompBeads (BD Biosciences) according to manufacturer's protocol and voltage gating established with unstained cell controls. All analysis of flow cytometry data was performed using FlowJo software.

2.3.15 Statistical Analysis

Significance was determined via unpaired, two-tailed *t*-test when $p < 0.05$. Error bars in figures depict standard deviations for the data sets.

2.4 Results and Discussion

In the field of neural tissue engineering, there exists a need for a universal platform to investigate the regulation of neural stem cell fate *in vitro*. The CTX0E03 human neural stem cell line is utilized here to demonstrate the versatility of the bioactive, PEG-based hydrogel scaffold. Cell interaction with the matrix was evaluated both in surface seeded, 2D cultures and with encapsulated cultures to study behavior in a 3D microenvironment.

2.4.1 Integrin Presentation by Human Neural Stem Cells

As described above, cells form adhesions with the surrounding extracellular matrix primarily via integrin binding to specific ligand sites. By identifying which integrins are highly expressed by a cell population, one could potentially predict which substrates will promote adhesion and therefore should be considered in the design of an artificial culture environment. An initial characterization of integrin expression by the human neural stem cell line, CTX0E03, was performed through the use of a commercially available integrin profiling assay. For this technique, the cells were first dissociated with a non-enzymatic chelating solution to preserve intact integrins on the cell surface. The cell suspension was seeded into hydrated microwells containing immobilized antibodies against specific integrin subunits or integrin pairs. After allowing cells to settle and interact with the antibody-coated surface, unbound cells were washed away and the remaining quantified in an absorbance-based assay. In contrast to western blot or PCR based techniques, this approach provides rapid screening of integrins that are actively presented on the cell surface. As shown Figure 15, negligible cell binding was

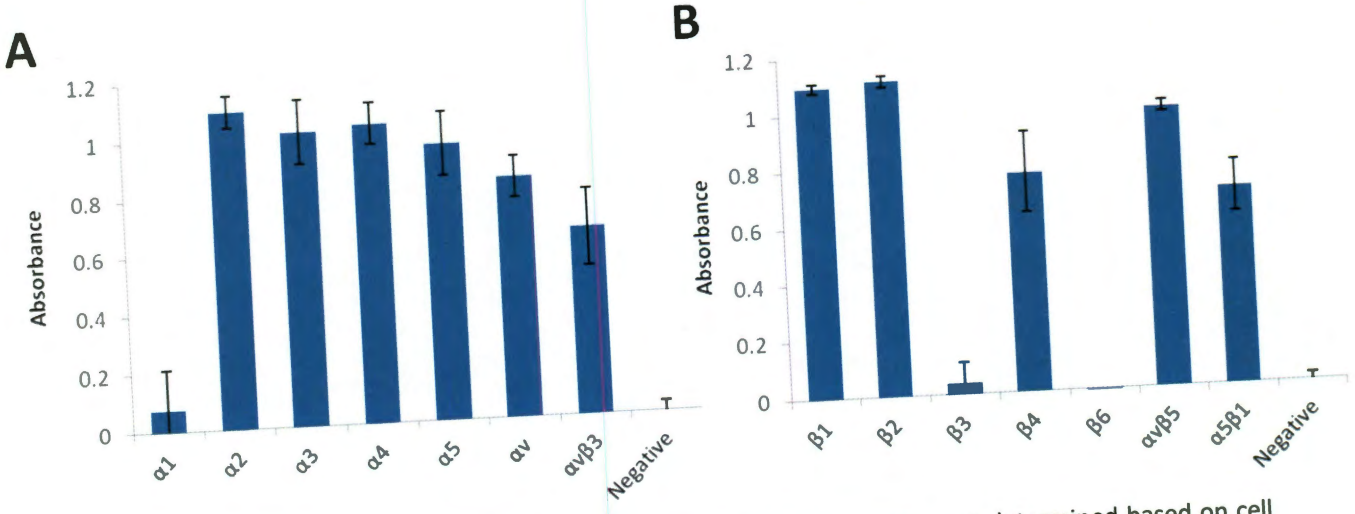

Figure 15. Integrin expression profile of CTX0E03 cells. Integrin expression was determined based on cell capture by an alpha integrin-binding (A) or beta integrin-binding (B) antibody array. Moderate to high expression was detected for all integrins investigated here, with the exception of α_1, β_3, and β_6.

observed in wells containing antibodies against α_1, β_3, and β_6 integrins. Moderate binding occurred for α_v, $\alpha_v\beta_3$, β_4, and $\alpha_5\beta_1$, while the strongest binding occurred for α_2, α_3, α_4, α_5, β_1, β_2, and $\alpha_v\beta_5$.

Although a comprehensive analysis of neural stem cell integrins has not been reported in the literature, several studies have evaluated mRNA or protein expression for particular integrins of interest. A review of the literature found that the results presented here generally agree with published findings. In particular, primary human neural stem cells have been characterized by low α_1, β_3, and β_6 integrin expression, and positive expression of integrins α_2, α_3, α_5, α_v, β_4, and β_5.[89,90] High expression of β_1 integrin has been repeatedly observed for neural stem cell populations and even been used as a marker to sort neural progenitors from primary brain tissue.[89,91-94] One contradiction between the integrin array data and published findings, however, was the presence of α_4 and β_2 integrins.[89] It is possible that the conditionally immortalized cell line differs from primary neural stem cells in this respect.

From these results, one can see that the CTX0E03 line displays a variety of surface integrins and may be capable of adhering to a wide array of substrates. Although the cell line is expanded on laminin-coated TCPS, the well characterized RGD motif was chosen for initial development of an artificial scaffold. An RGD presenting matrix should enable binding by $\alpha_v\beta_3$, $\alpha_v\beta_5$, and $\alpha_5\beta_1$ integrin pairs[83] that were shown here to be present on the CTX0E03 cell surface.[83]

2.4.2 Characterization of Peptide Modified Hydrogels

PEG Conjugation Efficiency: Multiple peptides were conjugated to an acrylate-PEG linker via succinimide chemistry. These included a linear and cyclic form of RGD, a tryptophan-containing RGD peptide, and finally a collagenase-degradable peptide, abbreviated as PQ which was reacted in a 2:1 ratio with the PEG linker. Since the presence of unconjugated acryl-PEG could

disrupt the polymer network, the efficiency for all these reactions was determined using gel permeation chromatography. In this technique, the reaction products are separated by size and quantified by an evaporative light scattering (ELS) detector. As shown in Figure 16, the larger, conjugated product (black trace) will move more quickly through the column and present as a left-shifted peak when compared to the unmodified PEG-SCM (red trace). Based on the absence of a measurable peak at the location of the unmodified SCM, it was determined that near 100% conjugation occurred for all of the reactions.

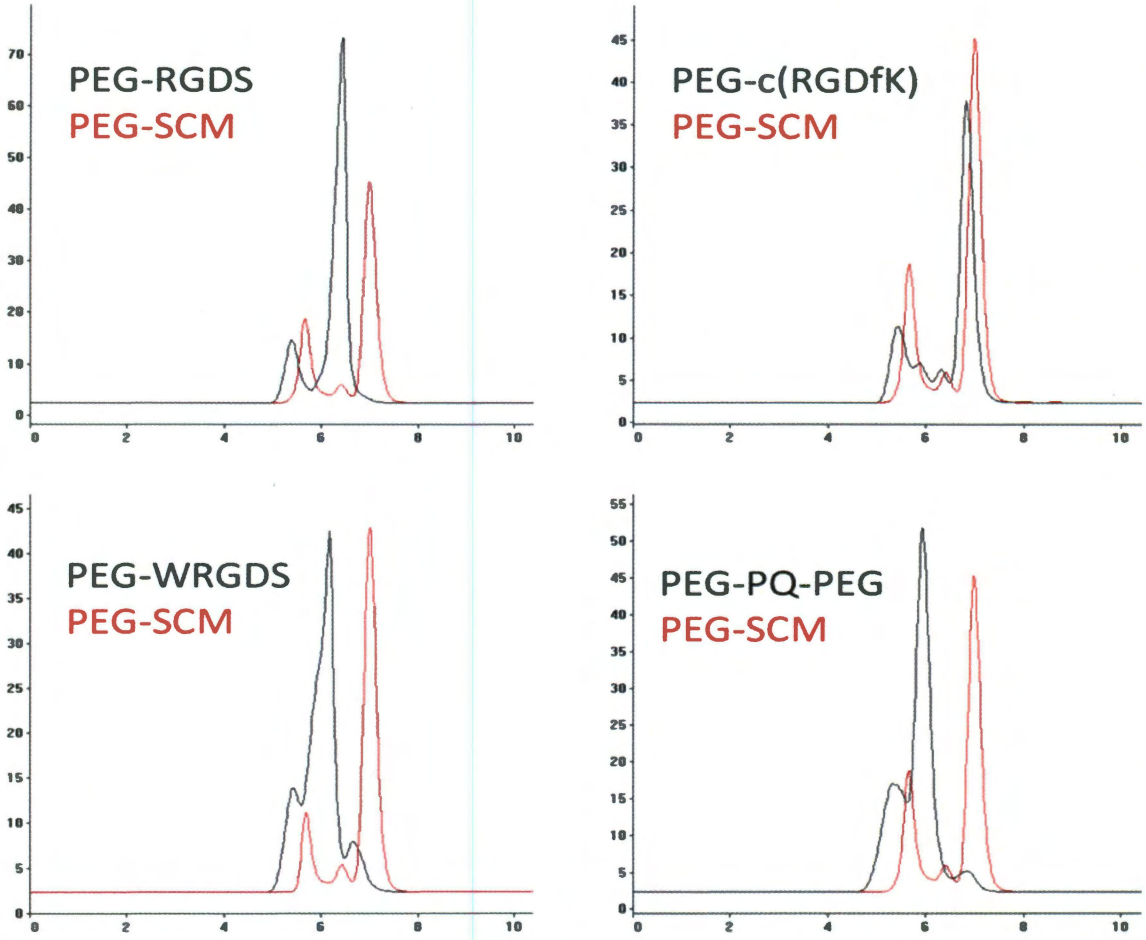

Figure 16. GPC analysis of PEG-peptide conjugates. Unmodified acryl-PEG-SCM sample is provided as a reference trace in red, and the product of the PEG-peptide conjugation reaction is shown in black. Near 100% conjugation efficiency was observed for all reactions.

For the PEG-WRGDS reaction, the presence of the tryptophan amino acid in the conjugated product should result in a characteristic absorbance peak at 280 nm. During GPC analysis, UV absorption can be monitored on the size-separated components in addition to the ELS signal. As shown in Figure 17, a peak in the UV absorbance signal was observed to coincide with the ELS signal from the PEG-WRGDS confirming successful conjugation.

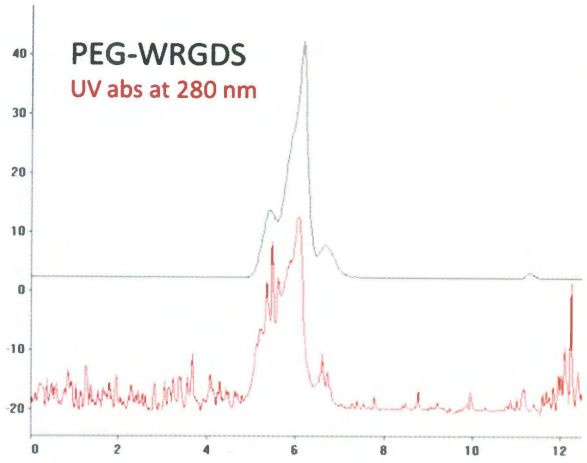

Figure 17. GPC analysis of PEG-WRGDS showing tryptophan absorbance peak. ELS (black) and UV absorbance (red) signal are shown. Characteristic UV absorbance from the tryptophan-containing PEG-WRGDS confirms conjugation was successful.

Enzymatic degradation: Enzymatic degradation of PEG-PQ-PEG hydrogel was characterized in a controlled study prior to cell experiments. The release of tryptophan-containing peptide fragments provides a simple measure of hydrogel degradation over time and was therefore used to characterize the protease-sensitive polymer. Figure 18 shows the degradation profile of the PEG-PQ-PEG scaffold in the presence of 100 μg/ml compared to two controls: degradable gel in buffer without collagenase and nondegradable PEGDA gel in collagenase solution. Solution absorbance increased only when degradable gel was incubated in the presence of protease, indicating that hydrogel degradation is mediated by enzymatic cleavage and not a hydrolytic process. Visual inspection after 72 h incubation confirmed that the PEG-PQ-PEG hydrogels fully degraded when in collagenase solution while degradable samples without collagenase and nondegradable PEGDA gels remained intact. It is important to note that a high collagenase concentration was chosen to allow observation of degradation within a reasonable time frame.

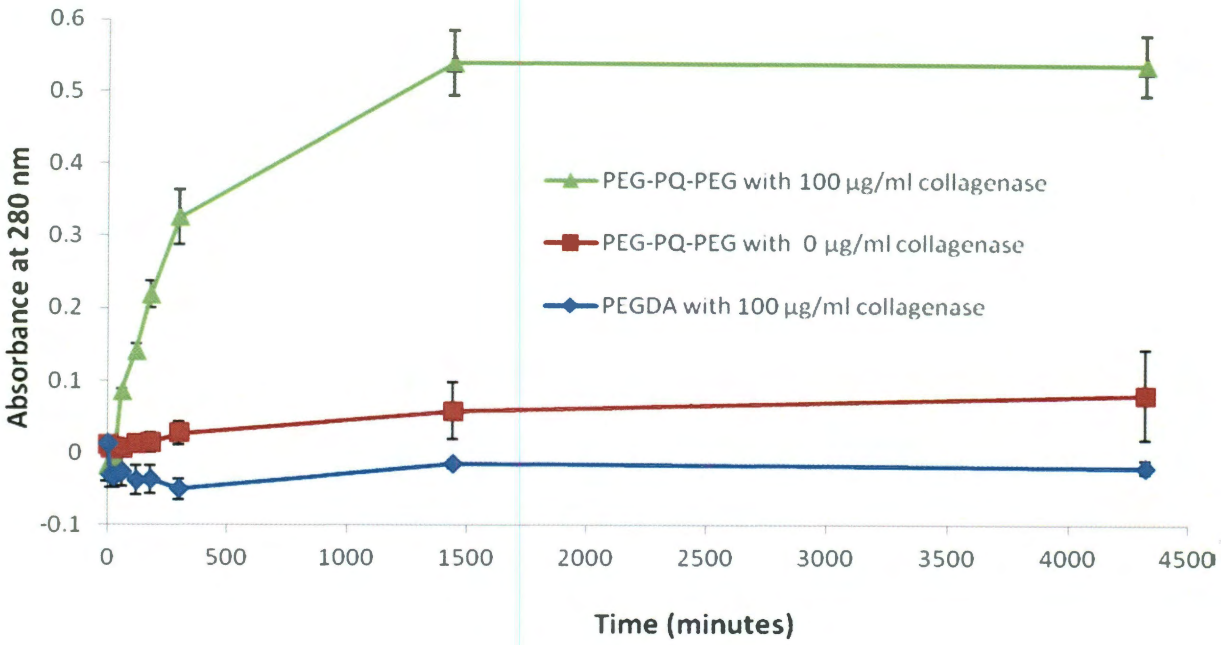

Figure 18. Collagenase degradation of PEG-PQ-PEG hydrogel. Degradation profile is shown for hydrogel scaffolds in buffer with or without 100 µg/ml collagenase. Degradation can be observed as increasing absorbance over time due to the cleavage and release of tryptophan-containing peptides into solution.

Analysis of PEG-Peptide Incorporation: The hydrogel scaffold is formed from a liquid polymer precursor solution by addition of photoinitiator and exposure to an activating light source. Addition of acryl-PEG-peptides to the precursor solution allows these components to be covalently linked into the scaffold for presentation to the seeded cells. In order to determine the efficiency of the incorporation of PEG-peptides into the matrix, a model RGD peptide containing tryptophan was used. The ring structure of tryptophan results in a characteristic absorbance peak at 280 nm that is linearly proportional to the concentration of the amino acid in solution. To measure incorporation, hydrogel disks were synthesized with a known concentration of PEG-WRGDS and placed in buffer solution to soak. The absorbance of the soak solution was measured over time and used to determine the percent of uncrosslinked PEG-peptide that diffused from the hydrogel. As shown in Figure 19, after 48 h approximately 61% of the starting

amount of PEG-WRGDS remained in the hydrogels that were exposed to crosslinking light for 1 min. For hydrogels that were exposed for 35 seconds, only 46% remained in the gels at the same time point. Direct measurement of the gel absorbance at the final time point found that at a minimum, 95% of the starting moles of WRGDS were fully accounted for (data not shown).

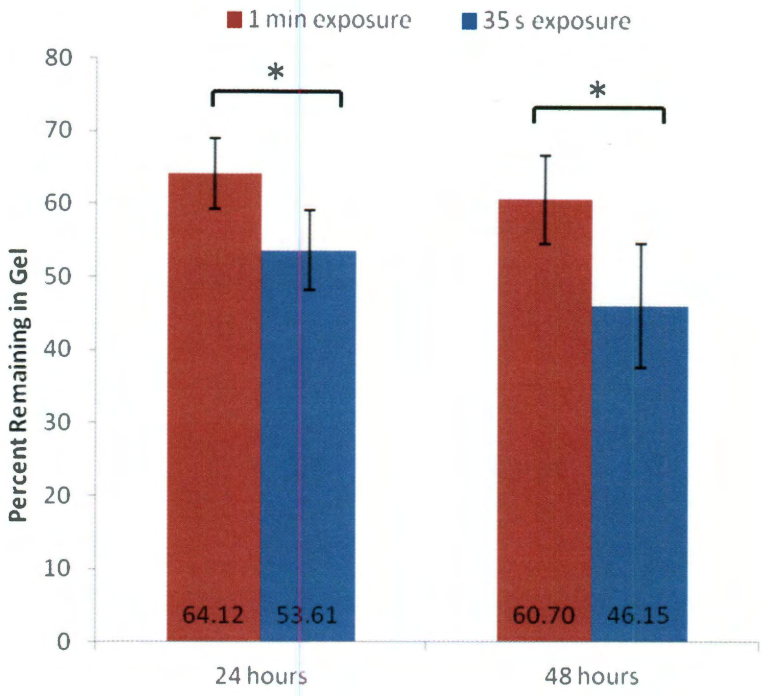

Figure 19. Incorporation of PEG-WRGDS. Quantification of incorporated PEG-WRGDS in the hydrogel matrix is based on soak solution absorbance at 280 nm. Hydrogels exposed for 1 min to the crosslinking light source showed improved retention of the PEG-WRGDS at both time points compared to a 35 s exposure indicating that more complete gelation of the hydrogel occurred. * $p < 0.05$

There was no significant difference observed between 24 and 48 h time points for either exposure group. These observations indicate that the hydrogel is more completely crosslinked following the longer exposure time, and therefore future experiments were conducted with a 1 min exposure unless otherwise indicated. It is proposed that the incorporation efficiency of PEG-WRGDS is representative of the other PEG-peptides used in this work. Therefore for all

subsequent experiments, the concentration of ligand presented to the cells can be approximated as 60% of the starting concentration reported for the polymer precursor solution.

2.4.3 Investigation of NSC Adhesion and Spreading

Initial cell studies evaluated the ability of the CTX0E03 line to adhere and spread on the hydrogel surface. Both linear and cyclic forms of RGD were tested at a range of concentrations from 0 to 6 mM and compared to a control group of cells seeded onto laminin-coated TCPS (Figure 20). Cell

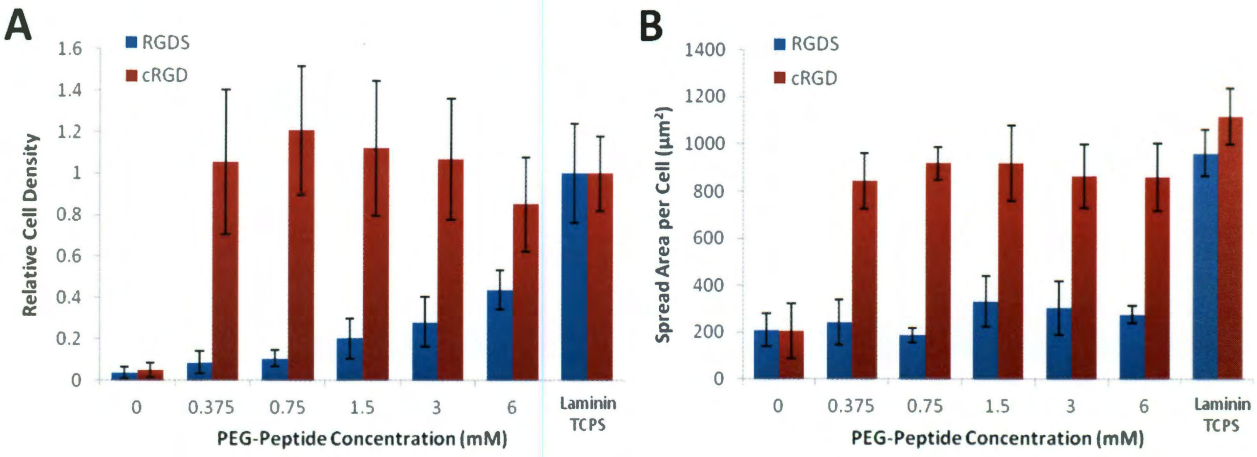

Figure 20. Quantification of CTX0E03 adhesion (A) and spreading (B) on the surface of hydrogel scaffolds modified with varying concentrations of PEG-RGDS or PEG-c(RGDfK) as compared to controls with 0 mM PEG-peptide or laminin-coated TCPS. The cyclic form of the RGD peptide promoted significantly greater cell adhesion and spreading as compared to linear RGD for all concentrations tested. $p < 0.05$

response was evaluated by staining the nuclei and actin of the fixed cell samples with DAPI and rhodamine-phalloidin, respectively. It was observed that cell adhesion to linear RGDS increased with increasing PEG-peptide concentration, however even at the highest tested concentration of 6 mM, the modified hydrogel substrate promoted significantly less adhesion when compared to laminin-coated TCPS. In addition, the linear RGD supported only minimal spreading of the adherent cells. In contrast, cyclic RGD peptide promoted equivalent cell adhesion when compared to laminin-coated TCPS for all concentrations tested. The PEG-c(RGDfK) modified

surfaces did support spreading of the seeded cells, however even at the highest concentration, there was still a significant difference between the hydrogel and TCPS control. Representative images from the laminin-coated TCPS and c(RGDfK) modified hydrogel groups are shown in Figure 21. One can see that a possible explanation for the measured difference in the area cell could be the difference in cell morphology between the two surfaces. On laminin-coated TCPS, the majority of the cell edges were characterized by wide, lamellipodia-like extensions, while on the PEG-c(RGDfK) hydrogel surface the this feature was not observed. This distinction indicates that the cells may be responding differently to the c(RGDfK) motif compared to laminin adhesive sites, however further studies are required to rule out confounding factors such as differences in the substrate stiffness.

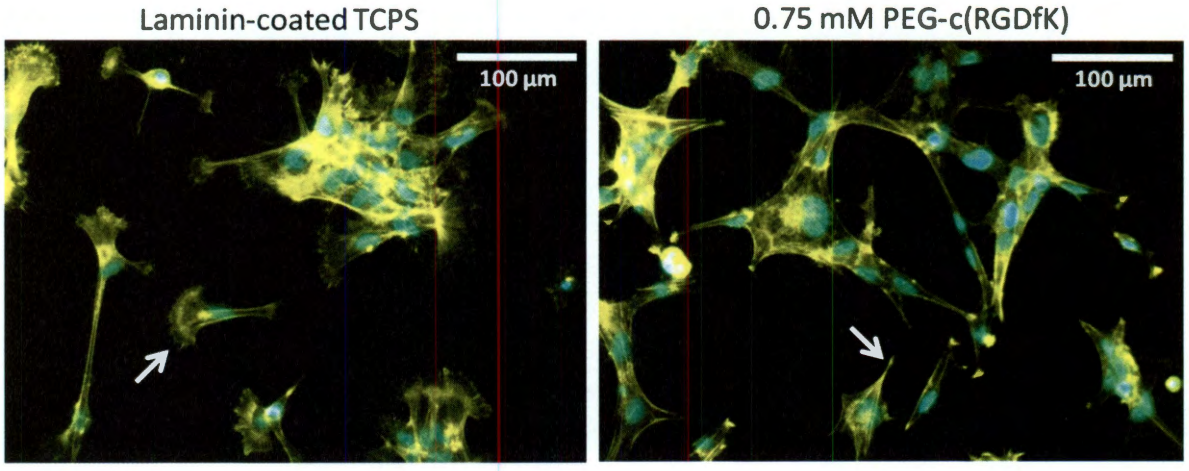

Figure 21. Representative images of cells spreading on laminin-coated TCPS or c(RGDfK) hydrogels that have been stained with DAPI (blue, nucleus) and phalloidin (false-colored yellow, actin). White arrow highlights the difference in the spread morphology observed between the two surfaces.

An additional evaluation of cell response to the low range of c(RGDfK) concentrations (Figure 22) found that cell adhesion to the hydrogel begins to drop at a ligand concentration of 0.03 mM, however cell spreading was not affected until a concentration of 0.003 mM was reached.

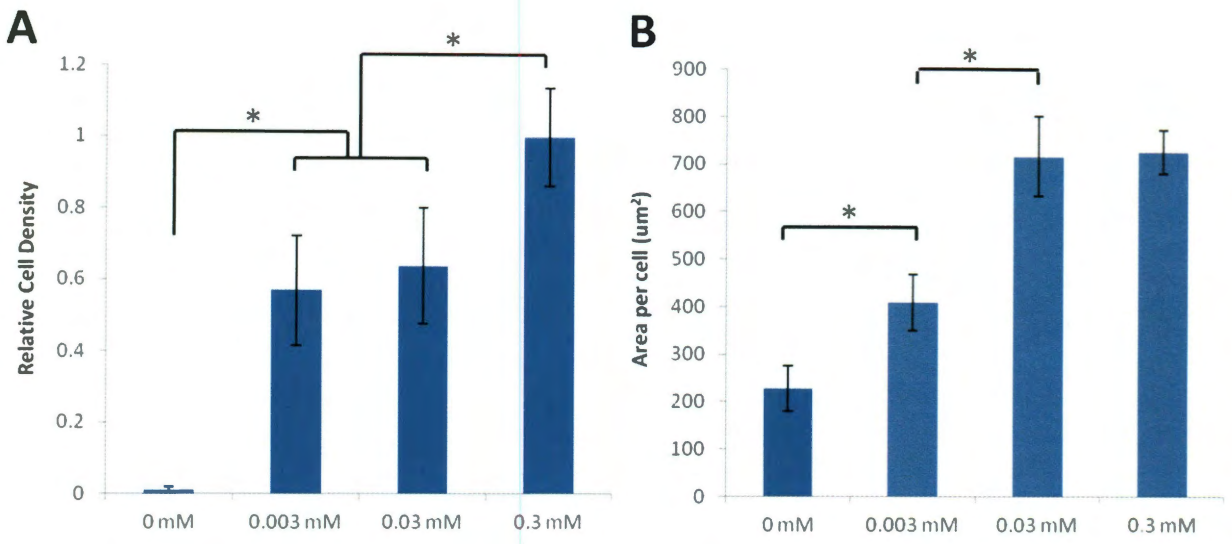

Figure 22. Quantification of NSC adhesion (A) and spreading (B) on hydrogels modified with a lower range of PEG-c(RGDfK) concentrations. Cell adhesion is significantly decreased when the peptide concentration drops from 0.3 to 0.03 mM while cell spreading is not impacted until a concentration of 0.003 mM PEG-c(RGDfK) is reached. * $p < 0.05$ for the noted comparisons

Since it has been shown in the literature that too much adhesive ligand can negatively impact cell response in some cases[70], the minimum effective concentration of PEG-c(RGDfK), or 0.3 mM, was chosen for subsequent experiments. Based on these results, the cyclic-RGDfK peptide was found to be over 1000-fold more effective at promoting neural stem cell adhesion compared to linear RGDS. Previous reports in the literature have found that the cyclic form of RGD-containing peptides were 20 to 100 times more effective as an inhibitor of cell adhesion than their linear counterparts when in solution.[95,96] It has additionally been reported that an immobilized cyclic RGD has even higher affinity for the integrin receptors than its soluble form.[97] Such a dramatic improvement in cell adhesion and spreading as shown here, however, has not been previously observed.

Both RGDS and c(RGDfK) are known to be able to bind $\alpha_v\beta_3$ and $\alpha_5\beta_1$ integrin pairs, however the cyclic peptide is reported to have a higher specificity for $\alpha_v\beta_3$.[96,98,99] A final study was performed

to attempt to identify if one of the two integrin pairs plays a larger role in promoting CTX0E03 interaction with the c(RGDfK)-modified hydrogel surface. As shown in Figure 23, neural stem cell adhesion was significantly impacted when cells were incubated with blocking antibodies against either the $\alpha_v\beta_3$ integrin pair or the β_1 integrin subunit prior to seeding. Only the β_1 integrin blocking antibody, however, caused a significant decrease in cell spreading compared to a positive control. From this data one can conclude that both sets of integrins were utilized by the NSCs when binding to synthetic substrate. It is recommended for future studies that a more comprehensive evaluation of the possible integrins involved be conducted.

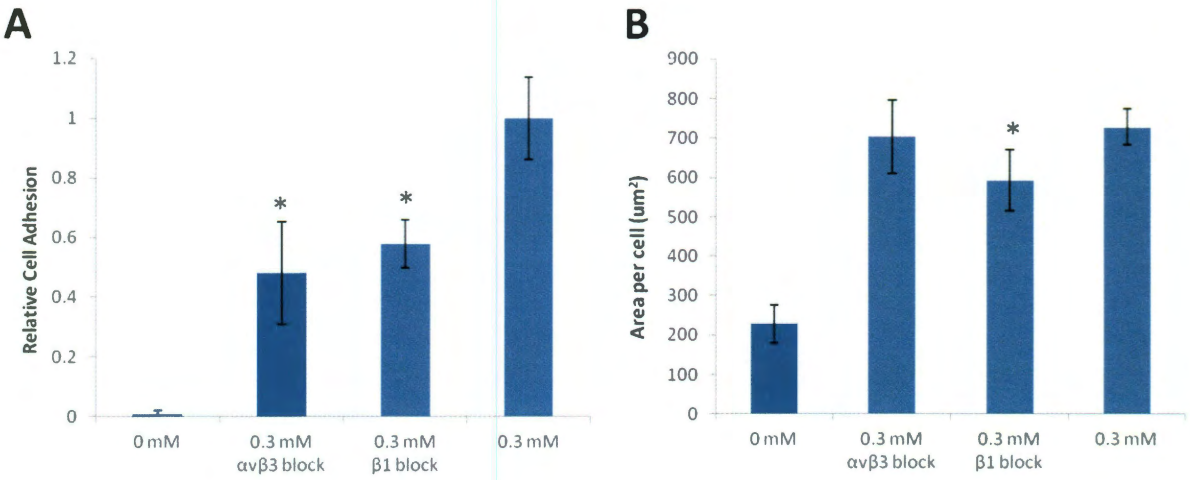

Figure 23. Quantification of NSC adhesion (A) and spreading (B) on 0.3 mM PEG-c(RGDfK)-modified hydrogels after incubation with blocking antibodies against $\alpha_v\beta_3$ or β_1 integrins. Both blocking antibodies caused significant decrease in cell adhesion to the hydrogel surface, however only the β_1 blocking antibody caused a measurable decrease in cell spreading. * $p < 0.05$ compared to control without blocking antibody

2.4.4 Expansion of NSCs on Hydrogel Substrates

The optimal hydrogel composition containing 0.3 mM PEG-c(RGDfK) was next evaluated with the neural stem cells under proliferative conditions to determine if the synthetic matrix can support expansion of the cell line *in vitro*.

Proliferation Analysis: To determine if the growth rate of the cells varied between laminin-coated TCPS and the c(RGDfK)-presenting hydrogel surface, cells were seeded on both substrates and cell number quantified at multiple time points with the fluorescent-based CyQuant Assay. Fluorescence intensity from the CyQuant reagent was linearly proportional to the cell count (standard curve not shown), allowing accurate quantification of the cell number at each time point. Analysis of cell proliferation (Figure 24)found that the laminin-coated TCPS and c(RGDfK) hydrogel permitted an equivalent rate of cell expansion with a calculated doubling time of approximately 42 h by exponential regression fit.[100] This measured population doubling time was in perfect agreement with the published value of 36 to 48 h for the CTX0E03 cell line.[80]

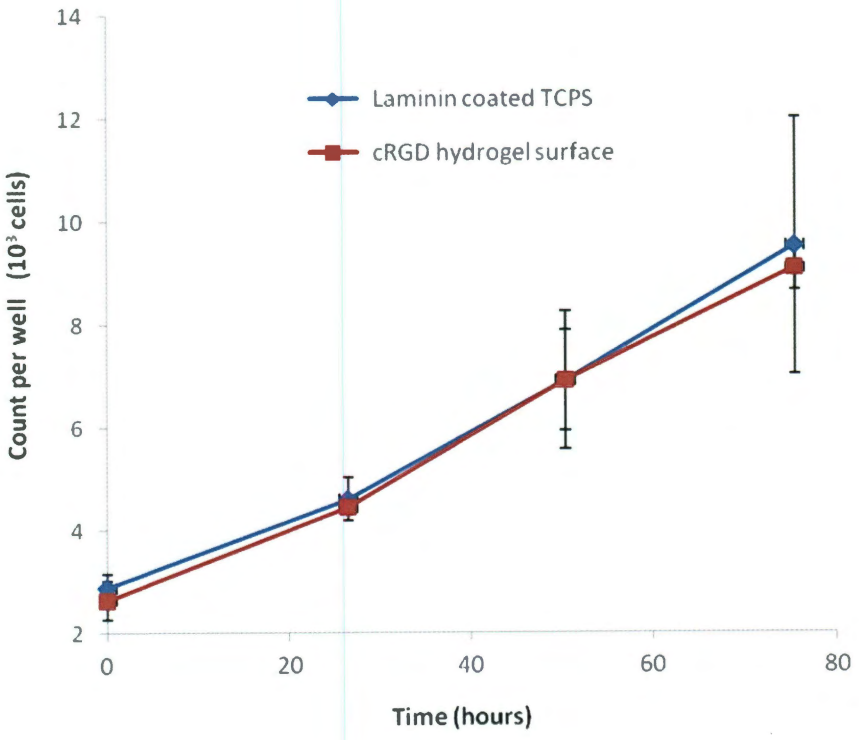

Figure 24. Analysis of NSC proliferation using the CyQuant Proliferation Assay. Comparison of CTX0E03 cell proliferation between laminin-coated TCPS and the PEG-c(RGDfK) hydrogels showed both surfaces support an equivalent rate of cell proliferation with a calculated doubling time of approximately 42 h.

An alternative method for characterization of cell proliferation is to stain for markers of actively dividing cells. The Ki-67 antigen is commonly used via immunostaining to label the nuclei of non-quiescent cells. It was thus used in this work to compare the proliferative phenotype between the hydrogel and TCPS culture surface. CTX0E03 cells cultured on laminin-coated TCPS or PEG-c(RGDfK) hydrogels were stained for DAPI and the Ki-67 marker and analyzed with ImageJ software as shown in Figure 25. Quantification of the percent of Ki-67 positive nuclei is shown in

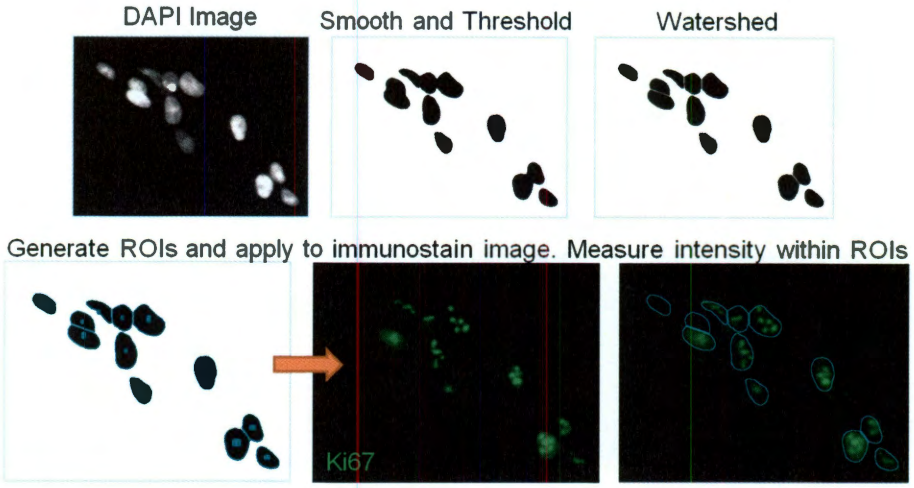

Figure 25. Process flow demonstrating the method developed to evaluate the percent of Ki-67 positive cells using ImageJ software. Stain intensity was measured within regions of interest (ROIs) defined by DAPI positive nuclei.

Figure 26 along with representative images of the labeled cells on the two substrates. Briefly, cell nuclei were defined by the DAPI signal and used to generate regions of interest (ROIs). These ROIs were applied to the corresponding Ki-67 image and used to measure the fluorescence intensity. A cutoff value for identification of positive cells was chosen as twice the measured background fluorescence. As with the proliferation curve, no significant difference was observed for CTX0E03 cells cultured on laminin-coated TCPS vs. the bioactive hydrogel. This further indicates that the hydrogel provides an equivalent surface for the expansion of the neural stem cell line.

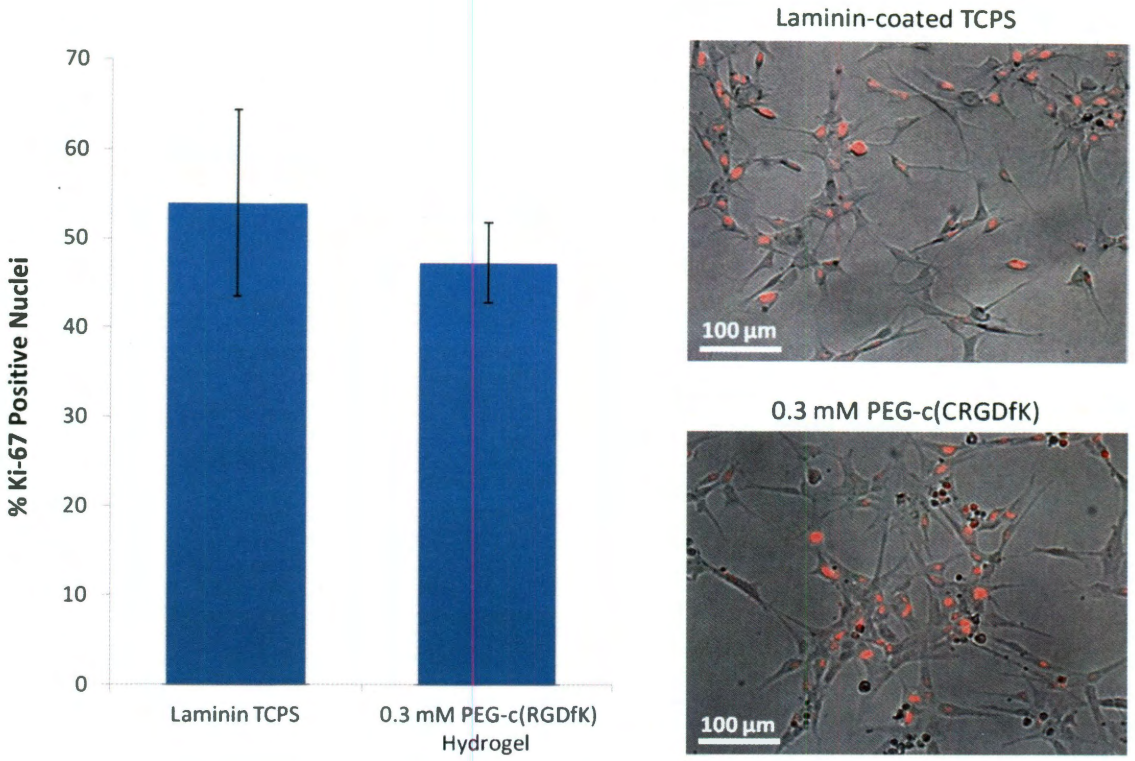

Figure 26. Quantification of Ki-67 immunostaining and representative images of CTX0E03 cells on laminin-coated TCPS or the c(RGDfK) modified hydrogel surface with Ki-67 positive nuclei labeled in red. No significant difference in Ki-67 expression was observed between the two culture surfaces for $p < 0.05$.

Maintenance of Undifferentiated Phenotype: In addition to assessing the rate of proliferation, it is important to confirm that the expanding cell population maintains the proper undifferentiated phenotype when cultured on the hydrogel surface. This parameter was assessed by immunostaining for two conserved markers of undifferentiated NSCs: the transcription factor, SOX2, and the intermediary filament, nestin.[12] ImageJ software was used to analyze the stained cell cultures on both laminin-coated TCPS and the c(RGDfK) hydrogel in a similar technique as for Ki-67 quantification. In Figure 27, representative images of the cultured cells as well as quantified marker expression are presented. One can see from this data that on both substrates approximately 95% of the cells were positive for SOX2 and similarly 95% were nestin positive. No significant difference was observed for marker expression between the two

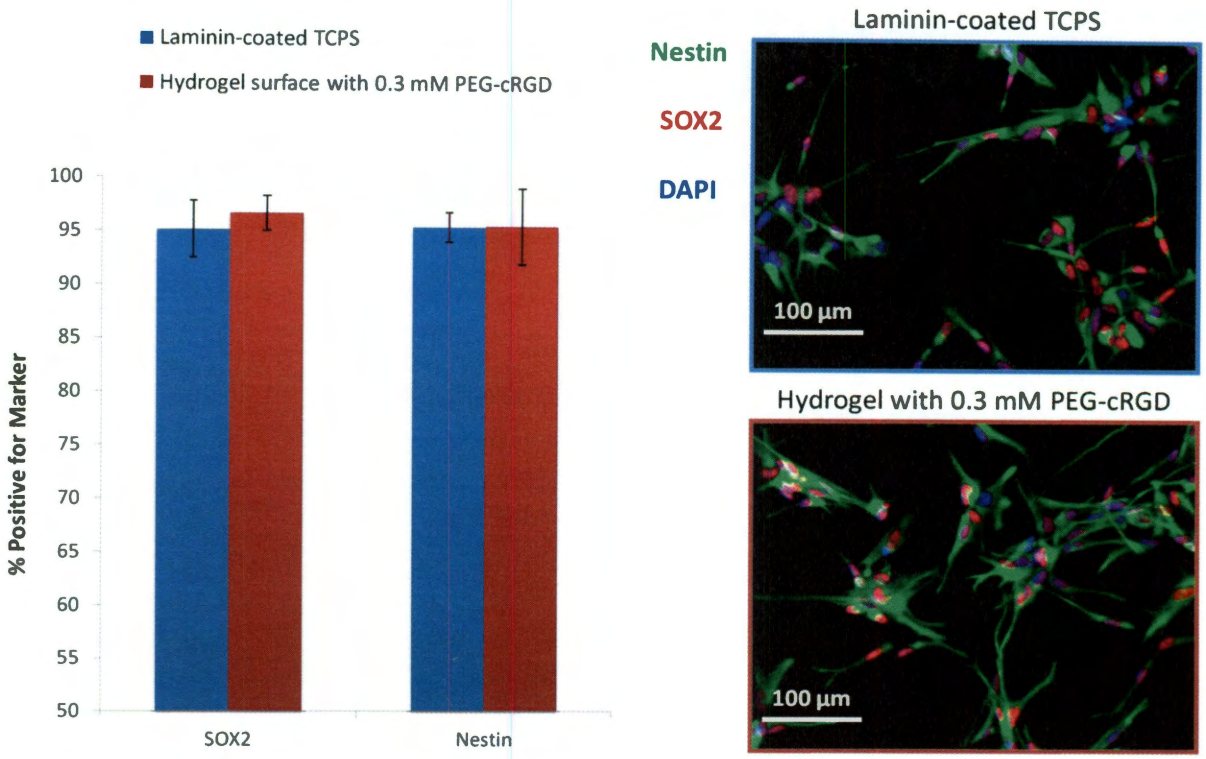

Figure 27. Quantification of NSC marker expression and representative images of CTX0E03 cells cultured on laminin-coated TCPS vs. PEG-c(RGDfK) modified hydrogels. No significant difference in expression of SOX2 or nestin was observed indicating that the proper NSC phenotype is maintained for the cells on either surface for $p < 0.05$.

culture substrates confirming that the hydrogel material does not promote differentiation of the neural stem cells and is therefore a suitable material for the study of NSC behavior *in vitro*.

2.4.5 Hydrogel Substrate for the Study of NSC Differentiation

The ultimate goal of the synthetic scaffold is to provide a platform on which to investigate factors that regulate NSC behavior and fate specification. It has been shown above that the hydrogel can support undifferentiated neural stem cell expansion. The next objective is therefore to show that the material preserves the differentiation potential of the CTX0E03 cell line by supporting development of both neuronal and glial lineages. The human NSC line used in this work has been conditionally immortalized such that cells will divide indefinitely in the

presence of FGF, EGF, and the synthetic drug, 4-OHT. Withdrawal of these components from the media is reported to trigger spontaneous differentiation along glial and neuronal lineages.[80] These lineages can be identified by specific markers such as the neuron-specific cytoskeletal component class III β tubulin or the astrocyte-specific glial fibrilliary acidic protein (GFAP). It has been previously published and subsequently confirmed here that the cell line will differentiate along both expected lineages when cultured for a period of 2 weeks on the laminin-coated TCPS surface.[80] Figure 28 shows a low (A) and high (B) magnification view of the typical differentiated phenotype at this 2 week time point. The cells were observed to become elongated and extend multiple long projections that formed a tightly interwoven mesh across the surface of the substrate. The majority of cells were found to express the glial, GFAP marker, while βIII Tubulin positive cells were more sporadic or found in clusters at sites of high cell density as depicted by DAPI staining. CTX0E03 cells, which were similarly cultured for 2 weeks in differentiating media on the surface of the PEG-c(RGDfK) hydrogels, are shown in low (A) and high (B) magnification in Figure 29. It was noted that the overall morphology and marker expression is highly reminiscent of the laminin-coated TCPS cultured cells. Again sporadic neuronal populations were found at regions of high cell density and were surrounded by a meshwork of interwoven GFAP positive cellular processes. It was not possible to accurately quantify the differentiated lineages from these immunostained samples due to the high cell density and the development of the dense, interwoven network. It can be concluded, however, that the c(RGDfK) modified hydrogel provided a suitable substrate for the support of CTX0E03 differentiation in a similar capacity as the traditional, laminin-coated TCPS substrate. For all of these studies a 10% by weight PEGDA hydrogel with 0.3 mM PEG-c(RGDfK) was used, however one distinct advantage that this system provides over TCPS is the ability to test a wide range of substrate stiffness and ligand density.

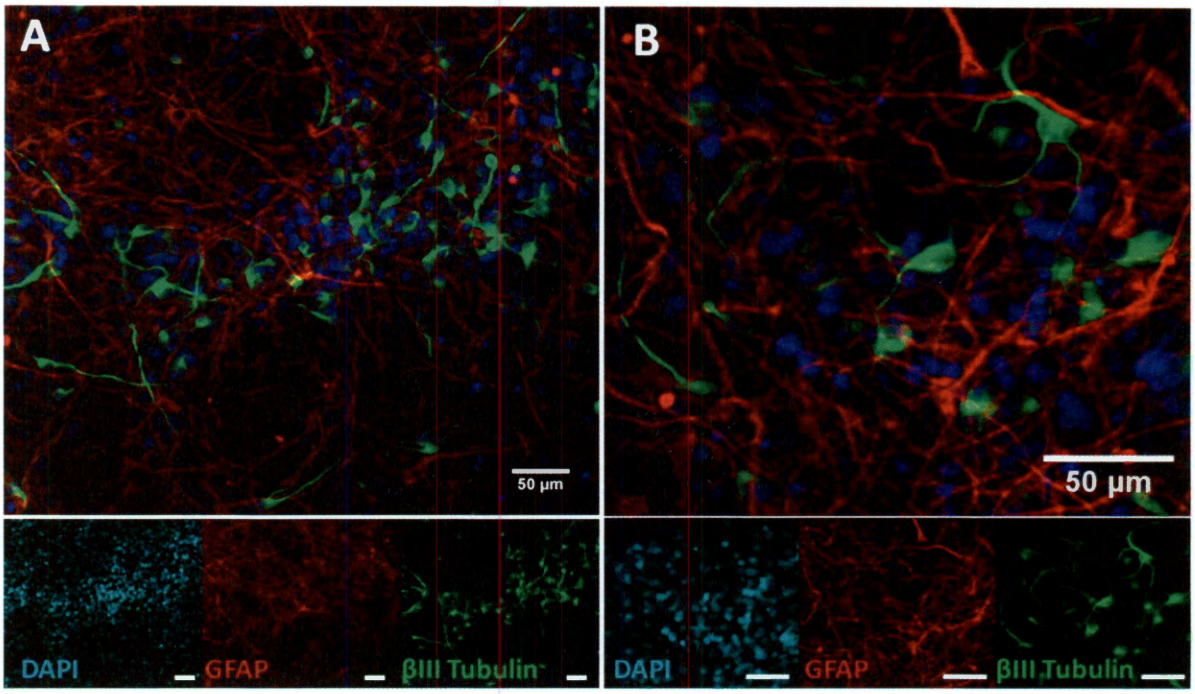

Figure 28. CTX0E03 differentiation on laminin-coated TCPS: βIII Tubulin positive neuronal cells and GFAP positive glial committed cells are identified after 2 weeks culture in differentiating media. Low (180X, A) and high (340X, B) magnification views are presented.

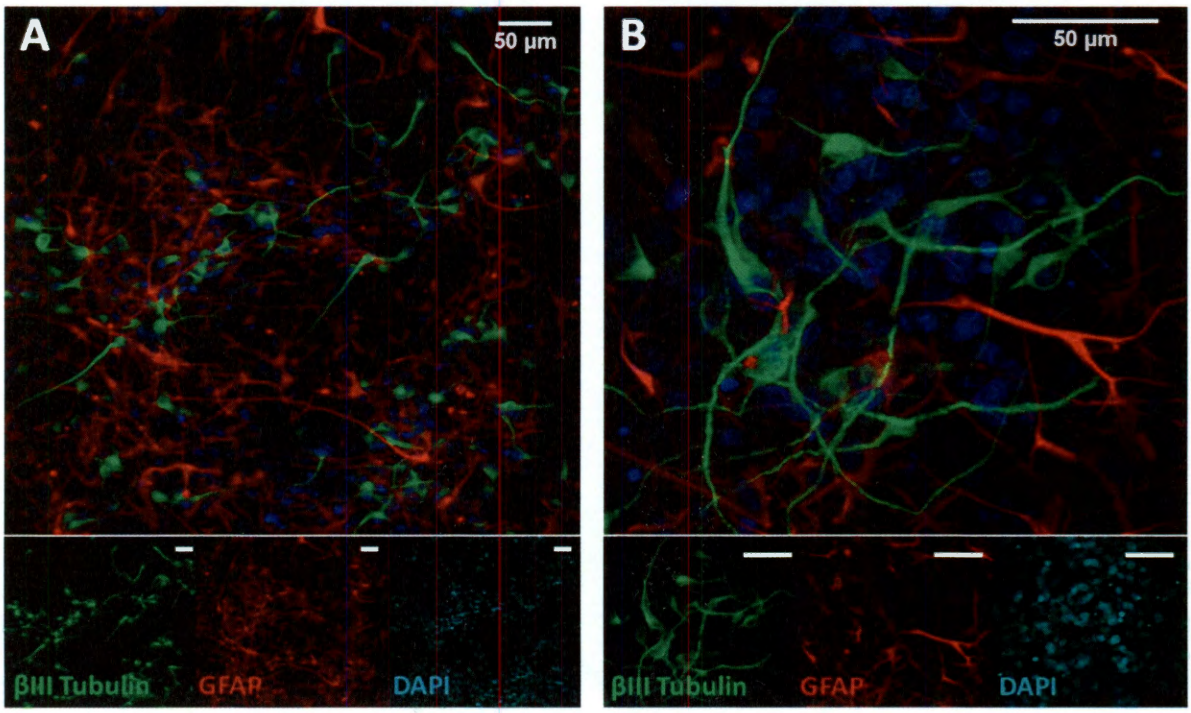

Figure 29. CTX0E03 differentiation on c(RGDfK) modified hydrogels: βIII Tubulin positive neuronal cells and GFAP positive glial committed cells are observed after 2 weeks culture in differentiating media on the synthetic matrix. Low (160X, A) and high (380X, B) magnification views are presented.

2.4.6 Analysis of Encapsulated Cell Viability

Another distinct advantage of the bioactive hydrogel scaffold presented here over typical culture substrates is its ability to support 3 dimensional encapsulation and culture of the neural stem cells. *In vivo*, these cells reside in a complex 3D environment surrounded by a framework of extracellular matrix and supporting cell types. For the first step in recapitulating this microenvironment in the hydrogel, sensitivity of the CTX0E03 cell line to the microencapsulation conditions was evaluated. Specifically, the effect of the photoinitiator alone was compared to photoinitiated encapsulation in the PEGDA hydrogel for a range of light exposure times between 35 s and 1 min. These exposure times are relevant, as it was shown above that hydrogels were not fully crosslinked after only a 35 s exposure, thus causing diffusion of uncrosslinked ligand (represented by WRGDS) and depletion of adhesive sites from the matrix over time. It was important to confirm that the preferred 1 min exposure did not negatively affect cell viability. As shown in Figure 30-A, CTX0E03 cells that were passaged and exposed to hydrogel precursor solution containing Eosin Y photoinitiator but without exposure to light retained

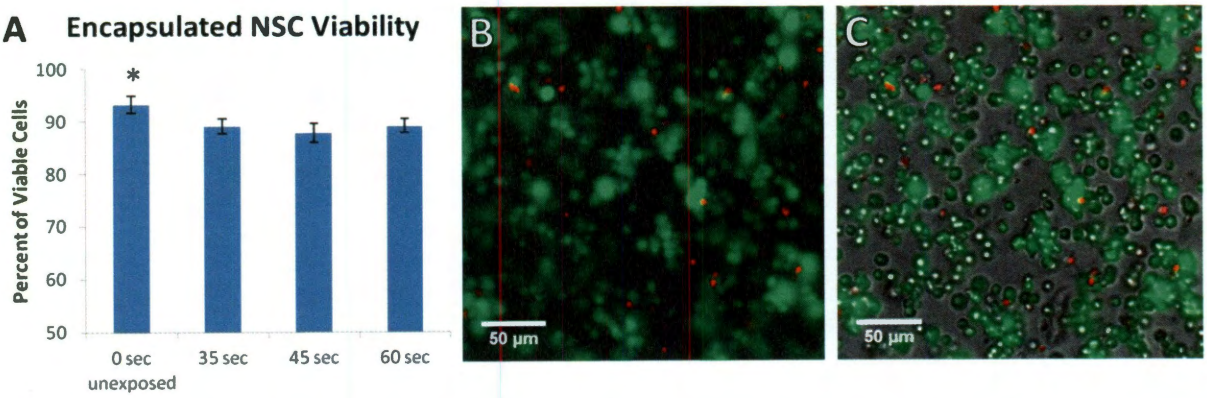

Figure 30. CTX0E03 viability analysis following encapsulation in the hydrogel matrix. A decrease in viability was observed upon encapsulation as compared to unencapsulated control, however no significant difference in viability was observed between the three exposure times tested for encapsulation (A). Fluorescent image (B) and brightfield overlay (C) shows even distribution of live (calcein AM, green) and dead (ethidium homodimer, red) CTX0E03 cells encapsulated for 1 min in the hydrogel scaffold. * $p < 0.05$ compared to encapsulated samples.

a viability of 93%. Figure 30-A shows that cell viability was slightly reduced to approximately 89% following encapsulation in the hydrogel regardless of the amount of time they were exposed to the crosslinking white light source. Representative fluorescent and brightfield overlay of live (green) and dead (red) cells in a 1 min crosslinked hydrogel is also included (Figure 30-B,C) to show the even distribution of the encapsulated cells. From this data, one can conclude that the 1 min exposure time, which provides improved hydrogel crosslinking as determined in section 2.4.2, does not cause a measurable reduction in cell viability as compared to the shorter exposure times tested here. For subsequent studies of encapsulated cells, an exposure time of 1 min was therefore used unless otherwise noted.

2.4.7 Demonstration of Three Dimensional NSC Culture

For long-term studies of encapsulated cell behavior, the hydrogel matrix must be capable of degrading to permit natural cell functions such as spreading and migration. To this end, the nondegradable PEGDA hydrogel backbone was replaced with a collagenase sensitive polymer, PEG-PQ-PEG. This material is generated with an MMP-2 and 9 sensitive peptide sequence embedded in the polymer chain allowing cell-secreted enzymes to locally degrade the crosslinked hydrogel scaffold. For all of the following encapsulated cell studies, polymer weight percent was reduced to 5% as the 10% hydrogel was observed to be too densely crosslinked to permit NSC spreading and organization (data not shown). Adhesive ligand concentration was maintained at 0.3 mM PEG-c(RGDfK).

Initial demonstration of the 3D scaffold was performed with NSCs encapsulated and cultured under growth conditions for 1 week. Immunostaining was used to evaluate cell morphology and expression of the undifferentiated NSC markers, nestin and SOX2. As shown in the following DIC image (Figure 31-A), the cells spread to form interconnected networks in the synthetic matrix.

Figure 31-B again shows the cell organization in a z-projection from a 75 µm thick confocal image stack of an immunostained sample. Although accurate quantification of marker expression was not feasible from these images, the vast majority of cells were observed to be positive for both nestin and SOX2 expression.

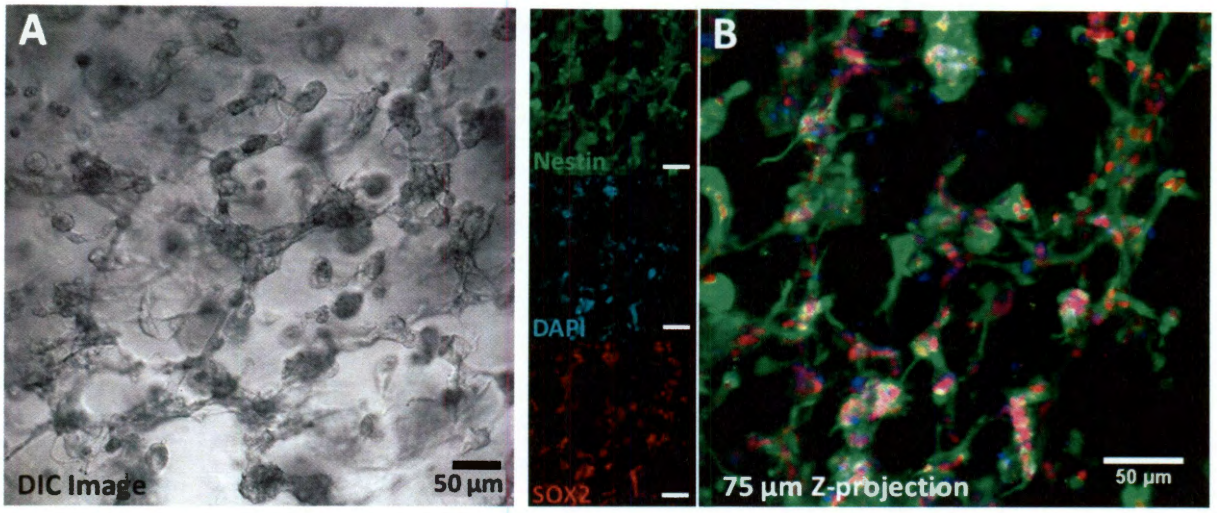

Figure 31. Encapsulated CTC0E03 cells after 7 days in culture under growth conditions. DIC image (A) shows morphology of the interconnected network of cells which has formed in the scaffold. 75 µm thick Z projection (B) shows nestin and SOX2 expression by the encapsulated cells.

The next step in demonstrating the utility of the hydrogel scaffold for 3D culture was to investigate CTX0E03 differentiation following encapsulation. Equivalent lineage markers as for surface seeded cells were used to characterize neuronal (βIII tubulin) or glial (GFAP) committed cells after 2 weeks in the hydrogel matrix. In Figure 32, low (A) and high (B) magnification z-projections allow observation of the cellular organization and marker expression. Additionally, for Figure 32-A, the z projection includes the plane of cells growing on the surface of the scaffold. These cells can be seen to form dense, island- like clusters with a relatively high proportion of βIII tubulin positive cells. These cell clusters were interconnected via a branching network of long, GFAP positive projections. Figure 32-B provides a higher magnification image

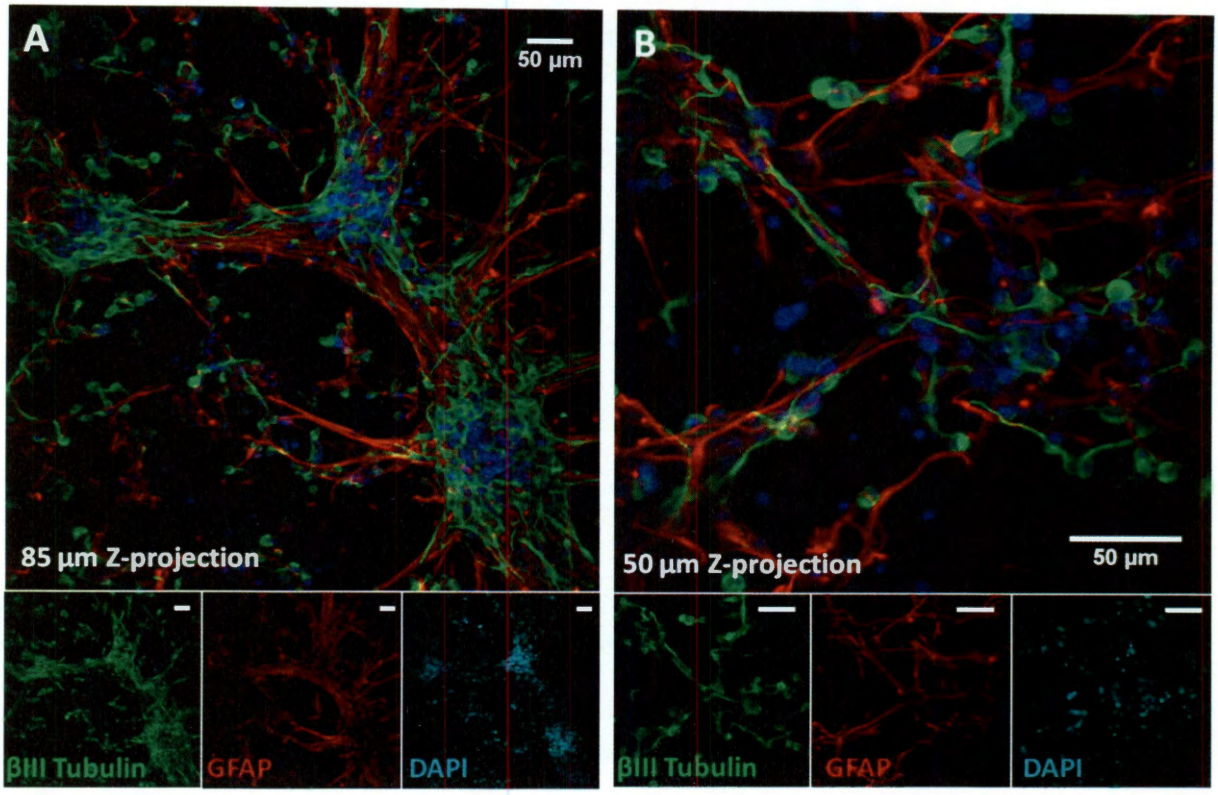

Figure 32. Immunostaining of encapsulated CTX0E03 cells showing neuronal (BIII Tubulin, green) and glial (GFAP, red) differentiated cells along with DAPI positive nuclei (blue). Cells were observed to form dense clusters on the surface of the gel (A) and extensive networks in the bulk of the hydrogel matrix (B).

of the cell network that formed deeper in the scaffold. Again the cells were elongated and characterized by long, thin projections. Both glial and neuronally differentiated cells were clearly distinguishable by exclusive marker expression. An additional observation is that the neuronal cells appear adjacent to and extend along the larger network of GFAP projections. A higher magnification example of this is shown in Figure 33. Although time-lapse imaging would be required to confirm, this organization suggests that the neural cells are utilizing the astrocyte network as a path for migration through the scaffold. Glial guided neuronal migration is a well-documented phenomenon both *in vivo* and *in vitro.*[101] Observation of a natural process such as this within the artificial matrix is a strong indication that the material is highly mimetic of the native ECM.

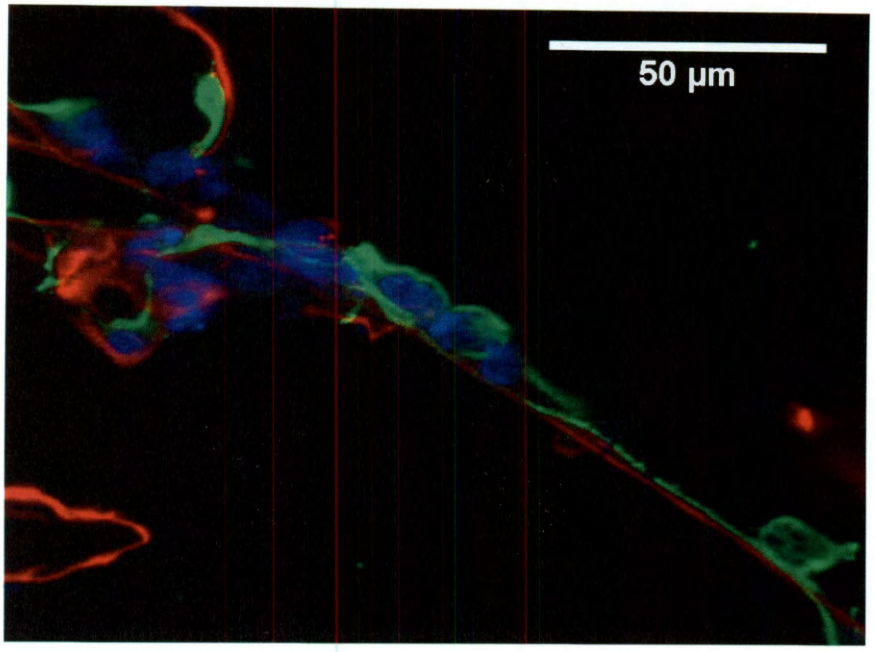

Figure 33. High magnification (700X) confocal image showing βIII tubulin positive cells (green) extending along GFAP positive projections (red) with nuclei labeled in blue.

Based on these results, the hydrogel scaffold was found to be an excellent matrix for encapsulation and *in vitro* study of neural stem cells in a 3D microenvironment. The cells expressed appropriate markers when cultured under growth or differentiating conditions and were capable of adhering to and remodeling the matrix as evidenced by the reorganization of encapsulated cells to form complex, branching networks. Although only the PEG-c(RGDfK) adhesive ligand was demonstrated here, the degradable scaffold could potentially be modified with a wide array of bioactive components in a precise manner that is not achievable with naturally derived scaffolds. It is therefore proposed as a significant improvement over the previously reported materials investigated for 3D culture of neural stem cells.

2.4.8 Flow Cytometry for NSC Population Analysis

Immunostaining provides an excellent means to evaluate the morphology and structural organization of both surface seeded and encapsulated cells. Due to the complexity of the dense

cell networks formed by the CTX0E03 cell line in culture and especially during differentiation, however, this approach does not permit quantitative analysis of the resulting cell populations. Flow cytometry was therefore utilized in order to more rigorously characterize the resulting cell populations on laminin-coated TCPS compared the c(RGDfK)-presenting hydrogel scaffold.

CTX0E03 cells were cultured under both growth and differentiating conditions on the hydrogel and TCPS surfaces. At the final time point (1 week for growth or 2 weeks for differentiating conditions), cells were passaged and stained with fluorescently labeled primary antibodies against the same antigens used for immunocyotchemistry. Although information on the spatial organization of cell populations is lost with this technique, multi-color flow cytometry provides significant advantages in that up to six fluorescent markers, as well as forward scattering (size), and side scattering (granularity) characteristics can be evaluated simultaneously for each individual cell. Data acquired on tens of thousands of cells per sample are compiled to generate a comprehensive survey of the various cell populations.

In Figure 34 and Figure 35, representative flow cytometry scatter-plots are presented for cells cultured on laminin-coated TCPS or PEG-c(RGDfK) modified hydrogels under growth and differentiating conditions. Quad-gating of undifferentiated NSC markers was used to determine the percent of nestin and SOX2 positive cells (Q2) under growth conditions for each sample. Neuronal and glial lineage markers were defined with box gates to allow comparison of lineage specification between culture conditions for differentiated samples. It can be additionally seen that the differentiated cell populations have a distinct scatter profile as compared to undifferentiated cells. A direct comparison of the growth and differentiated samples on laminin-coated TCPS is shown in Figure 36 to highlight these differences.

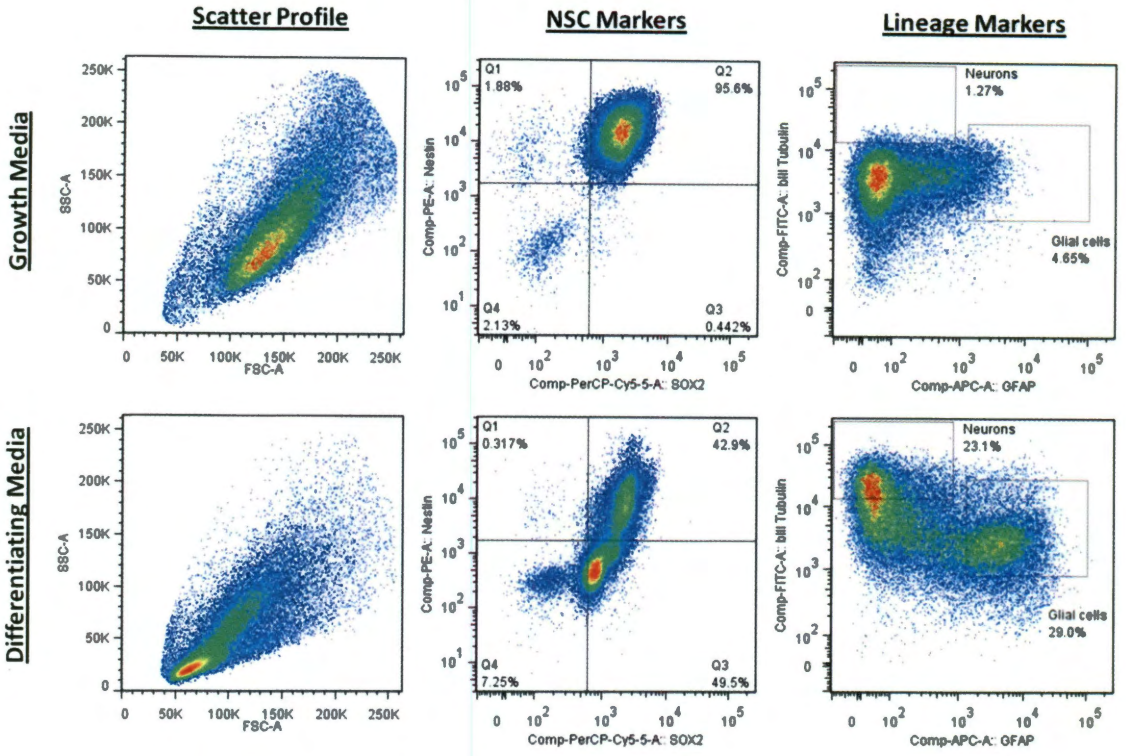

Figure 34. Representative flow cytometry results for cells cultured on laminin-coated TCPS showing scatter profile, undifferentiated marker expression, and lineage marker expression under growth and differentiating conditions. Undifferentiated cultures are largely SOX2 and nestin positive, while differentiated cultures show development of distinct GFAP and βIII tubulin-positive populations as expected.

As expected, the cells under growth conditions primarily expand as a single population with high nestin and SOX2 expression. Following 2 weeks in differentiation media, the NSC markers nestin and SOX2 become down-regulated in a portion of the population and some cells begin to up-regulate GFAP and βIII tubulin. A decrease in both forward and side scattering also indicates cells size and granularity decreases as the cells undergo differentiation. It has been reported that neurons are characterized by a distinct, low scattering profile. In order to clarify which cell populations were responsible for the changes in scattering and marker expression observed here, a direct comparison of the differentiated populations as defined by the box gates, is shown in Figure 37.

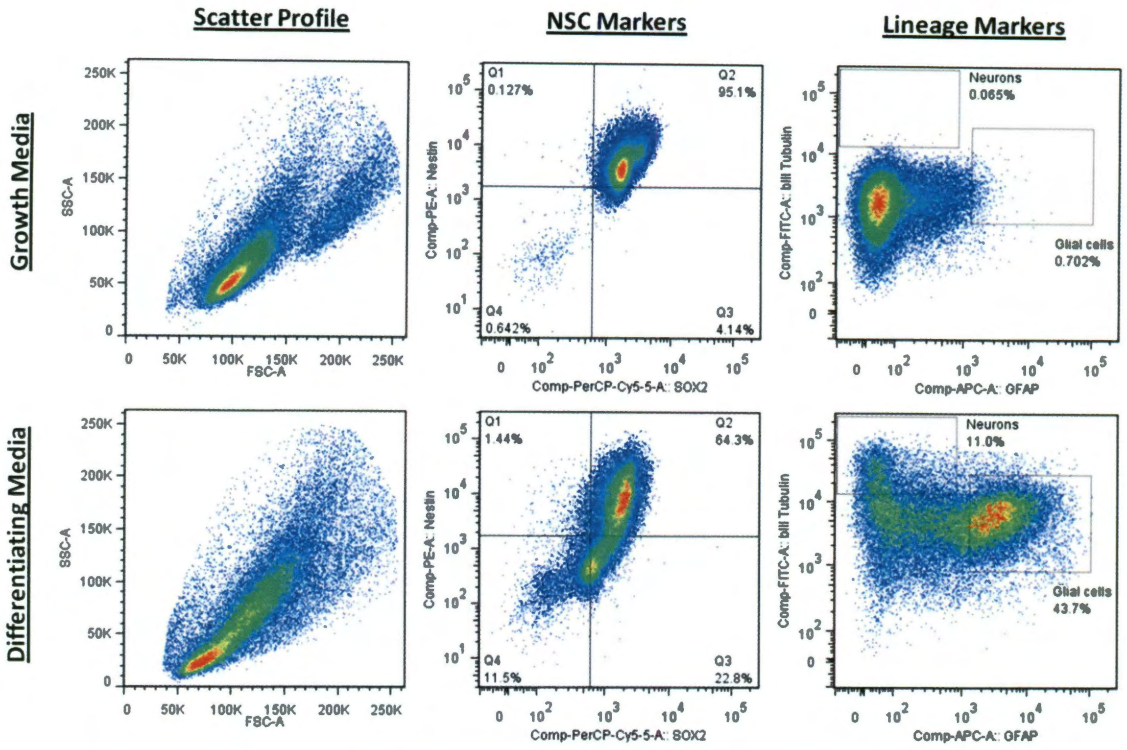

Figure 35. Representative flow cytometry results for cells cultured on PEG-c(RGDfK) modified hydrogels showing scatter profile and marker expression profiles under growth and differentiating conditions. Cells are primarily SOX2 and nestin positive under growth conditions and develop into distinct GFAP and βIII tubulin-positive populations upon differentiation.

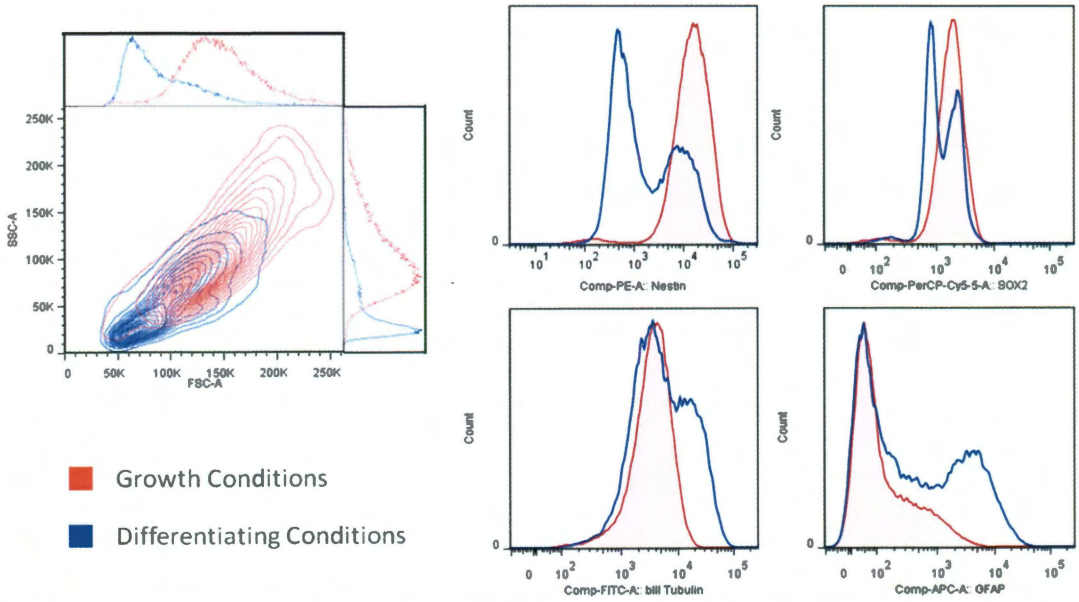

Figure 36. Comparison of growth and differentiated cultures on laminin-coated TCPS. Histogram overlays show decreasing nestin and SOX2 expression and increasing bIII Tubulin and GFAP expression upon differentiation as expected. Differentiated cultures also exhibit decreased forward and side scattering.

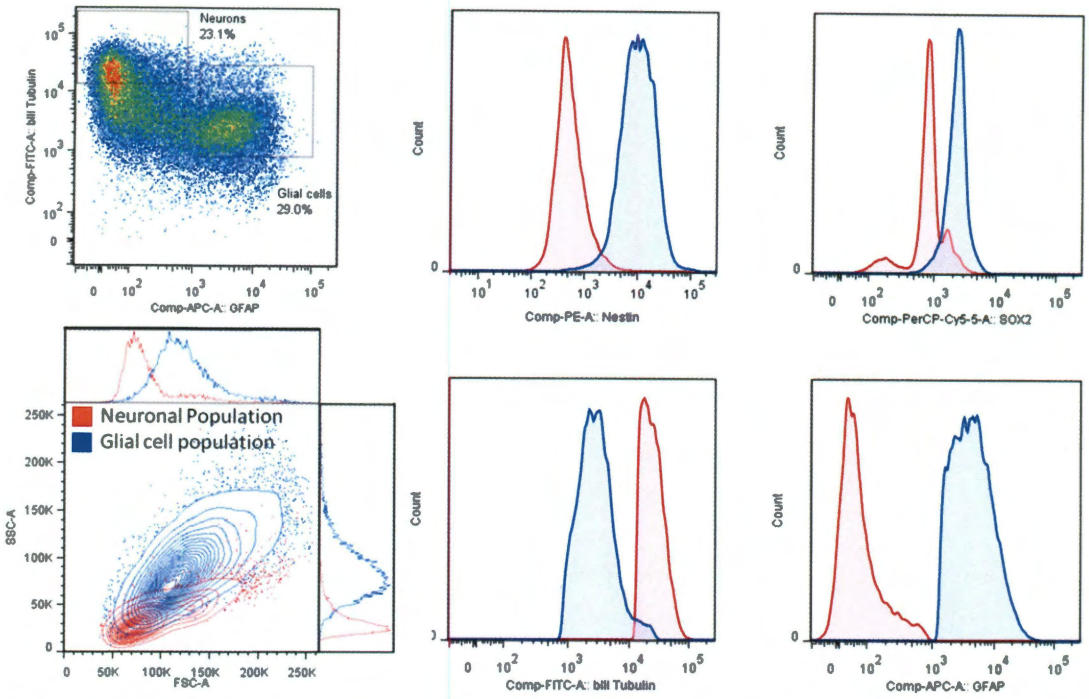

Figure 37. Comparison of neuronal and glial populations as gated from CTX0E03 cells differentiated for 2 weeks on laminin-coated TCPS. Neuronal cells show decreased forward and side scattering as well as a decrease in SOX2 and nestin expression compared to the glial population defined here.

Comparison of the neuronal and glial populations derived from CTX0E03 cells differentiated on laminin-coated TCPS confirms the development of distinct scattering populations. Specifically, neuronal cells were observed to have very low side scattering and forward scattering behavior as compared to the glial differentiated cells. It was also observed from this comparison that the two populations show significant differences in nestin and SOX2 expression, with neurons down-regulating these markers as compared to the GFAP-positive glial cells. This data indicates that the neuronal population may be more terminally differentiated after 2 weeks than the glial population. It is recommended for future studies that longer time points be evaluated to observe if the glial population will similarly turn off these NSC markers.

Quantification of the flow cytometry data between the hydrogel and TCPS culture conditions is shown in Figure 38. In agreement with immunocytochemical analysis, approximately 95% of

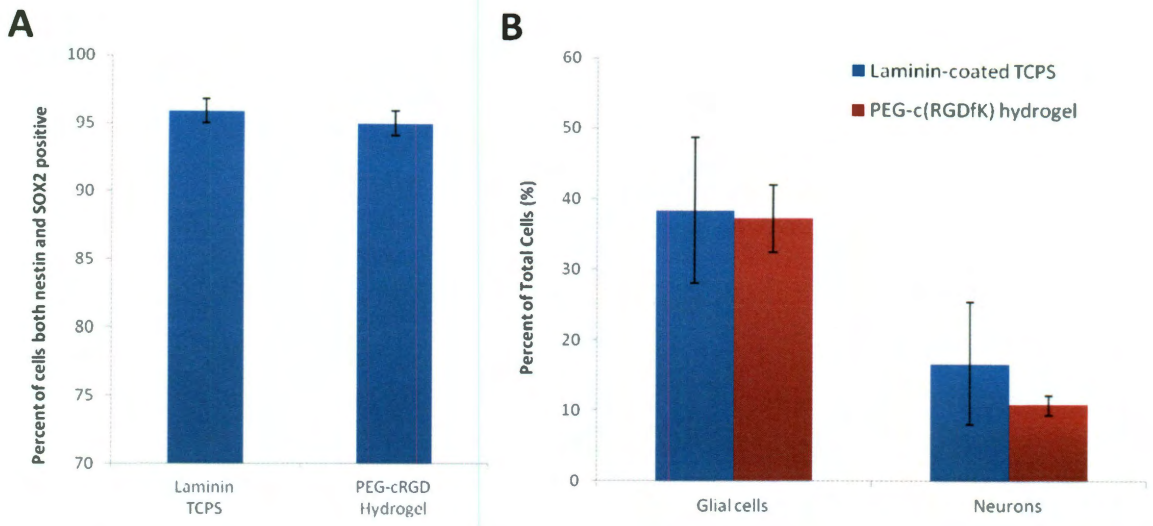

Figure 38. Flow cytometry analysis of cells cultured on laminin-coated TCPS vs. the PEG-c(RGDfK) modified hydrogel matrix. Under growth conditions (A), approximately 95% of cells were found to be both nestin and SOX2 positive for both substrates. Differentiation was not found to be significantly different between the two culture materials (B) with approximately 37% of cells following a glial fate and 10 to 15% of cells following a neuronal fate. $p < 0.05$

the cells cultured in growth media on either substrate were found to be positive for the undifferentiated NSC markers, SOX2 and nestin. Assessment of the differentiated cultures found that with the gated populations as defined here, approximately 37% of the differentiated cells have committed to a glial lineage, while between 11 and 17% of cells have committed to a neuronal fate. No significant difference was observed between cells differentiated on the laminin-coated TCPS vs. the PEG-c(RGDfK) hydrogel. It can therefore be concluded that the hydrogel material with 0.3 mM c(RGDfK) can provide an equivalent substrate for the growth and differentiation of the CTX0E03 cell line.

In addition to the surface seeded cultures, flow cytometry analysis was similarly used to characterize the encapsulated cell populations. However, due to limitations on the size of the encapsulated cell cultures as well as poor cell recovery following hydrogel degradation at the end of the culture period, only a single, pooled sample was able to be evaluated for growth and

differentiated conditions. The flow cytometry data presented in Figure 39 for encapsulated the populations should therefore be considered only as an example, which may not be representative of the actual cell response.

One notable characteristic of the encapsulated growth condition sample as compared to surface seeded cells was the significantly higher and more variable GFAP expression across the population. *In vivo,* the type B neural stem cells are known to express GFAP, however *in vitro* cultured neural stem cells and NSC lines rarely express this marker. Up-regulation of GFAP under encapsulated growth conditions may indicate that either that the cells were starting to undergo glial directed differentiation, or that they may have taken on a more *in vivo*-like expression

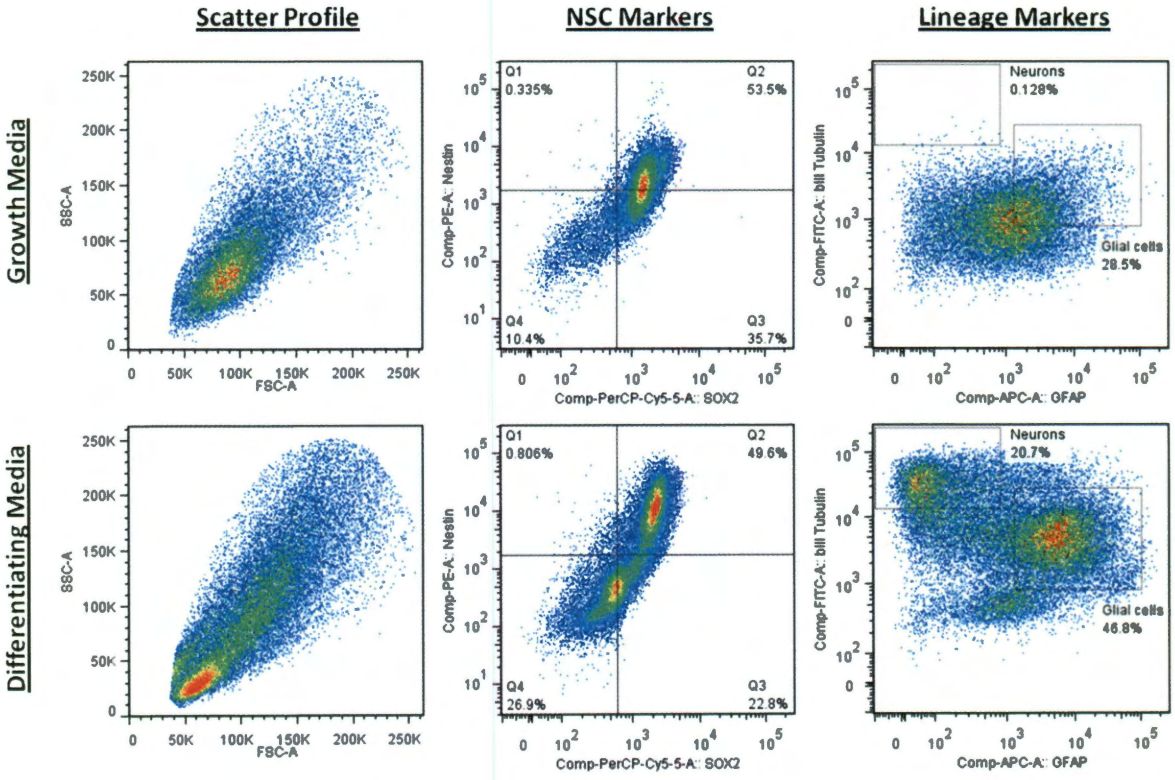

Figure 39. Flow cytometry results for cells encapsulated within c(RGDfK) modified degradable hydrogels. Scatter profile and marker expression under growth and differentiating conditions are shown. It should be noted that only a single pooled sample was evaluate for each media condition and results may not be representative.

profile. Both possibilities are intriguing and warrant further investigation with larger sample groups and additional time points. Encapsulated cells that had been differentiated for 2 weeks were found to develop into both neural and glial populations within the range found for surface seeded samples. There does appear, however to be fewer cells "in limbo" between the two possible differentiated states defined here, with over 61% of the total cell population falling into either the neuronal or glial cell gates. It is possible, as suggested from analysis of the growth condition group, that the encapsulated cells were more driven towards a differentiated state than when cultured on a 2D surface. An additional observation from the differentiated scatter plot was the presence of a third cell cluster with low βIII tubulin and intermediate GFAP expression levels. Larger sample groups and analysis of additional lineage makers would be required to identify this population; however these cells may indicate that a portion of the encapsulated culture was directed towards a third lineage, for example towards an oligodendrocyte fate.

2.5 Conclusions

This work presents the development and characterization of a synthetic hydrogel scaffold with ideal properties for probing the response of neural stem cells *in vitro*. The CTX0E03 cell line used here was generated for clinical use in humans and thus provided a relevant cell model for demonstrating the utility of the scaffold. An initial evaluation of the behavior of surface seeded cultures identified a cyclic, RGD containing peptide, c(RGDfK), as a potent mediator of cell adhesion and spreading. Further comparison of this c(RGDfK)-modified surface with the traditional culture substrate of the NSC line showed that it supported an equivalent rate of cell proliferation and maintained proper undifferentiated phenotype based on expression of recognized NSC markers.

Since the ultimate goal of neural tissue engineering is to repair or regenerate damaged neural cells and tissue, it was critical that the NSCs retained their ability to differentiate along the appropriate lineages when cultured on the artificial matrix. The multi-lineage potential of CTX0E03 cells was confirmed by immunostaining against conserved markers of the committed neuronal and glial lineages following a two week differentiation period. It was demonstrated that both surfaces maintained NSC potential and permitted development of the expected differentiated cell types. In addition, the apparent morphology and organization of the cells following differentiation was indistinguishable between the two culture surfaces. Finally, flow cytometry was presented here as a powerful tool for quantitative analysis and comparison of the resulting cell populations across all substrates and culture conditions.

Ultimately, a key benefit of the bioactive hydrogel scaffold over traditional substrates such as TCPS is its ability to support encapsulated culture of the cells. Growth and differentiating culture conditions were similarly evaluated with CTX0E03 cells encapsulated in the bulk of degradable hydrogel scaffolds. It was confirmed that the material maintained appropriate NSC marker expression under permissive conditions, and that the material supported the development of both neuronal and glial lineages following growth factor withdrawal. Furthermore, both culture conditions were observed to develop into extensive, three dimensional cell networks indicating cell-mediated degradation and remodeling of the scaffold has occurred.

It is well accepted that cell behavior can be markedly different in a three dimensional environment as opposed to two dimensional culture. When embedded in the hydrogel matrix, the neural stem cells are provided with a more natural microenvironment that is reminiscent of the NSC niche. It is subsequently hypothesized that the behavior of 3D cultures will be more representative of true neural stem cells *in vivo.*

Only a single adhesive and degradable peptide sequence was fully investigated here, however the hydrogel scaffold presents a versatile environment in which any number of bioactive signals could be incorporated. Future studies could additionally make use of the light-based tethering of signaling molecules to generate 2D or 3D patterned substrates for investigation with the cells. Spatially controlled ligand presentation may, for example, be utilized to generate microenvironments within the scaffold with distinct patterns of laminin and fibronectin availability that mimic the organization in the niche. In all it is proposed that the synthetic hydrogel matrix will be a valuable tool for future investigations of neural stem cell behavior and the pathways that regulate NSC fate.

3 Immobilized Growth Factors for Spatial Control of NSC Behavior

3.1 Introduction

3.1.1 Soluble Signals in NSC Regulation and Lineage Determination

Many components of the neural stem cell niche, such as the vasculature and the specialized basal lamina, are likely to impose their effect on the NSC through soluble signals.[48,74] Two growth factors in particular, epidermal growth factor (EGF) and FGF-2, are now considered standard components of isolation and expansion protocols for NSCs.[3,6,13,102,103] These well-known mitogens both promote the proliferation of NSCs, and in addition FGF-2 maintains neurogenic potential.[3,13,72] As mentioned above, the fractones maintain a unique affinity for the neurogenic mitogen, FGF-2.[74] One experiment in which labeled FGF-2 was introduced into the ventricles showed that the bulbs of the fractones were even able to sequester the growth factor from the cerebral spinal fluid (CSF).[74] Fractones positive for N-sulfate heparin sulfate proteoglycan showed the greatest FGF-2 binding and were associated with a higher number of proliferating NSCs.[74]

Besides these two mitogens, a large number of factors have now been characterized for their effects on NSCs. Figure 40 reviews the primary downstream effects for a number of these soluble and bound signaling interactions in the context of neural stem cell fate.[11] In addition to FGF, several other soluble signals associated with the vasculature are included in the diagram and have been shown to influence stem cell behavior *in vitro* and in the *in vivo* niche.[6,45,48,72,104] These include Leukemia inhibitory factor (LIF), platelet derived growth factor (PDGF), and vascular endothelial growth factor (VEGF).[6,48,102,104] Longer range signaling may occur via neurotransmitter release from axons that extend into the niche from other regions of the

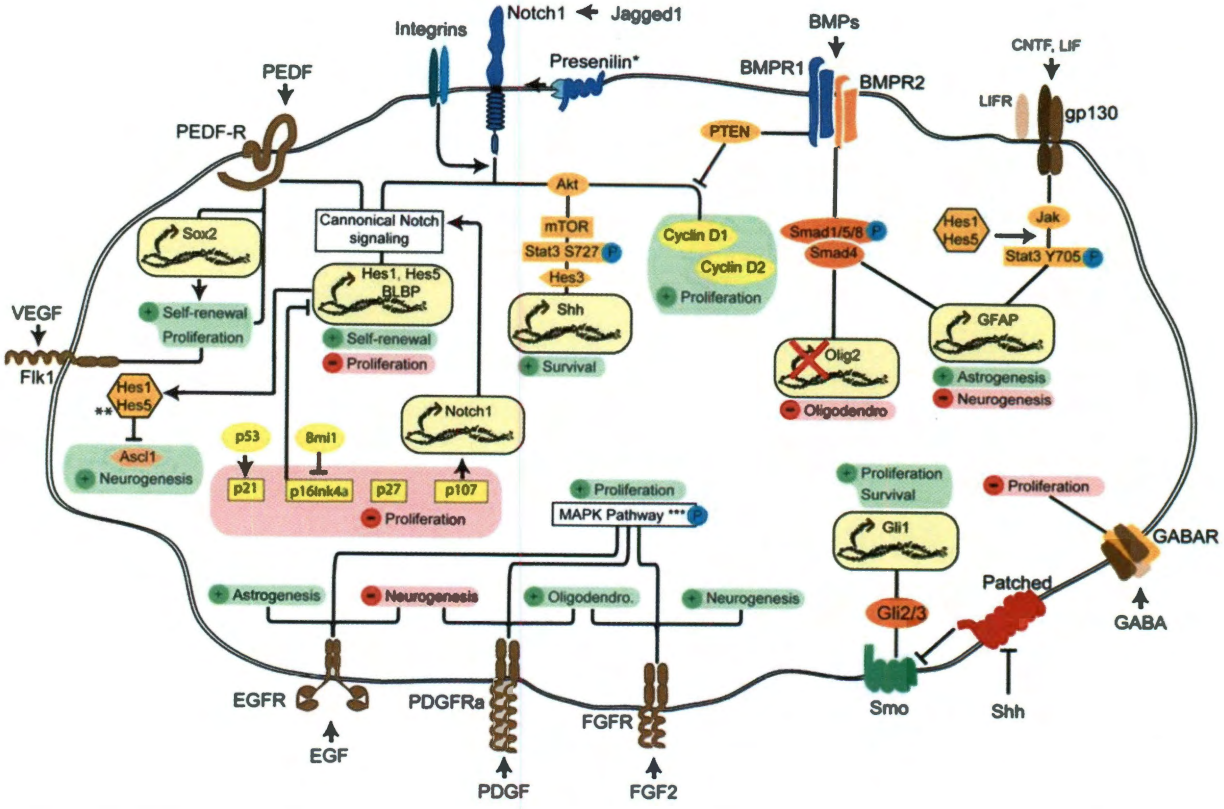

Figure 40. Diagram of the various signaling inputs and their influence on neural stem cell fate.[11] Soluble and insoluble signals from the extracellular microenvironment can interact to result in a variety of downstream cell responses. Green highlighted text indicates up-regulation, while red highlighted text indicates down-regulation of the specified cell response. Figure from Basak et al. 2009.

brain.[48,72] The neurotransmitter, GABA, for example, has been shown to promote neuronal differentiation and maturation, contrary to its typical inhibitory action outside the niche.[48] Although missing from this diagram, NGF or nerve growth factor is another well studied regulator of cell behavior within the central nervous system.[105] Previous investigations have shown that neurosphere-forming cells express NGF receptors.[105] This factor has been found to promote neural differentiation of precursor cells, encourage maturation of neurons, and also induce a neuroprotective effect *in vivo*.[105] Its effect on the primitive neural stem cell, however, is not yet fully understood. One complication in the study of many of these growth factors is that the response of stem cells can vary widely based on other biochemical components in the

microenvironment, previous mitogen exposure, and the developmental stage from which they were originally harvested (e.g. embryonic vs. adult).[16,20] Providing a defined system to investigate the factors that govern NSC fate and especially neurogenic differentiation would help to unravel these regulatory pathways and may ultimately lead to the development of an improved cell therapy.[3,16]

For this work, two contrasting growth factors were chosen for investigation within the synthetic scaffold. To demonstrate control of stem cell proliferation, CTX0E03 response to FGF was evaluated with the growth factor presented both in solution as well as tethered to a hydrogel substrate. To demonstrate control of neuronal differentiation, NGF was similarly evaluated in solution and tethered to the matrix for its ability to promote neurite extension by the model, PC-12 progenitor line.

3.1.2 Strategies for Growth Factor Immobilization

A variety of methods have been developed for immobilization of whole proteins. For temporary applications, a non-covalent approach may be appropriate. Some examples include physical entrapment, simple adsorption of the protein to a substrate, binding of a His_6-tagged protein to chelated Nickel ions, or specific binding of the protein by immobilized antibodies.[106] These non-covalent methods, however, may be susceptible to disruption by environmental factors such as pH, salt concentration, and displacement by other proteins in solution. As such, they provide limited utility under conditions suitable for long term cell culture and were not considered for this work.

Covalent tethering approaches can be generally categorized by the functional group targeted for coupling. Nucleophiles such as a thiols (cysteine residues) and primary amines (lysine residues and the amino terminus) are common targets. Although thiol linkage can be achieved with the

Michael's reaction (Figure 41-B), naturally occurring cysteine residues are often inaccessible or located within the active site of the protein leading to disrupted activity after bioconjugation.[62,106,107] Deliberate modification of the protein sequence to include an additional cysteine residue specifically for the purpose of conjugation is one possible solution, but this approach can be considerably time consuming. A much more convenient and rapid technique involves the reaction of a succinimide group with the primary amines on a protein (Figure 41-A). Maintaining the pH of this reaction at 8.5 allows specificity for primary amines over other nucleophilic groups which may be present. Primary amines can be found at the amino terminus as well as on lysine residues and frequently may be located on the solvent accessible surface of a natively folded protein. Additionally, succinimide to amine chemistry is well established and has been widely used for the attachment of PEG chains to proteins and other biological molecules in order to increase solubility, stability, and circulation time.[61,67,68,108,109]

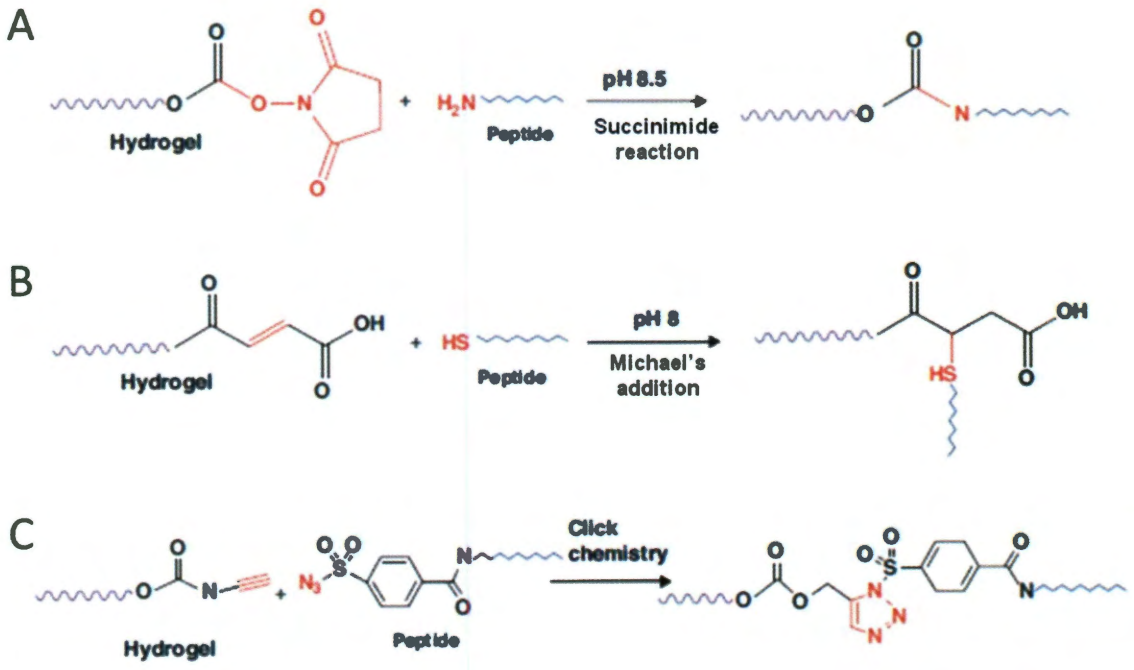

Figure 41. Commonly used reaction schemes for covalent conjugation to proteins or peptides.[107]

Immobilization of vascular endothelial growth factor, platelet derived growth factor, and fibroblast growth factor are just some examples published in the literature using this reaction scheme.[67,68,109] Another, relatively new approach for bioconjugation is referred to as "click chemistry" (Figure 41-C).[110] For this method, an azide is reacted with an alkyne to form the conjugated biomolecule.[106,111] This approach can also be adapted for site-specific conjugation. Example applications of click chemistry include surface immobilization of biotin, covalent labeling of oligonucleotides, and functionalization of the surface of viral particles. [112]

3.2 Objectives

The ability of the hydrogel system to present tethered growth factors to NSCs was demonstrated here using FGF and NGF, two proteins with well characterized effects on neural progenitor proliferation and differentiation, respectively. The proteins were first conjugated to mono-acrylate PEG linkers via succinimide chemistry and characterized for conjugation efficiency. The pegylated growth factors were then analyzed for retention of bioactivity following conjugation and finally investigated as tethered signals in the hydrogel matrix for their influence on neural progenitor behavior *in vitro*.

3.3 Materials and Methods

All materials were purchased from Sigma unless otherwise noted.

3.3.1 Cell Culture

Rat pheochromocytoma cells (PC-12, passage 6-12, ATCC) were used in addition the CTX0E03 cell line since they are an established model for studying the activity of nerve growth factor. PC-12 cells were cultured as non-adherent clusters in RPMI media supplemented with 10% heat-inactivated horse serum, 5% fetal bovine serum (FBS, Atlanta Biologicals), 2 mM L-glutamine,

100 U/ml penicillin, and 100 μg/ml streptomycin at 37° C in 5% CO_2 environment. Media was exchanged every other day by centrifuging the cell suspension for 5 min at 300xg and then resuspending the cell pellet in fresh media. Cell clusters were disrupted by pipette aspiration and subcultivated at a 1:5 ratio once per week or when the cells reached a concentration of approximately $2x10^6$ cells/ml.

3.3.2 Synthesis of PEG-Protein Conjugates

To generate PEG-protein conjugates, recombinant human FGF basic (FGF, R&D Systems) and nerve growth factor basic (NGF, R&D Systems) were first dissolved at 100 μg/ml in ice-cold, filter-sterilized HEPBS buffer (20 mM N-(2-Hydroxyethyl)piperazine-N'(4-butanesulfonic acid) and 100 mM NaCl, pH 8.7). Acryloyl-PEG-succinimidyl valerate (acryl-PEG-SVA MW 3400 Da, Laysan Bio) was separately dissolved in ice cold HEPBS buffer at 2 mg/ml and immediately sterilized via filtration (0.2 μm). For conjugation to FGF, protein solution and acryl-PEG-SVA solution were combined to achieve final reaction concentrations of 40 μg/ml protein and 15:1 molar ratio of PEG to protein. For conjugation to NGF, final reaction conditions of 40 μg/ml protein and either 2:1, 5:1, or 10:1 ratio of PEG to protein were tested. All reactions were vortexed at 4 °C overnight and stored in undiluted aliquots at -80°C.

3.3.3 Western Blot Determination of Conjugation Efficiency

To determine efficiency of the conjugation reaction, a Western blot was performed on the protein and PEG-protein conjugates. Samples were loaded at 125 ng protein per lane and run at 80V for 2 h on a 4-15% Tris-HCL polyacrylamide gel (ReadyGel, Biorad). Bands were then transferred to a nitrocellulose membrane, blocked in 5% milk block, and stained with 1:300 dilution of rabbit anti-FGF primary antibody (Abcam) for PEG-FGF samples or rabbit anti-NGF primary antibody (R&D Systems) for PEG-NGF samples. Secondary antibody incubation (goat

anti-rabbit HRP conjugate, Santa Cruz Bio) at 1:500 dilution was followed by visualization with an ECL chemiluminescent Western blotting analysis system (GE Healthcare). Stained blots were imaged with an LAS 4000 (FujiFilm) and images analyzed in ImageJ software.

3.3.4 Analysis of PEG-Protein Bioactivity in Solution

Fibroblast growth factor is expected to promote neural stem cell proliferation. To assess bioactivity of the PEG conjugates, the CellTiter96 proliferation assay (Promega) was used. Briefly, CTX0E03 cells were seeded at 15,000 cells/cm^2 in differentiating media lacking growth factors (EGF, FGF, 4-OHT) in a 96 well plate. Media was supplemented with FGF or PEG-FGF at final concentrations of 40, 10, 2.5, 0.625 or 0 ng/ml. After 72 h in culture, 20 µl CellTiter96 reagent was added to each well according to the manufacturer's protocol and absorbance was read 490 nm after a subsequent 4 h incubation at 37 °C.

Two methods for determining nerve growth factor bioactivity were performed. For quantification of neurite extension, PC-12 cells were seeded at 20,000 cells/cm^2 in a laminin-coated 48 well plate. Media was supplemented with NGF or one of the PEG-NGF conjugates at a final concentration of 100, 50, 10, 1, or 0 ng/ml. Cells were cultured for 1 week with fresh media and growth factor added every other day. Finally cells were imaged by phase contrast microscopy (Zeiss Axiovert 135) and ImageJ software was used to quantify total neurite length per view field.

Due to tendency of PC-12 cells to form clusters in culture, an alternative protocol was used to allow quantification of the percent of neurite positive cells in response to NGF or PEG-NGF exposure. Cells were first primed for three days in 50 ng/ml NGF supplemented media in a laminin-coated flask. Next, the cells were passaged and seeded at 20,000 cells/cm^2 in a laminin-coated 48 well plate. Media was supplement with 0 or 40 ng/ml of NGF or PEG-NGF and cells

were cultured for 72 h. Finally, samples were fixed for 1 h in 4% PFA, permeabilized for 10 min in 0.5% tritonX-100, and stained with 1 μM DAPI in PBS for 1 h. Images were taken by phase contrast and fluorescent microscopy (Zeiss Axiovert 135) and analyzed in ImageJ.

3.3.5 Analysis of PEG-Protein Incorporation into the Hydrogel Matrix

The efficiency of PEG-protein incorporation into the hydrogel matrix was determined by measuring protein diffusion from the scaffold over time. The amount of protein released into solution was quantified with a CBQCA Protein quantification assay (Life Technologies) in which the CBQCA reagent becomes highly fluorescent upon reaction with primary amines in the presence of potassium cyanide. Since this assay quantifies primary amines, the Eosin Y + TEOA photoinitiator system was replaced by 2-2-dimethoxy-2-phenylacetophenone (Irgacure 651) to avoid interference from the buffer solution. Polymer precursor solution (10% 10 kDa PEGDA in PBS with 10 μl/ml of a 300 mg/ml acetophenone in NVP stock solution) was prepared with 0 or 20 μg/ml PEG-FGF or 2:1 PEG-NGF. Non-immobilized hydrogel disks (10 μl volume, 3 per group) were synthesized with a 3 min exposure under UV light (Dolan-Jenner) and incubated in 100 μl PBS on a rocker at RT for 24 or 48 h. For each time point, soak solution was removed and stored at -80 °C. Solution protein concentration was determined according to manufacturer's protocol. Briefly, a 90 μl volume from each thawed sample was transferred to a black bottom 96 well microplate. To each well was added 40 μl of a 2.5 mM potassium cyanide (KCN) stock solution and 20 μl of a 0.5 mM CBQCA stock solution both of which were prepared in 0.1 M sodium borate buffer, pH 9.3. The samples were allowed to react on a rocker at RT for 1 h before reading on a fluorescent plate reader (SPEX FluoroLog-3 Spectrofluorometer) with excitation at 465 nm and emission at 550 nm. Concentrations were compared to a similarly made standard curve of 0 to 1 μg/ml PEG-FGF or PEG-NGF solution in PBS.

3.3.6 Analysis of Tethered PEG-Protein Bioactivity

Soluble factors may require internalization to initiate downstream signaling and cell response. For this reason, retention of bioactivity was next evaluated with the PEG-conjugated proteins tethered into the hydrogel matrix. For fibroblast growth factor, sterile-filtered polymer precursor solution (10% 10 kDa PEGDA in HBS with 1.5% TEOA, 3.4 µl/ml NVP 10 µM eosin Y, and 0.3 mM PEG-c(RGDfK)) was prepared both with and without 1 µg/ml PEG-FGF. Immobilized hydrogels (10 µl volume, 3 per group) were synthesized as described in section 2.3.7 and incubated in 1 ml HBSS at RT for 24 h. CTX0E03 cells were seeded at 10,000 cells/cm^2 in differentiating media lacking FGF, EGF, and 4-OHT and incubated at 37 °C for 48 h. Following incubation, samples were fixed for 1 h in 4% PFA, permeabilized for 15 min with 0.5% Triton X-100, and blocked overnight at 4°C with 5% BSA. Samples were then incubated in primary antibody (rabbit anti Ki-67, 1:200, Vector Labs) at 4 °C overnight in PBS with 0.5% BSA, followed by 4 X 1 ml PBS rinses and secondary antibody incubation (Donkey anti-rabbit Alexa Fluor 555) at 4 °C overnight in PBS with 0.5% BSA . Final PBS rinses and DAPI staining (2 µM DAPI in PBS for 1 h) were all performed at RT. Samples were imaged by phase contrast and fluorescent microscopy (Zeiss Axiovert 135) and analyzed in ImageJ to determine cell density and percent of cells positive for the proliferative, Ki-67 marker.

Bioactivity of tethered NGF was assessed with the PC-12 cell line. Filter-sterilized polymer precursor solution (10% 10 kDa PEGDA in HBS with 1.5% TEOA, 3.4 µl/ml NVP 10 µM eosin Y, and 3 mM PEG-c(RGDfK)) was prepared containing 0, 0.5, 5, and 20 µg/ml of the 2:1 reacted PEG-NGF. Immobilized hydrogels (10 µl volume, 3 per group) were synthesized according to the protocol described in section 2.3.7, and incubated in 1 ml HBSS at RT for 24 h. PC-12 cells (primed for 3 days in media with 50 ng/ml NGF) were seeded on the hydrogel surface at 20,000

cells/cm^2 and incubated at 37 °C for 72 h. Samples were then fixed, stained with DAPI, and analyzed for percent of neurite positive cells in the same manner as described for solution NGF bioactivity in section 3.3.4.

3.3.7 Statistical Analysis

Significance was determined via unpaired, two-tailed *t*-test when $p < 0.05$. Error bars in figures depict standard deviations for the data sets.

3.4 Results and Discussion

The purpose of this work is to demonstrate the ability of the hydrogel system to present immobilized signals to neural stem cells *in vitro*. Two growth factors, fibroblast growth factor and nerve growth factor, were chosen for their contrasting effects on NSC behavior. Cell response to each of these factors has been well characterized and as such they present ideal models for initial evaluation of the system. For the first step, the proteins must be conjugated to a PEG linker. Due to the sensitivity of proteins to organic solvents, the reaction was performed in aqueous buffer with acryl-PEG-SVA, a more water-stable variant of the PEG-SCM reagent used previously in section 2.3.4. For FGF, the reaction ratio of PEG to protein was chosen based on the number of available primary amines in the recombinant protein sequence. For NGF, multiple ratios were tested as previous literature has shown that PEG conjugation can reduce bioactivity.[108]

3.4.1 Western Blot Analysis of PEG Conjugates

A Western blot was performed on the unmodified protein and PEG-SVA-reacted protein to assess the conjugation efficiency of the reaction. In this technique, PEG-conjugated protein will appear as a higher molecular weight smear due to single or multiple PEG chain additions. As

seen in Figure 42, the recombinant FGF protein appears as a dark band at the expected molecular weight of 17 kDa. A fainter band at approximately 34 kDa suggests some protein was present as a dimer. For the PEG-FGF conjugate, a faint 17 kDa band is observed in addition to a smear of higher molecular weight components. These results indicate that successful conjugation of the growth factor to the PEG linker has occurred.

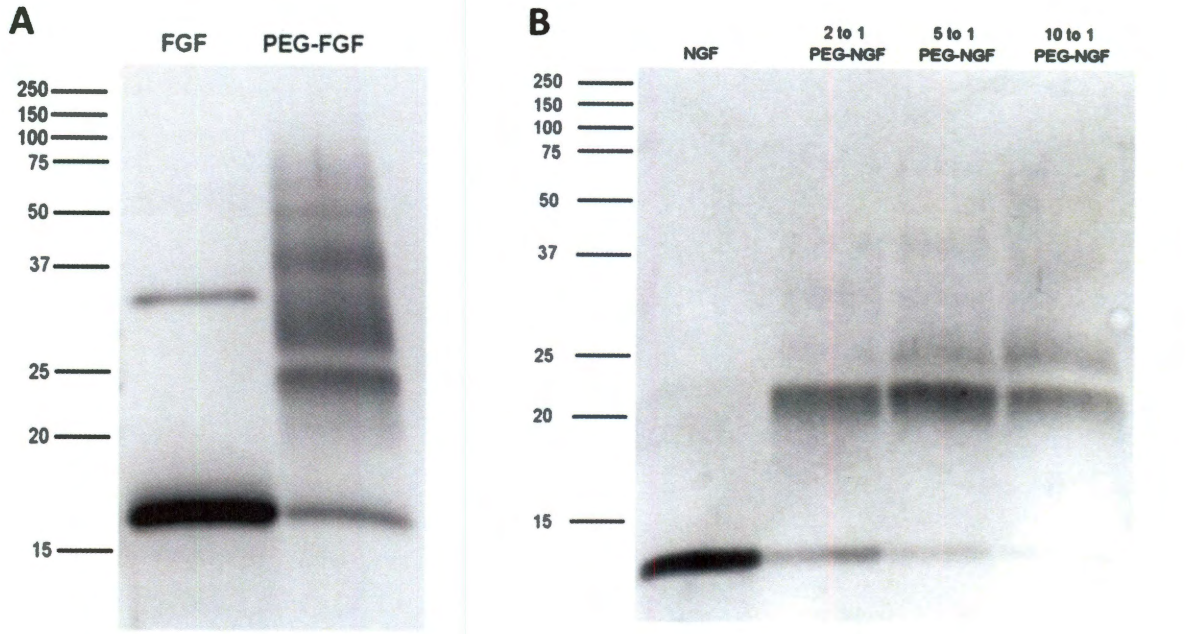

Figure 42. Western blot analysis of PEG conjugated FGF and NGF proteins. Higher molecular weight smear indicates presence of the PEG bound protein. For FGF, a conjugation efficiency of approximately 85% was observed based on lightening of the 17 kDa band from the unconjugated control. For NGF, conjugation efficiencies of 95, 98, and 100% were observed for 2:1, 5:1, and 10:1 reaction ratios of PEG to protein, respectively.

Comparison of the 17 kDa band intensity between FGF and PEG-FGF samples showed a reaction efficiency of approximately 85% at the 15 to 1 ratio of PEG-SVA to FGF protein. Previous literature has demonstrated successful conjugation of FGF to PEG hydrogels in order to direct the migration of fibroblast cells *in vitro*. Comparison to the published study found that the efficiency of the reaction presented here was lower than previously observed.[67] This discrepancy

is likely due to the variation in reactivity and aqueous half-life of the bi-functional PEG-SVA vs. the previously available PEG-NHS reagent, which was supplied by a different manufacturer.

For conjugation to nerve growth factor, three reaction ratios of PEG to protein were evaluated. Although a higher ratio can improve conjugation efficiency, it may also result in reduced protein bioactivity if the polymer reacts to a region of the protein involved in receptor binding. By testing three ratios, one can optimize the retention of protein bioactivity vs. completeness of the conjugation reaction. By Western blot analysis (see Figure 42), all three reaction conditions resulted in successful conjugation based on the presence of the higher molecular weight smears. Comparison of the density of the unconjugated NGF band (13 kDa predicted MW) across the samples showed a conjugation efficiency of 95, 98, and 100% for ratios of 2:1, 5:1, and 10:1 PEG-SVA to NGF.

3.4.2 PEG-Protein Bioactivity in Solution

Conjugation of PEG chains to a protein may impact the ability of the protein to bind and activate target receptors on the cell surface. It is therefore important to determine the effect of the PEG reaction on the bioactivity of the FGF and NGF proteins. FGF is recognized as a primary mitogen for neural progenitors. The CellTiter96 Assay was therefore chosen as a simple means to quantify proliferation of CTX0E03 cells in response to FGF or PEG-FGF supplemented media. With this assay, a linear relationship can be observed between the cell concentration and media absorbance due to metabolic conversion of an MTS reagent into a formazan product with peak absorption at 490 nm. CTX0E03 cells were seeded at equal density and cultured in varying concentrations of FGF or PEG-FGF for three days before comparison of the final cell concentration using the CellTiter96 assay. Note that concentrations are given based on FGF protein in solution, thus molarity of the growth factor is equivalent for these comparisons. The

results of this assay (Figure 43) showed that cell proliferation in response to FGF and PEG-FGF was equivalent for the 10 ng/ml and 40 ng/ml concentrations. At lower concentrations (0.625 and 2.5 ng/ml) the FGF performed slightly better than the conjugated growth factor however this difference was only statistically significant for the 2.5 ng/ml concentration. Previously published work investigated only a single concentration (50 ng/ml) of pegylated protein to assess the effect of the conjugation reaction on FGF bioactivity.[67] The data presented here indicates that the PEG modification may have a very slight impact on the bioactivity of the growth factor; however at higher concentrations this difference is not significant.

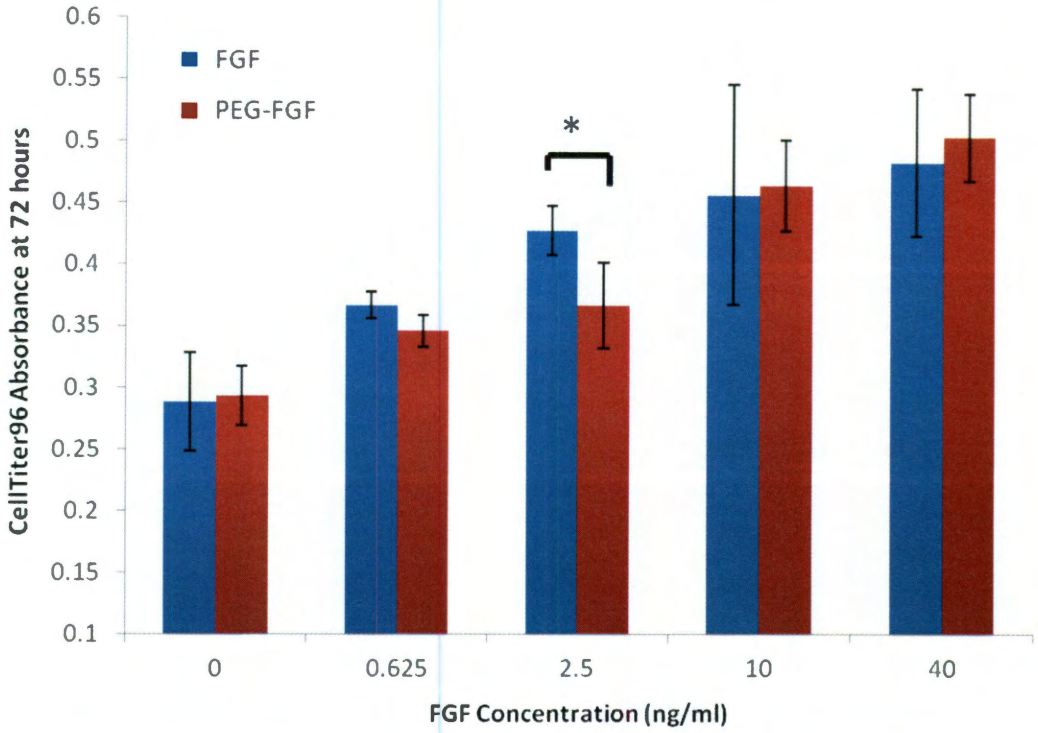

Figure 43. CellTiter96 assay of CTX0E03 proliferation in response to varying concentrations of FGF or PEG-FGF supplemented media after three days in culture. Proliferation was found to be equivalent between the unmodified and PEG conjugated factor for all but the 2.5 ng/ml concentration. * $p < 0.05$

The model PC-12 cell line was used for investigation of the bioactivity of nerve growth factor in solution. Upon exposure to NGF, this cell line is known to undergo differentiation and extension of neurites. Two criteria were used to quantify the cell response for these studies: total neurite

length, and percent of the cell population that underwent differentiation. Neurite extension was quantified from phase contrast images using the NeuronJ plugin to trace and measure the total length per view field. Representative images of the cell response after one week exposure to the growth factors are shown in Figure 44 along with the quantification of this response in Figure 45. From these results, one can see that unmodified NGF induced robust neurite extension from

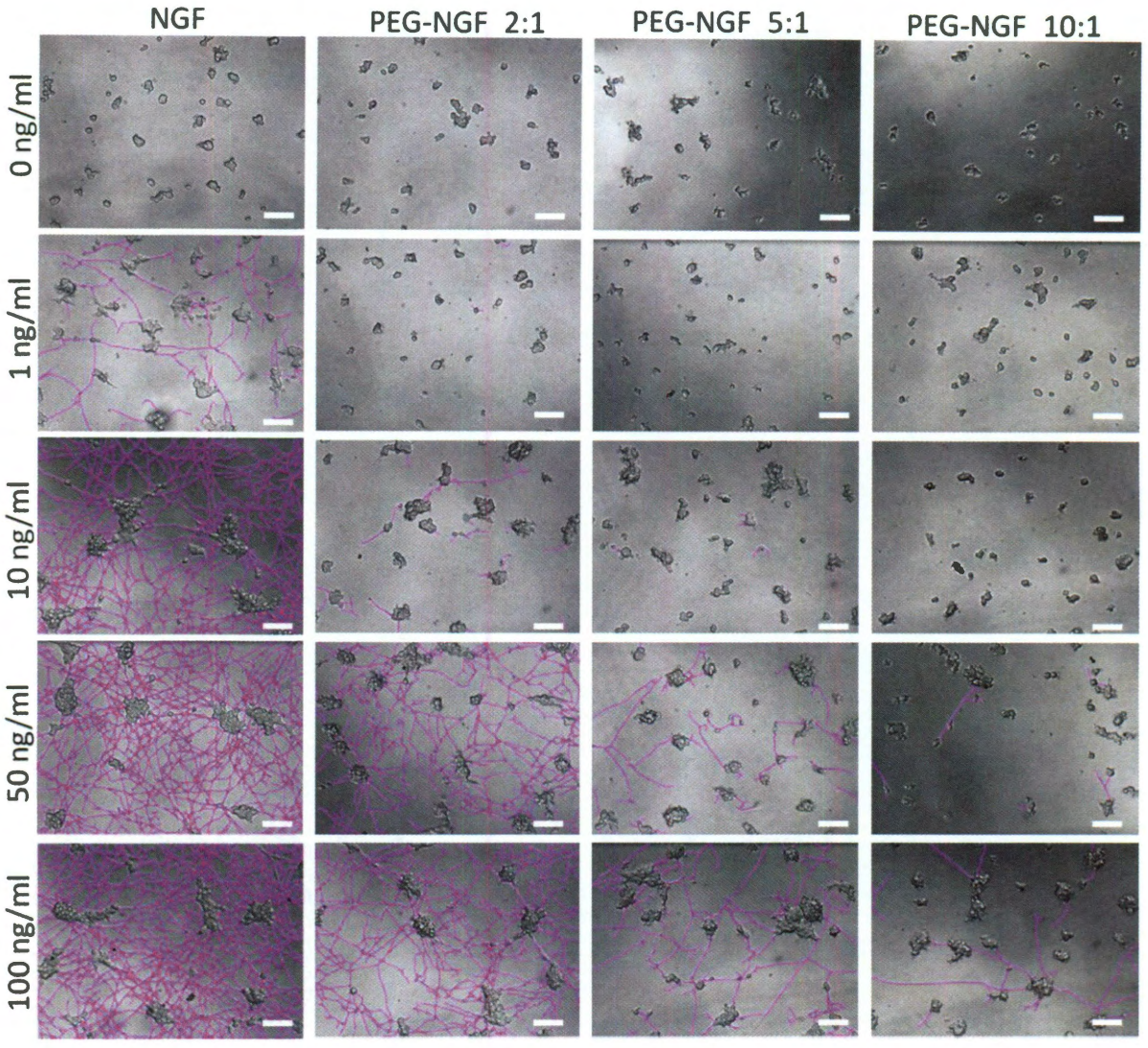

Figure 44. Representative Images of PC-12 neurite extension in response to NGF or PEG-NGF in solution. Neurites were traced in the NeuronJ plugin for ImageJ to allow quantification and are shown here in fuchsia. It can be observed that neurite extension is greatest for the unmodified NGF protein. Increasing ratio of PEG to NGF used during the conjugation reaction results in reduced bioactivity as shown here. Scale bars represent 100 μm.

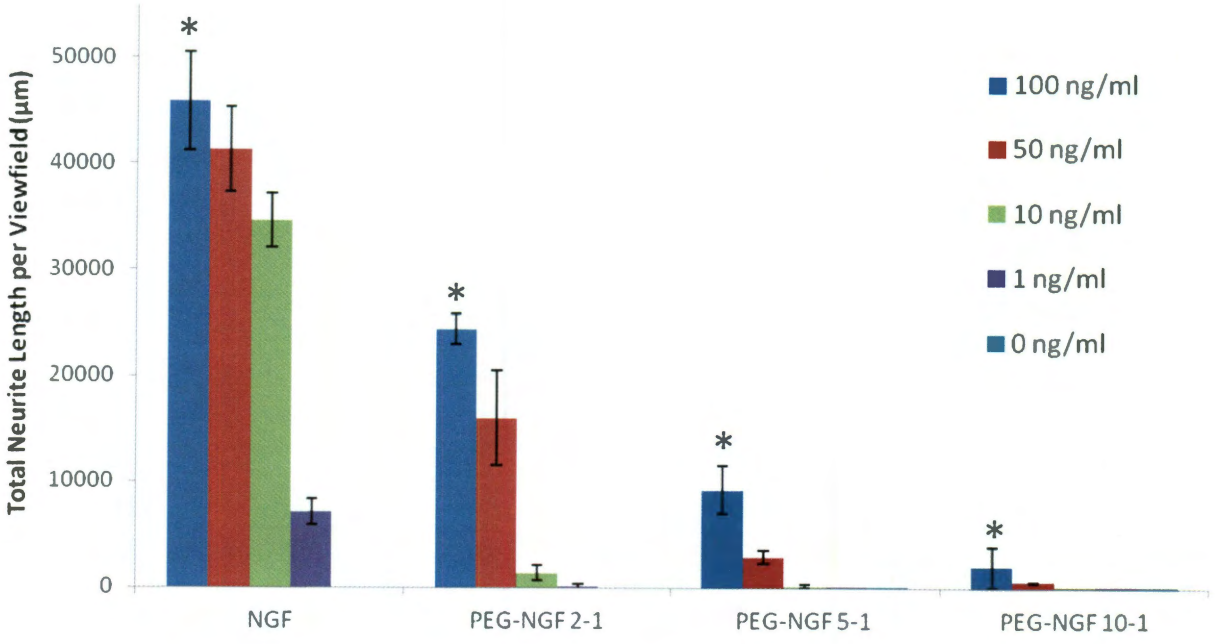

Figure 45. Quantification of neurite extension by PC-12 cells after 1 week exposure to NGF or PEG-NGF in solution. Response to 100 ng/ml concentration shows statistically significant difference between all sample groups with bioactivity inversely related to the ratio of PEG to NGF used during the conjugation reaction. * $p < 0.05$

the cultured cells in a dose dependent manner. PEG conjugated growth factor was also able to induce neurite extension, however bioactivity was significantly reduced. Additionally, an inverse relationship can be observed between the neurogenic response and the ratio of PEG to NGF used in the coupling reaction.

Similar results are obtained when quantifying the percent of neurite positive cells (Figure 46). For this study, a shorter exposure time and DAPI counterstaining aided in the analysis of the individual cell response. Again the bioactivity of the growth factor was reduced as the ratio of PEG to protein was increased. This suggests that the coupling of a greater number of PEG chains per protein results in greater disruption of the interaction between NGF and the cell surface receptor.

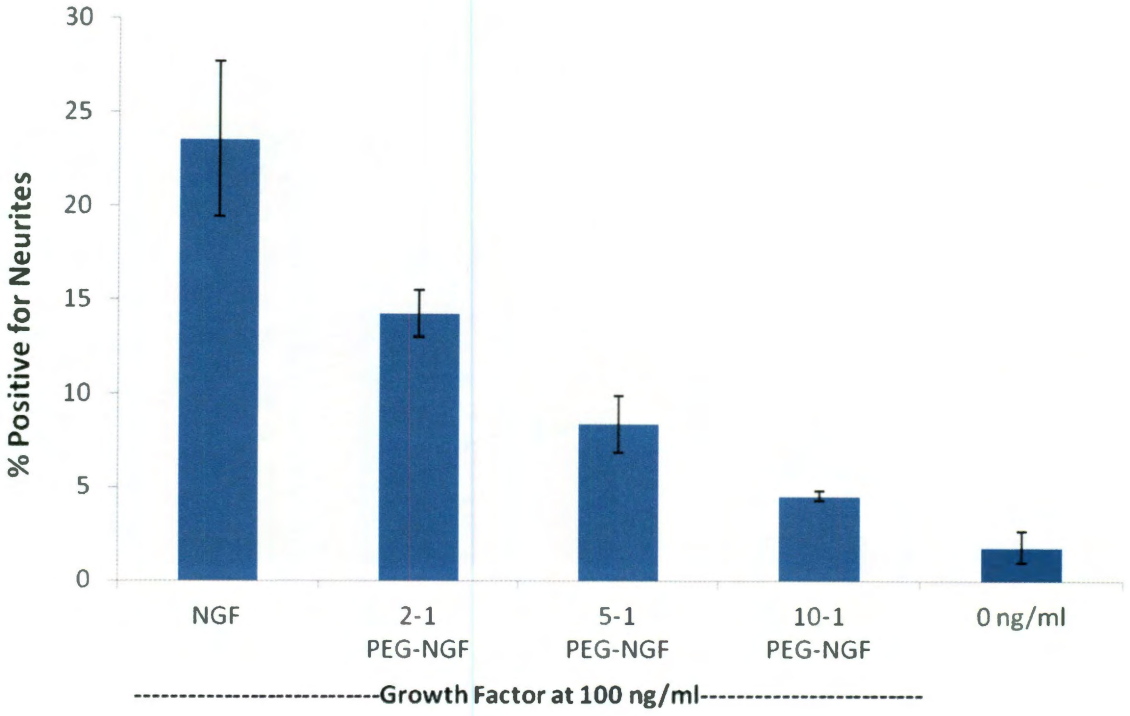

Figure 46. Quantification of the percent of neurite extending PC-12 cells after 72 h exposure to soluble NGF. Decreased bioactivity is observed with increasing ratio of PEG to NGF. All values are significantly different from each other with $p < 0.05$.

The structure of the folded NGF protein and its TrkA receptor complex are presented in Figure 47. Lysine residues along the protein backbone are identified in blue and present possible sites for PEG-SVA coupling in addition to the N terminus. The TrkA receptor primarily binds to the saddle-like depression in center of the NGF homodimer as shown in Figure 47-B.[113] Although the N terminus and C terminal lysine are solvent accessible and readily available for coupling, reaction of PEG-SVA to the lysine residues at position 32 and 34 may be responsible for the reduction in bioactivity observed, especially at higher ratios of PEG to protein. The results observed here were found to be consistent with those published in the literature. Previous studies have reported approximately 100 to 200 fold reduction in bioactivity when the growth factor was tagged using succinimide chemistry with a PEG-linked fluorophore at a 10 molar

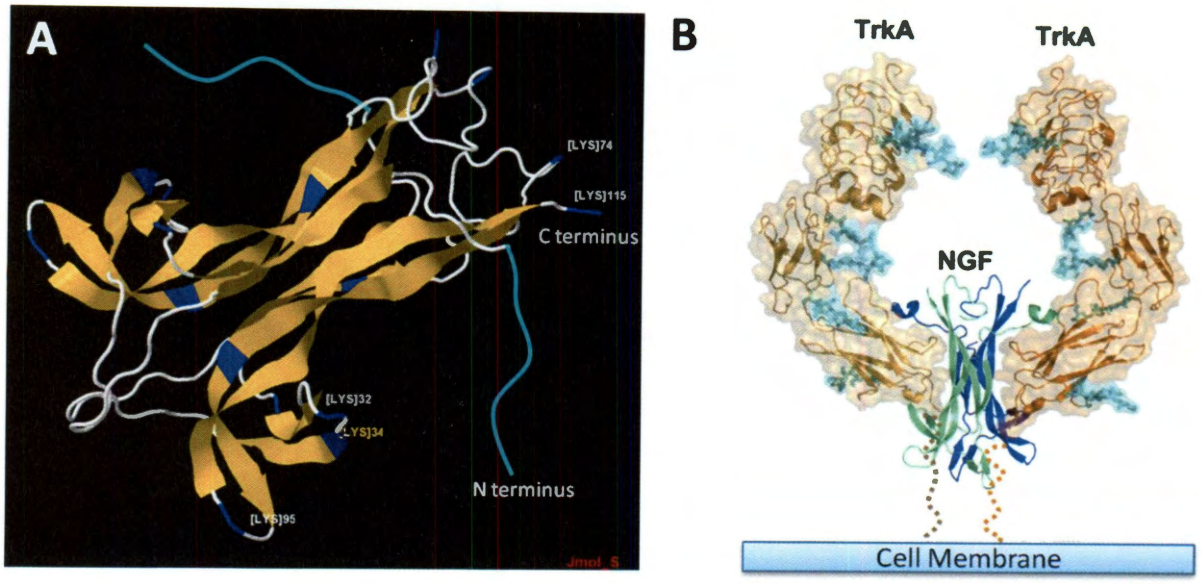

Figure 47. Folded structure of nerve growth factor (A, produced in Jmol) with lysine residues labeled in blue. The portion of the N terminus not visible in the crystal structure has been added in cyan.[114] Binding of the growth factor with the TrkA receptor (B) on PC-12 cells promotes survival and neurite extension.[113] Figure from Wehrman *et al.* 2007.

excess.[108] By comparison, the 2:1 PEG-NGF synthesized here showed approximately 5-fold reduction in bioactivity and thus presents a significant improvement. It was therefore chosen for all tethered studies within the hydrogel system.

3.4.3 Analysis of PEG-Protein Incorporation into the Hydrogel Matrix

Efficiency of PEG-protein incorporation into the hydrogel matrix was determined by using the commercially available CBQCA assay to quantify the amount of protein which diffuses out of the hydrogel and into a soak solution. The CBQCA reagent reacts with primary amines on proteins and peptides in the presence of cyanide to produce a highly fluorescent product. The TEOA component of the Eosin Y-initiated polymer solution contains a primary amine and would likely oversaturate the assay, preventing accurate quantification of the protein concentration. Furthermore, the Eosin Y photoinitiator has significant autofluorescence within the same range as the CBQCA reagent. To avoid interference from these compounds, a different photoinitiator

system was used to generate the hydrogels for the assay. Irgacure 651 is a UV activated photoinitiator that shows minimal autofluorescence at 465 nm excitation. Hydrogel disks were synthesized with an extended exposure time of 3 min to ensure complete crosslinking. It is proposed that protein incorporation will be comparable between the photoinitiator systems when the crosslinking reaction is taken to completion in both cases. As shown in Figure 48, by the 48 h time point it was found that no significant reduction of incorporated PEG-FGF was observed, however approximately 36% of the PEG-NGF had diffused from the hydrogel. The lower incorporation by PEG-NGF was not surprising based on the likelihood that fewer PEG linker chains are present on each molecule of protein due to the lower ratio of the PEG to NGF used for the conjugation reaction (2:1 vs. 15:1 for FGF).

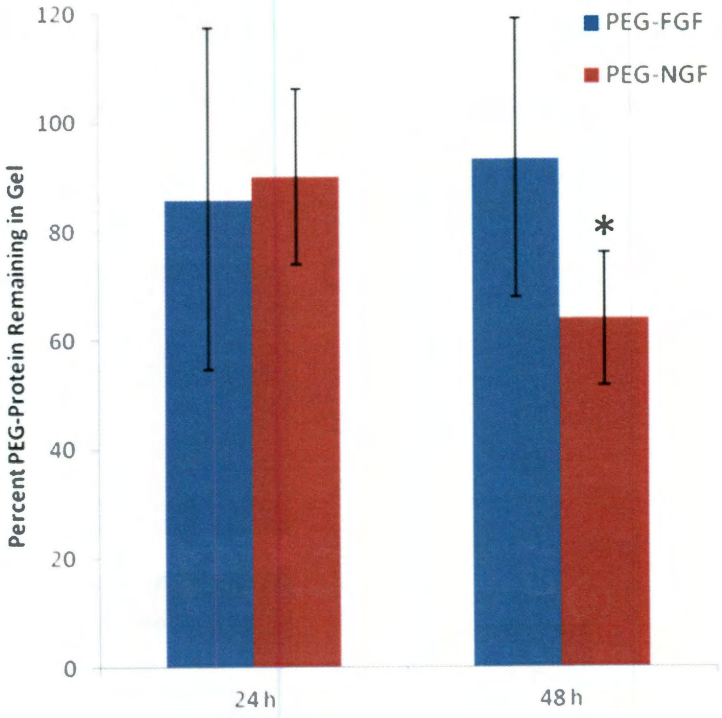

Figure 48. Analysis of PEG-FGF and PEG-NGF incorporation in the hydrogel matrix. Approximately 64% of the PEG-NGF remained incorporated after the 48 h incubation period. * $p < 0.05$ compared to 24 h time point.

3.4.4 Tethered PEG-Protein Bioactivity

Investigation of tethered growth factor influence on surface-seeded neural stem cells was first evaluated for the fibroblast growth factor. PEG-FGF was incorporated in the bulk of immobilized hydrogel disks at a 1 μg/ml concentration. During photo-initiated crosslinking, the acrlyl-terminated PEG linker should allow covalent tethering of the protein to the hydrogel matrix. Cells were cultured on the surface of the hydrogels in differentiating media lacking FGF, EGF, and 4-OHT for three days prior to imaging and analysis of cell density. As shown in Figure 49, a significant increase in cell number was observed for the FGF-modified hydrogels as compared to control gels with 0 μg/ml PEG-FGF. Representative brightfield images are also presented in the figure to demonstrate the apparent differences in cell density and distribution. Previous studies have shown that similarly immobilized FGF can induce oriented spreading of fibroblast cells[67], however this is the first demonstration of PEG-FGF modified hydrogels for the control of neural stem cell proliferation.

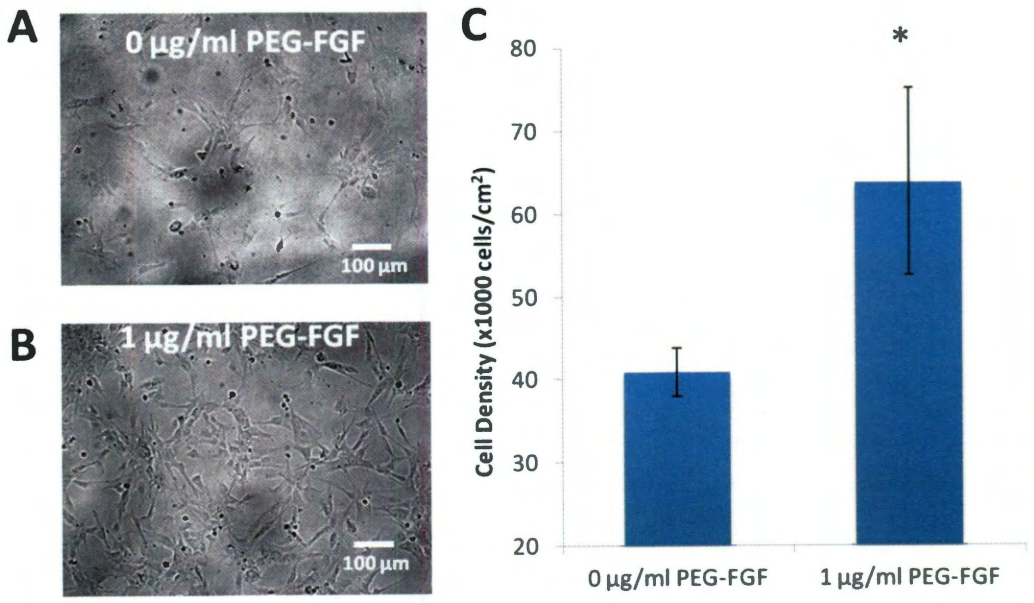

Figure 49. Comparison of CTX0E03 proliferation on the surface of hydrogels containing 0 μg/ml (A) or 1 μg/ml (B) of tethered PEG-FGF. A significant increase in cell number was observed for the growth factor modified gels as compared to 0 μg/ml control (C). * $p < 0.05$

To study the bioactivity of immobilized nerve growth factor, the PC-12 line was again utilized. The cells were seeded on hydrogel disks containing 0 to 20 µg/ml 2:1 PEG-NGF incorporated in the bulk. After 72 h in culture, the samples were fixed and cell response was quantified by determining the percent of neurite positive cells. As shown in Figure 50, a significant increase in neurite positive cells was observed for hydrogels containing 5 and 20 µg/ml PEG-NGF.

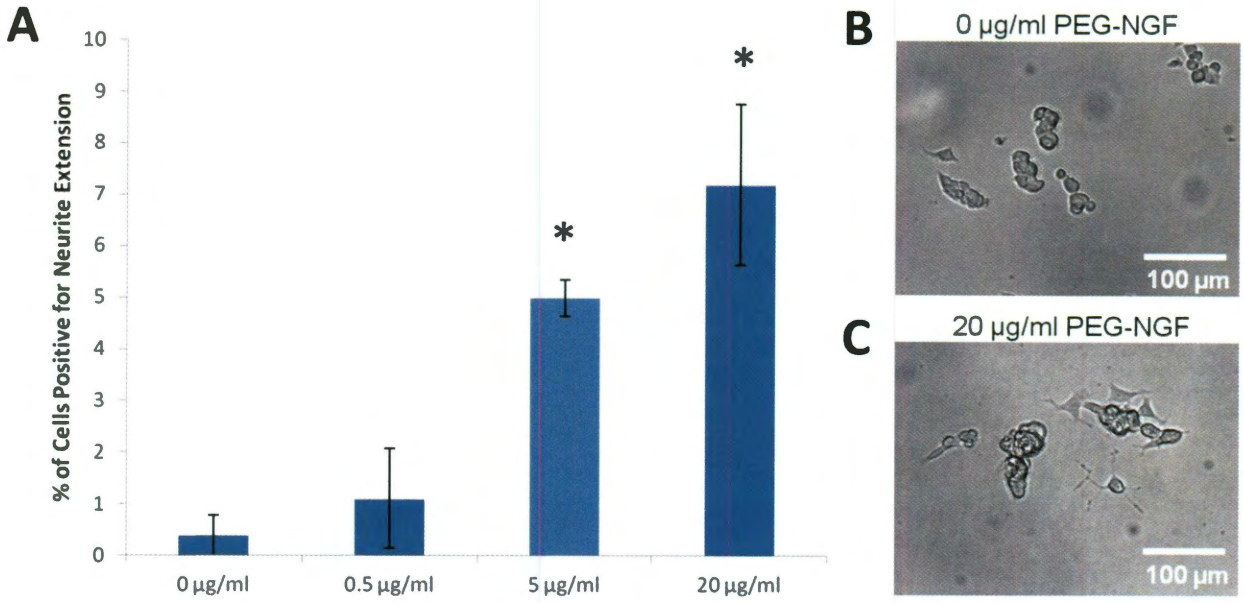

Figure 50. Quantification of the percent of neurite positive cells after 72 h culture on hydrogel disks with immobilized PEG-NGF (A). A significant response was observed for the 5 and 20 µg/ml concentrations as compared to control gels without growth factor. Representative images of the 0 µg/ml (B) and 20 µg/ml (C) samples are also shown. * $p < 0.05$ as compared to 0 µg/ml control

The overall cell response, however, was significantly lower when compared to solution bioactivity results. For example, at a concentration of 100 ng/ml in solution, the PEG-NGF induced neurite outgrowth in approximately 15% of the cell population. For the immobilized protein, a 20 µg/ml concentration resulted in only about 5% of the population responding despite the 200-fold increase in signal concentration.

Multiple factors may be responsible for this difference between solution and tethered bioactivity. First, when cells are grown in 2D on a modified surface, they will only interact with signal they are directly contacting and thus the spread area of the cell can dictate the amount of signal that is received. Another consideration is the mechanism by which a receptor triggers a downstream signaling response. For some pathways, internalization of the receptor-ligand complex may be required to initiate a response.[115] In the case of NGF, however, primary signally pathways do not require internalization.[113] Finally, the ability of the growth factor to initially bind and activate the receptor may be physically restricted by the PEG tether. As was shown in Figure 47, the NGF protein interacts in a deep pocket of the TrkA receptor. The 3400 MW PEG linker may simply be too short to allow proper assembly of this receptor-ligand complex. It is recommended for future studies that a variety of PEG linker lengths should be investigated to determine if this is the mechanism for the reduced bioactivity observed here.

3.5 Conclusions

This work demonstrates the capacity of the hydrogel matrix to present covalently tethered proteins to neural stem cell cultures *in vitro.* Two well characterized and contrasting growth factors, fibroblast growth factor and nerve growth factor, were chosen to show control over NSC proliferation and differentiation respectively. Successful conjugation was verified by an increase in the protein molecular weight as measured by western blot analysis. Furthermore, retention of bioactivity was confirmed for both factors in solution. For PEG-FGF, bioactivity remained comparable to the unmodified protein. For NGF, PEG conjugation resulted in reduced bioactivity, which may be caused by the presence of potential coupling sites near the active binding domain of the native protein. Finally, each growth factor was immobilized in the

hydrogel scaffold and re-evaluated to confirm its ability to influence the behavior of surface seeded neural progenitors.

In addition to the two growth factors presented here, a wide array of PEG-linked protein signals could be developed for immobilization using this approach. Furthermore, the photo-initiated crosslinking system provides the capacity for light-based patterning of incorporated signals in both 2 and 3 dimensions. This technique could therefore be used to generate patterns of growth factor availability within a hydrogel matrix that, for example, are reminiscent of the fractone-sequestered FGF reservoirs in the *in vivo* niche. Taken together, this work presents significant potential for developing a bioactive hydrogel matrix that mimics the complexity and biochemical organization of the *in vivo* NSC niche.

Another possible application for this technology could be for *in vivo* drug delivery or development of advanced cell-based constructs for neural tissue engineering. The ability of the hydrogel system with incorporated factors to promote a response *in vivo* has been previously demonstrated in the study of angiogenic factors using the cornea micropocket assay.[71] In the CNS, multiple factors have been identified with the capacity to activate endogenous repair systems. It is suggested that future work could investigate immobilization of these niche-stimulating or neuroprotective factors in order to develop more advanced therapeutic strategies for the treatment of CNS damage and disease.

4 Investigation of the Angiogenic Potential of Neural Stem Cells

4.1 Introduction

4.1.1 Cell-Cell Signaling in the Niche

A variety of important cell-cell interactions are expected to occur in the NSC niche based on the highly extended and interconnected morphology of the type B neural stem cells. These include interactions with endothelial cells of the vasculature, ependymal cells lining the ventricles, neurons through their axonal extensions, and perivascular astrocytes that contribute to fractone formation.[45,51,104] Other astrocytes, macrophages, and fibroblasts found in the niche may also play a role through growth factor secretion or ECM interactions.[45,51,72] In one example, astrocytes were found to promote the proliferation of NSCs and direct their differentiation toward a neuronal phenotype during *in vitro* co-cultures.[116] Doetsh *et al.* have even implicated the mechanical action of the ciliated ependymal cells in generating growth factor gradients to direct NSC migration.[48] In addition to paracrine affects, neighboring cells can also promote their influence through direct cell-cell contact. Components of adherens junctions including cadherins and β-catenin have been identified in the niche and are thought to influence NSC behavior.[5] In one study, for example, β-catenin over-expression was found to enhance neural progenitor proliferation *in vivo* leading to enlarged lateral ventricles in the rodent model.[117] Direct cell-cell connections through gap junctions are another way to allow rapid, long distance signal transmission and have been observed between niche astrocytes as well as among the ependymal cells.[22,48,72]

4.1.2 The Neurovascular Niche

Several groups have observed that within both proliferative zones of the CNS, neural stem cells are found in close proximity to microvasculature.[5,6,45,48,118] Within the SGZ specifically, proliferating NSCs migrate towards and cluster at capillary ends or branch points.[119] These areas of the vasculature are traditionally associated with active angiogenesis, suggesting a link between NSC expansion and the formation of new blood vessels.[118,119] Contrasting theories still exist as to whether the vascular compartment or the neural stem cells provide the first signals initiating this interaction and cell clustering events.[119] Known stimulators of angiogenesis such as exercise, hypoxia, and testosterone have also been shown to increase neuroblast production and migration, further supporting a link between the two processes.[3,8,72,118] One key player that has been identified is vascular endothelial growth factor, or VEGF.[120] As shown in Figure 51, a positive feedback loop is established in which the endothelial cells and neural stem cells both secrete, and respond to the growth factor. As a result, both endothelial sprouting and NSC expansion and neuronal differentiation are stimulated. The newly formed neuroblasts have additionally been observed to use the network of blood vessels as a scaffold both during normal migration towards the olfactory bulb, and following stroke to reach areas of ischemic damage.[6,118,121]

Although the basic role of the vasculature is to transport oxygen and nutrients to the tissues, it can also interact through the surrounding extracellular matrix, secreted soluble factors, transported endocrine factors, and direct cell-cell contact.[118] To investigate some of these interactions, *in vitro* experiments have studied the behavior of endothelial cell co-cultures with the NSCs.[104] These experiments showed increased proliferation and neurogenesis of the NSCs when in the presence of endothelial cells.[45,48,104,122] Additionally, the endothelial cells are also

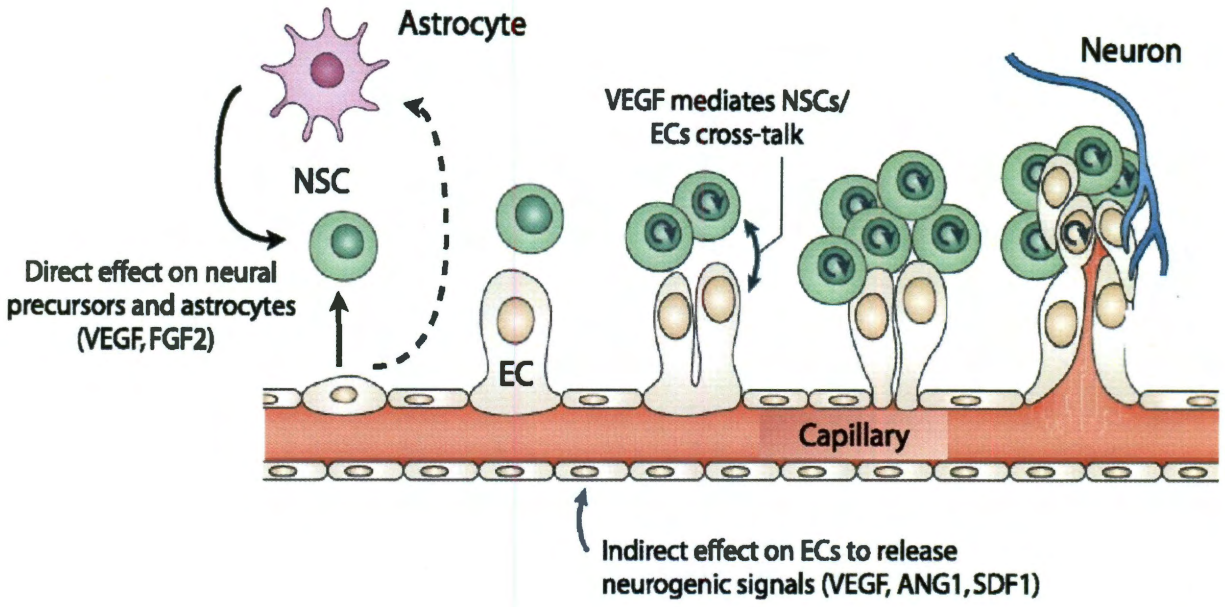

Figure 51. Graphical representation of the process of spatiotemporal coordination between neurogenesis and angiogenesis in the neural stem cell niche.[120] Both direct signals from the NSCs and indirect signals from other cellular components in the region are capable of stimulating endothelial sprouting. A positive feedback loop is then established between the two cell populations via secretion of VEGF and other soluble signals.[120] Figure from Ruiz de Almodovar *et al.* 2009.

stimulated under these conditions, leading to increased tubulogenesis.[104] Beyond a few identified proteins such as VEGF and brain-derived neurotrophic factor (BDNF), the full signaling interactions involved are still under debate.[104] It is clear however, that the vasculature of the niche plays a critical role and should be considered during the design of any tissue engineered construct.[45,48,104]

4.1.3 Vascular Lineage for Neural Stem Cell Differentiation

The theory of coordinated neurogenesis and angiogenesis described above is well accepted and widely studied in the literature. Another, much more controversial idea however, is that neural stem cells themselves retain the capacity to differentiate along vascular lineages. In 2000, Tsai *et al.* observed that rat cortical neural stem cells differentiated at varying culture densities developed into vastly different populations.[123] Although the typical neuronal, astrocyte, and

oligodendrocyte lineages were formed from high density cultures, very low density cultures showed almost complete absence of theses cell types. Instead, a population of almost exclusively alpha-smooth muscle actin (α-SMA) positive cells was observed.[123] In a subsequent study, these α-SMA positive cells were confirmed to express other markers of smooth muscle cells such as calponin and SM22, and were shown to contract in response to a variety of stimuli.[124] The combination of multiple, cell type-specific markers and a contractile phenotype indicated the cells had differentiated along a mural lineage.

More recently, Oishi *et al.* demonstrated the expression of endothelial markers such as PECAM-1 and VE-cadherin in a subpopulation of neural stem cells differentiated at low density in the presence of 10% fetal bovine serum. Isolation and expansion of this population found that they were capable of organizing into tubule-like networks when cultured in three-dimensional collagen gels. Taken together, the possibility for both mural and endothelial cells lineages to develop from a single population of embryonic neural stem cells presents an intriguing possibility for the generation of vascularized constructs in neural tissue engineering.

4.2 Objectives

The ability of the hydrogel scaffold to simulate the physical ECM and soluble signals of the *in vivo* niche has been demonstrated in previous sections. For this work, the cellular and specifically microvascular component of the niche is considered for its influence on neural stem cell behavior. Initial characterization of the angiogenic potential of the CTX0E03 cell line was performed, followed by investigation of a co-culture encapsulation of NSCs and primary endothelial cells within the degradable hydrogel matrix. Finally, a commercially available neural stem cell line transfected to constitutively express green fluorescent protein (GFP) was

investigated for its angiogenic potential *in vivo* using the cornea micropocket angiogenesis assay. Growth of the limbic vessels at the edge of the cornea toward cell-laden, degradable hydrogel disks with no added growth factors was used as an indicator of NSC-induced angiogenesis.

4.3 Materials and Methods

All materials were purchased from Sigma unless otherwise noted.

4.3.1 Cell Culture

Primary human umbilical vein endothelial cells (HUVECs passage 2 to 6, Lonza) were cultured at 37 °C in a 5% CO_2 environment in endothelial basal medium (EBM-2, Lonza) supplemented with the endothelial growth media bullet kit (EGM-2, Lonza). Media was exchanged every other day and subcultivation was performed at a ratio of 1:6 once the cells reached 85% confluency. Human cortical neural stem cells (CTX0E03) were cultured as described in section 2.3.1. Murine neuroepithelial cells transfected to express green fluorescent protein (NE-GFP-4C passage 3 to 6, ATCC) were cultured on TCPS that had been treated with 15 μg/ml poly-L-lysine in PBS for 2 h at RT. The NE-GFP-4C cells were cultured in Eagle's minimum essential medium (EMEM, ATCC) supplemented with 4 mM L-glutamine and 10% FBS and incubated at 37 °C in a 5% CO_2 environment. Media was exchanged every other day and subcultivation was performed at a ratio of 1:10 once the cells reached 90% confluency.

4.3.2 Characterization of NSC Pro-Angiogenic Features

CTX0E03 cells were seeded at high (100,000 cell/cm^2) and low (10,000 cells/cm^2) densities and cultured in differentiating media lacking EGF, FGF, and 4-OHT for 2 weeks on laminin-coated 24-well plates (protocol section 2.3.1). Additional wells were also seeded at 20,000 cells/cm^2 in

complete growth media and cultured for 3 days. Following this culture period, select wells were passaged with Accutase and reseeded at 10,000 cell/cm^2 to allow observation of individual cell morphology. To assess marker expression, a portion of the cells were fixed and stained with primary antibodies against smooth muscle alpha-actin (mouse anti-α-SMA, 1:200) and neuronal βIII Tubulin (rabbit anti-βIII Tubulin, 1:500, Abcam) followed by secondary antibodies (donkey anti-rabbit Alexa Fluor 488 and donkey anti-mouse Alexa Fluor 555, 1:500, Invitrogen) according to the immunostaining protocol in section 2.3.10. Images were acquired by phase contrast and fluorescence microscopy (Zeiss Axiovert 135).

To assess production of vascular endothelial growth factor (VEGF), 3 wells per group were exchanged with 0.5 ml fresh media at the final time point and incubated at 37 °C and 5% CO_2 for an additional 48 h. After the incubation period, the media was sampled and stored at -80 °C and the cells were passaged and counted by hemacytometer to determine final cell number per well. The amount of VEGF produced by the cell cultures was determined by analyzing the thawed media samples with a Quantikine human VEGF ELISA kit (R&D Systems) using VEGF standards according to manufacturer's protocol.

4.3.3 NSC Co-culture with Endothelial Cells *In Vitro*

HUVECs and CTX0E03 were passaged and separately resuspended in degradable polymer precursor solution (sterile-filtered 5% PEG-PQ-PEG in HBS with 0.3 mM PEG-c(RGDfK), 1.5% TEOA, 3.4 µl/ml NVP, and 5 µM eosin Y) at 30x10^6 cells/ml. Immobilized hydrogel disks of 10 µl volume were then generated according to the method described in section 2.3.7 as either a HUVEC monoculture, or a 4:1 mix of the HUVEC and CTX0E03 cell suspensions. For select samples, the two cell suspensions were pipetted adjacent to each other prior to gelation to provide a direct interface between the monoculture and co-culture conditions. The

encapsulated cell samples were cultured in 1 ml of HUVEC media for 7 days at 37 °C with media exchanges every other day. Samples were then fixed and immunostained with primary antibodies at 1:200 dilution (goat anti-CD31 (Santa Cruz Bio), mouse anti-α-SMA, and rabbit anti-nestin) followed by secondary antibodies at 1:500 dilution (donkey anti-goat, mouse, and rabbit conjugated to Alexa Fluor 488, 555, and 647 respectively, Invitrogen). Samples were imaged by confocal microscopy (Zeiss Live5 DuoScan) and analyzed in ImageJ.

4.3.4 Cornea Micropocket Assay of NSC-Induced Angiogenesis

The fluorescently-labeled NE-GFP-4C line was used to investigate the angiogenic potential of neural stem cells *in vivo*. The cells were passaged and resuspended at $15x10^6$ cells/ml in sterile polymer solution (10% PEG-PQ-PEG in HBS with 3 mM PEG-RGDS, 1.5% TEOA, 3.4 µl/ml NVP, and 5 µM eosin Y). Non-immobilized hydrogel disks 127 µm thick, 500 µm diameter were prepared using a slight modification to the standard protocol. Specifically, a 127 µm spacer was used in place of the 380 µm spacer and gels were punched with a 500 µm biopsy punch after gelation. Blank hydrogel disks without cells were prepared in a similar manner. Viability of the encapsulated cells was determined with a Live/Dead staining kit (Invitrogen) as previously described in section 2.3.12.

The hydrogel disks were implanted in the cornea of *Flk1-myr::mCherry* transgenic mice[125] in a modified version of the cornea micropocket angiogenesis assay as described by Poché *et al.*[126] Briefly, a partial thickness incision was made in the cornea and the corneal layers were separated using a Von Graefe knife to create a micropocket approximately 700 µm in length and 300 to 400 µm from the limbic vasculature. Blank or cell-encapsulated hydrogel disks were then inserted and the pocket was allowed to seal closed naturally. Non-implanted gels from each group were also maintained in NE-GFP-4C media *in vitro* and imaged after 3 days by brightfield

(Zeiss Axiovert 135) and confocal microscopy (Zeiss LSM 510 META). After 3 and 7 days, mice were euthanized and the corneas were removed and fixed in 4% PFA prior to flat-mounting and imaging on a confocal microscope (Zeiss LSM 510 META). All animals were used under a protocol approved by the American Association of Laboratory Animal Science and the Institutional Animal Care and Use Committee at Baylor College of Medicine.

4.3.5 Statistical Analysis

Significance was determined via unpaired, two-tailed *t*-test when $p < 0.05$. Error bars in figures depict standard deviations for the data sets.

4.4 Results and Discussion

The primary goal of this work is to characterize the CTX0E03 cell line with regards to its angiogenic potential, and to demonstrate the utility of the hydrogel scaffold for investigation of NSC-induced angiogenesis both *in vitro* and *in vivo*. For initial cell characterization, the CTX0E03 line was investigated as cultures on laminin-coated TCPS.

4.4.1 Characterization of NSC Pro-Angiogenic Features

It has been previously claimed that neural stem cells are capable of transdifferentiation to adopt a smooth muscle or pericyte fate.[123,124] Studies investigating this phenomenon reported that low cell density is one way to drive this differentiation pathway.[123] To test if the CTX0E03 cell line can develop smooth muscle cell characteristics, the cells were seeded at high and low densities on laminin coated TCPS and cultured in differentiating media. Following the differentiation period, the cells were assessed for morphology, angiogenic growth factor expression, and expression of smooth muscle alpha-actin. Figure 52-A and B shows the representative morphology of cells that had undergone either high or low density differentiation. A marked

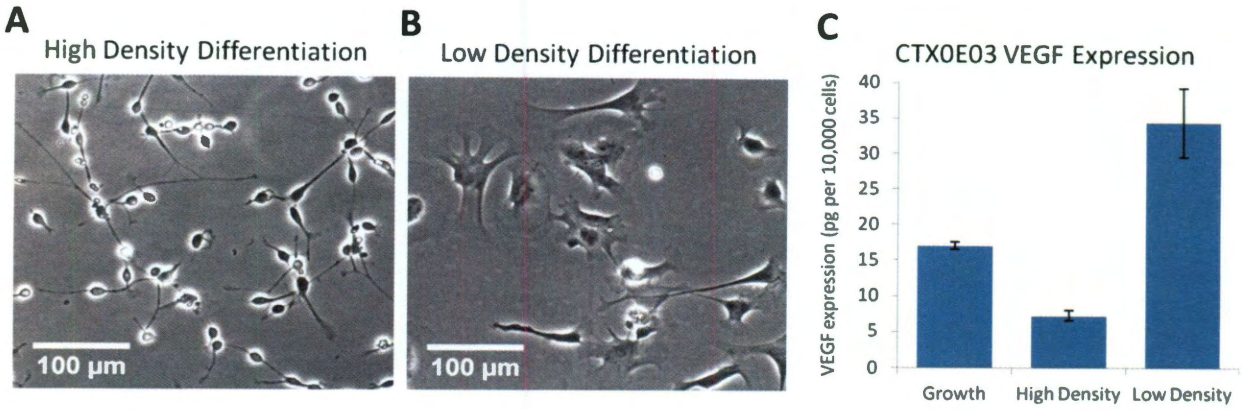

Figure 52. Representative phase contrast images show elongated, neuronal-like morphology of the CTX0E03 cells after high density differentiation (A) compared to the larger, spread cell morphology observed following low density differentiation (B). Normalized VEGF expression from the two differentiated cell cultures compared to cells in growth media show dramatically higher VEGF expression from the low density differentiated cells. All groups are significantly different from each other with $p < 0.05$.

difference is observed between the two conditions. Specifically, the high density differentiated culture primarily appears as small, highly elongated cells with a neuronal-like extensions and morphology. The low density differentiated culture, in contrast, generally showed much larger, spread morphology on the laminin-coated surface with lamellipodia-like projections along the cell edge. Such a dramatic difference in cell morphology provides strong evidence that the cells have differentiated along distinct lineages. An ELISA assay allowed comparison of secreted VEGF by the cell cultures from each condition and is quantified in Figure 52, C. It was found that when cultured in expansion media, CTX0E03 cells produce approximately 17 pg VEGF/10^3 cells over a period of 48 h. Following high density differentiation, the production of this angiogenic growth factor is significantly reduced to about 7 pg VEGF/10^3 cells. Low density differentiation, however, more than doubles the growth factor production. An increase in VEGF production suggests that these low density derived cultures are more inclined to interact with the vasculature and endothelial cells for example in an *in vivo* setting.

A final analysis of these two differentiated cultures was achieved by immunostaining against a marker of smooth muscle cells, α-SMA. In Figure 53-A and B, representative phase contrast images again show the difference in cell morphology. A small percentage of cells in the high density group are observed to express the α-SMA marker (Figure 53-C). For the low density group, however, the majority of the cell population was found to strongly express this cytoskeletal protein (Figure 53-D).

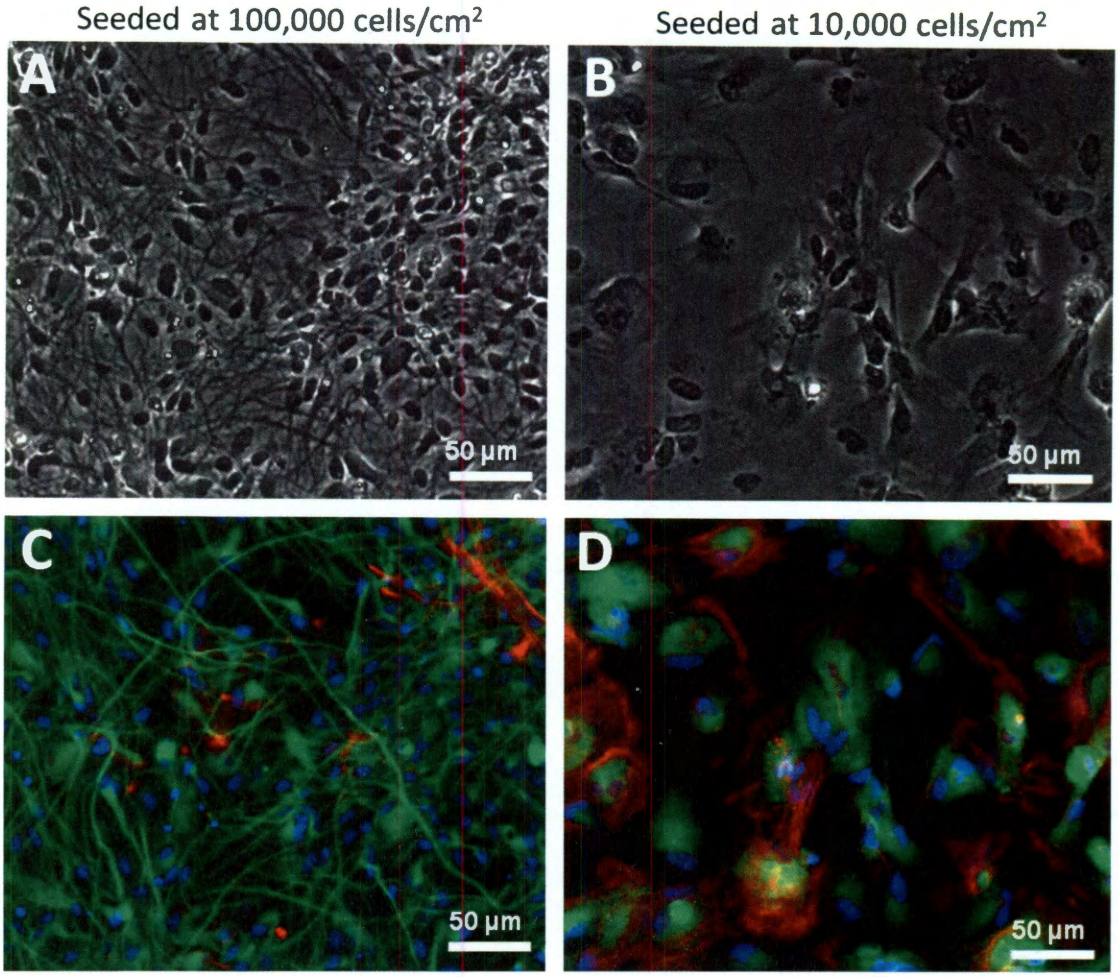

Figure 53. Representative phase contrast (A, B) and fluorescent images (C, D) of CTX0E03 cells differentiated at high density (A, C) or low density (B, D). Immunostaining was performed against neuronal βIII Tubulin (green) and α-SMA (red) with a nuclear counterstain (DAPI, blue). Low density differentiation was found to drive a large portion of the cell population towards a spread, α-SMA positive phenotype.

Although identification of α-SMA protein by immunostaining does not confirm smooth muscle or pericyte differentiation, it does provide additional evidence that CTX0E03 cells differentiated at low density are driven towards a much different phenotype than the elongated, neuronal and glial populations resulting from higher seeding densities. Furthermore, the cell-density dependent results observed here are in agreement with previously published literature concerning the possibility of a smooth muscle fate from cortical neural stem cells.[123]

It is important to remember that *in vitro* culture conditions (2D surface, monoculture interactions) are vastly different from the environment in which a neural stem cell would reside in the body. It is possible that the artificial conditions created here have resulted in aberrant differentiation of the cells which would not naturally occur otherwise. This work indicates only that the neural stem cells may retain the capacity to develop along an α-SMA-positive, VEGF secreting lineage, however further work would be required to investigate if this behavior is observed for NSCs *in vivo*.

4.4.2 NSC Co-culture with Endothelial Cells

It has been previously shown that co-cultures of pericyte precursors cells and endothelial cells can organize into a primitive vascular plexus.[71] Furthermore, endothelial cells co-cultured with neural stem cells have also be observed to self-organize *in vitro* and *in vivo* to a greater extent than the endothelial monoculture.[127,128] The bioactive hydrogel scaffold developed in this work provides an excellent environment for studying the angiogenic properties of the CTX0E03 neural stem cell line in a functional co-culture with endothelial cells. Importantly, the hydrogel provides minimal intrinsic bioactivity, which could interfere or confound the results.

To study this interaction, primary endothelial cells (HUVECs) were encapsulated alone, or in a 4 to 1 ratio with neural stem cells and maintained in HUVEC media for one week before fixation

and staining against cell-specific markers: CD-31 for endothelial cells and nestin for neural stem cells. Staining against α-SMA was also performed to determine if any of the neural stem cells expressed this smooth muscle cell marker. Confocal z-projections of the immunostained samples are shown in Figure 54. It can be observed that little or no organization occurred for the HUVEC monocultures. In contrast, co-cultured samples show development of a robust, interconnected network. Occasional α-SMA-positive cells were identified primarily along nestin-positive cell clusters as shown in Figure 54-B. The interface between these two conditions was also investigated by placing the monoculture and coculture hydrogel solutions in direct contact prior to gelation (Figure 55). Again, minimal spreading is visible on the HUVEC- only side of the dual-hydrogel construct, while the coculture region shows extensive spreading and organization.

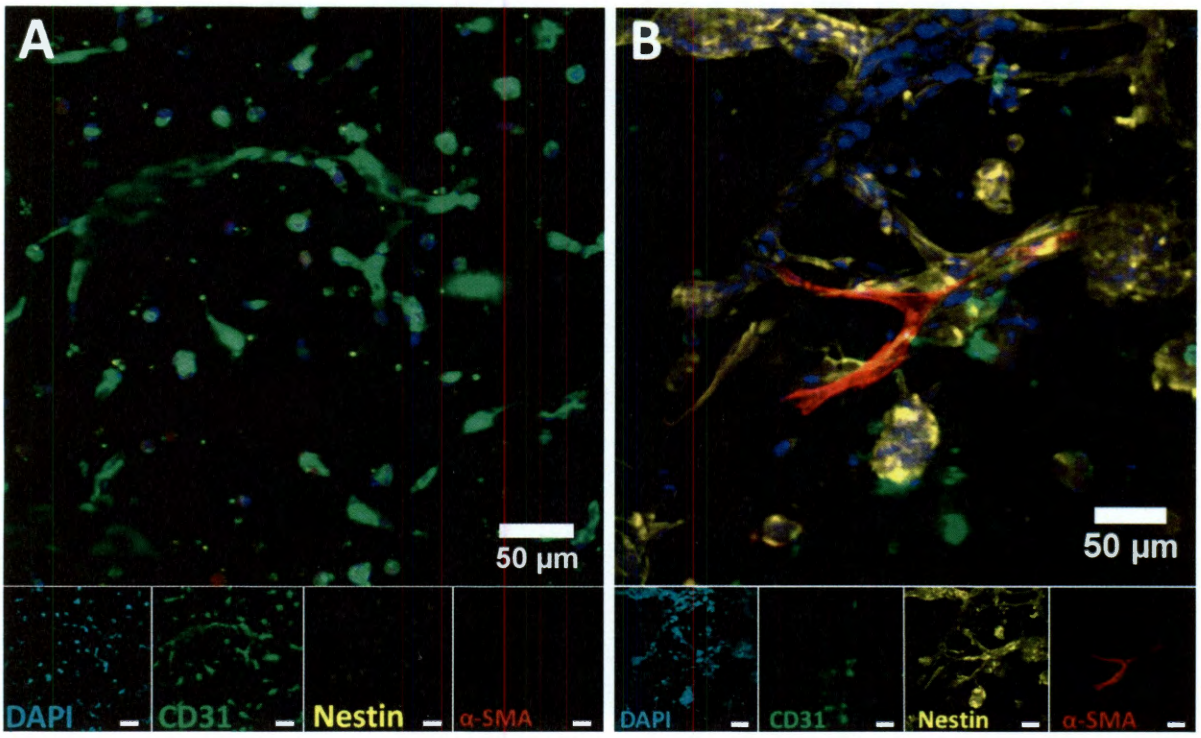

Figure 54. Confocal z-projections of an encapsulated HUVEC monoculture (A) and a 4:1 coculture of HUVECs and CTX0E03 neural stem cells (B). Minimal organization and cell elongation was observed for the encapsulated endothelial cells after 1 week in culture in the 3D hydrogel environment. The coculture with neural stem cells, however, showed extensive spreading and network formation, with occasional cells expressing α-SMA marker.

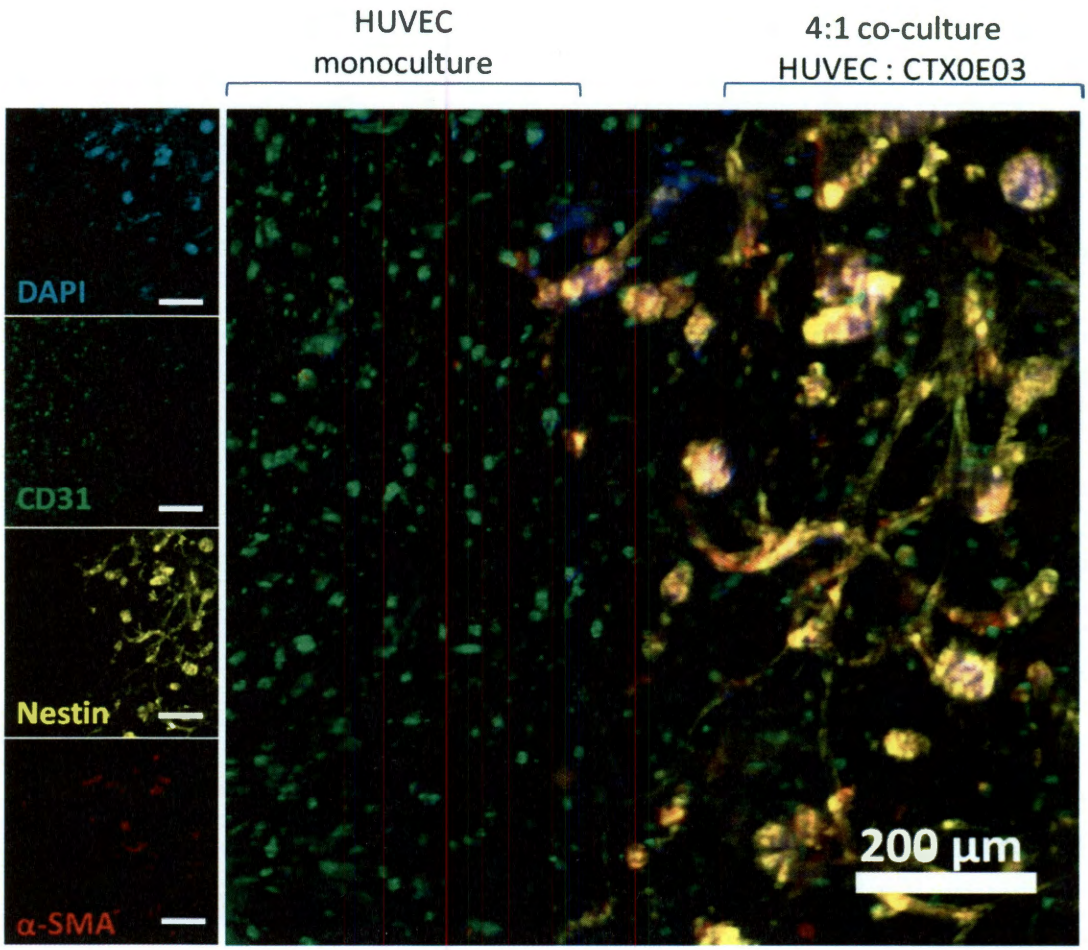

Figure 55. Confocal z-projection of the interface between a monoculture encapsulation of HUVECs and a 4:1 coculture with neural stem cells. Minimal organization is observed for endothelial cells alone; however co-encapsulation with neural stem cells resulted in the formation of an extensive 3D cellular network.

One unexpected finding apparent in all of these samples was the low frequency of CD31 positive cells in the coculture at the end of the incubation period. Observation of CD31 positive cells in the monoculture side of the dual-hydrogel sample (Figure 55) indicates that this loss of CD31 is a result of direct cell contact or short acting signals and not a secreted factor in the media of the culture. Additional studies are needed to determine if this observation is a result of down-regulation of the CD31 protein, or reduced viability of the endothelial population. It is proposed that time-lapse imaging or analysis of the cultures at earlier time points would be especially helpful in understanding the interactions within this complex system.

Although the CD31 marker is not prevalent in the coculture system, the tubule-like organization of the cells is similar to the primitive vascular networks formed by endothelial cells in 3D culture. Furthermore, spreading of α-SMA positive cells along these tubule networks is comparable to the arrangement of mural cells *in vivo,* where they extend along and stabilize the vasculature. Further investigation to verify the presence of a lumen in the cocultures structures are recommended in order to confirm vasculogenesis has occurred. Substitution of HUVECs with brain derived endothelial cells is also recommended for future studies in order to provide a more relevant coculture interaction similar to what would be found in the *in vivo* NSC niche. Although significant work remains, these preliminary studies demonstrate the utility of the hydrogel scaffold for investigating the interactions between endothelial cells and neural stem cells *in vitro*.

4.4.3 Cornea Micropocket Assay of NSC-Induced Angiogenesis

To investigate the angiogenic nature of NSCs in an *in vivo,* the cornea micropocket angiogenesis assay was employed. This assay is well established for the study of soluble signals that may promote or inhibit a vascular response in the animal model. For this technique, the factor of interest is typically loaded into a Hydron pellet and implanted into a small pocket that has been surgically generated between the outer layers of the cornea.[129] Diffusion of an angiogenic growth factor such as VEGF from the implanted device induces the limbic vessels at the base of the eye to sprout and grow in the direction of the growth factor gradient. As the cornea is normally an avascular tissue, the relative strength of this angiogenic response can be easily measured against a neutral background.

Recently, a modification of this protocol has been published in which the Hydron pellet was replaced with a PEGDA based hydrogel as the source of the angiogenic factors.[126] For this thesis

work, the hydrogel was investigated as a platform for the delivery of pro-angiogenic signals from encapsulated NSC cultures in the absence of exogenous signaling proteins.

To aid in the identification of the neural stem cells following implantation, the CTX0E03 cell line was replaced with a commercially available NSC line, NE-GFP-4C. These cells are derived from embryonic mice and have been transfected to constitutively express GFP. Lower risk of an immunogenic response is another expected benefit of the NE-GFP-4C cell line as compared to the xenogeneic, human-derived CTX0E03 line. An initial, proof of concept study was conducted to verify that the cells could be encapsulated in appropriately sized hydrogel disks for *in vivo* implantation with minimal impact on cell viability. The small dimensions of the corneal pocket as generated in the mouse model restricts the size of the construct to approximately a 500 µm diameter by 200 µm thick disk. The standard protocol for hydrogel synthesis was thus modified by using 127 µm thick PDMS spacers and punching with a 500 µm diameter biopsy punch after gelation. As shown in Figure 56-A and B, this process was successful in producing appropriately sized hydrogel constructs while maintaining high viability of the encapsulated NE-GFP-4C cells. After 3 days culture *in vitro,* the cells were observed to develop into dense, neurosphere-like

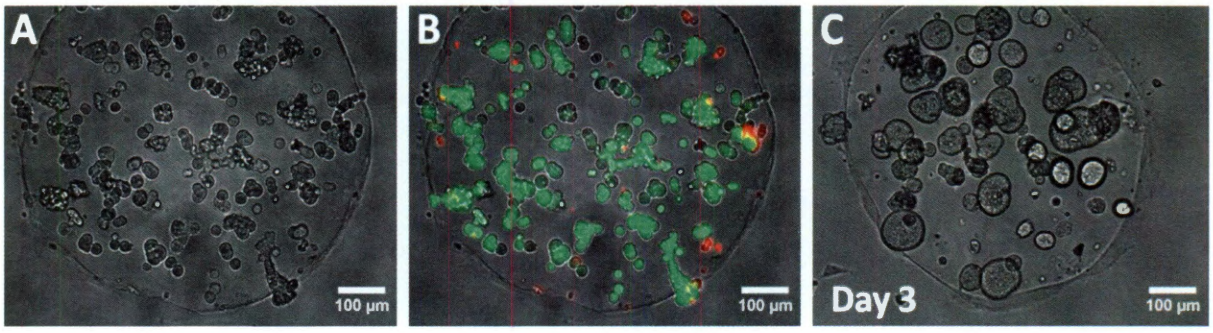

Figure 56. Brightfield (A) and brightfield/fluorescent overlay (B) of an encapsulated NE-GFP-4C culture stained with calcein AM (live, green) and ethidium homodimer (red, dead) to show cell viability. Representative Brightfield image of the encapsulated cells after 3 days in culture *in vitro* (C) shows development of neurosphere-like clusters indicating that the cells are proliferating within the hydrogel scaffold.

clusters as shown by the brightfield image in Figure 56-C. The formation of these aggregates indicates that the cells survived the encapsulation process and are proliferating within the hydrogel scaffold. Confocal images from several of these clusters confirm GFP expression by the encapsulated cells (Figure 57-A, B, and C). It was also noted that expression of the fluorescent protein varied both between cell clusters and among individual cells within a single cluster. Variation in gene expression is a common challenge with transfected cell lines. For the purposes of this experiment it should be considered that not all implanted cells will be traceable *in vivo*.

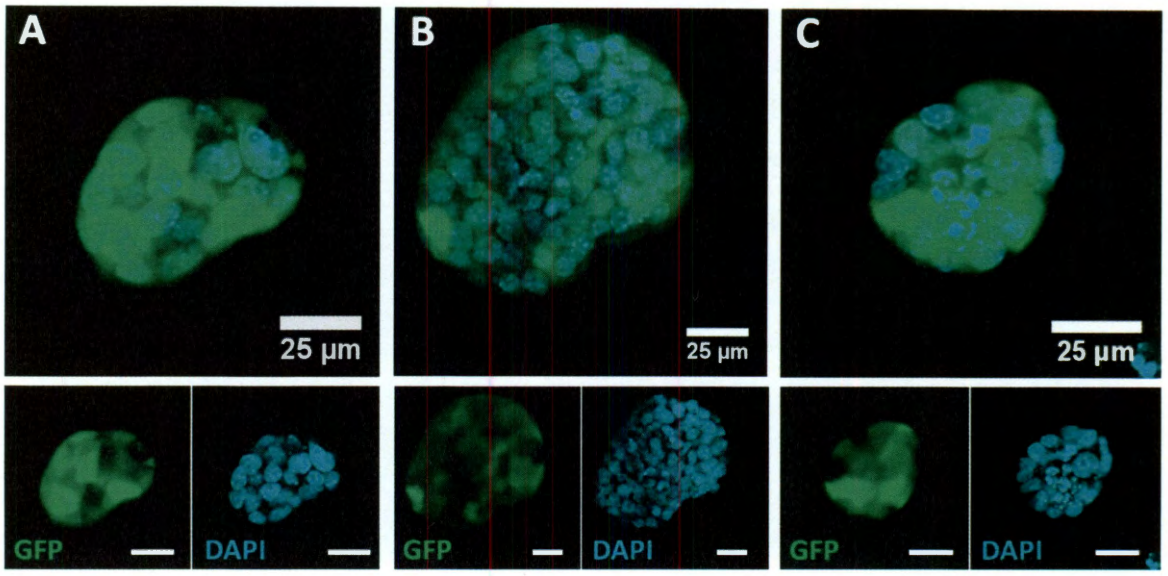

Figure 57. Confocal images from three different NE-GFP-4C clusters (A, B, and C) formed after 3 days *in vitro* in the hydrogel scaffold. Varying levels of GFP expression were observed between the individual cells.

A preliminary study in which these encapsulated cell constructs were implanted in the cornea micropocket assay resulted in similar development of the neurosphere-like clusters after 3 days *in vivo* (Figure 58). Fluorescent imaging of a fixed and flat-mounted sample identified many of these clusters as GFP positive (Figure 58-B, C), showing that the implanted cells continue to express the label and can therefore be distinguished from the host tissue.

heterogeneous expression of the GFP label by the implanted cells at this time point.

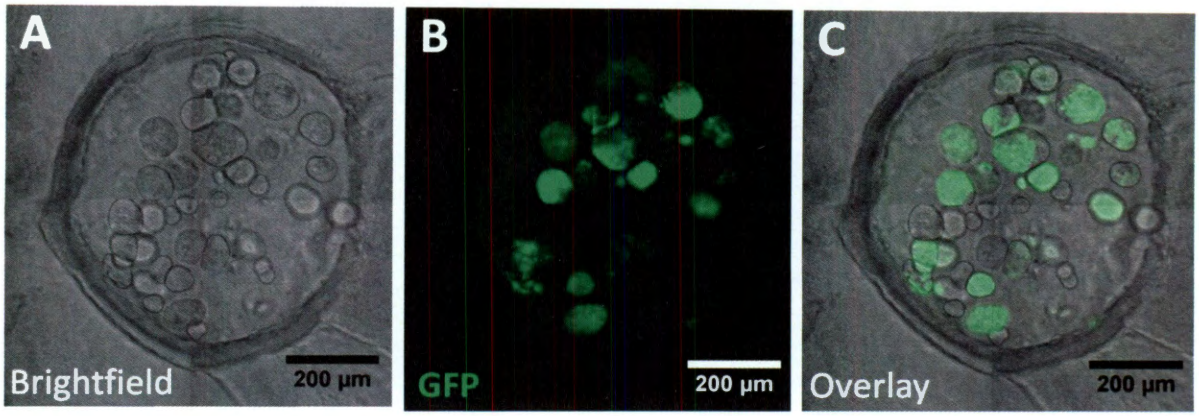

Figure 58. Brightfield (A), fluorescent (B), and overlay image (C) of hydrogel-encapsulated NE-GFP-4C cells 3 days after implantation in the mouse cornea. Cells were observed to form neurosphere-like clusters indicating cells survived and proliferated in the *in vivo* environment. Fluorescent image shows heterogeneous expression of the GFP label by the implanted cells at this time point.

At 7 days post-implantation, a portion of the encapsulated cell constructs were observed to have stimulated an angiogenic response from the limbic vessels in the animal model based on visualization of mCherry-labeled blood vessels extending toward the implant (Figure 59). For hydrogels implanted without encapsulated cells, no angiogenic response was observed. The growth of vessels toward the cell-laden hydrogel is similar, though not quite as extensive, as observed in previously published work with hydrogels releasing an angiogenic growth factor such as VEGF.[71] Additionally in these samples, GFP-positive neural stem cells were no longer isolated to the cell clusters but had migrated outward across the region covered by the implanted hydrogel. Figure 59-A shows a low magnification image of the edge of a hydrogel construct where one can see the spreading GFP-positive cell population as well as the in-growing vascular network. Higher magnification of the interaction between these host vessels and the implanted neural stem cells is provided in Figure 59-B. This close interaction, as well as the overall induction of vessel in-growth, provides evidence that soluble, angiogenic signals were secreted by the implanted cells. Further studies are recommended to identify which

factors are involved in promoting this response and to discover whether the NE-GFP-4C cells are differentiating in the *in vivo* microenvironment.

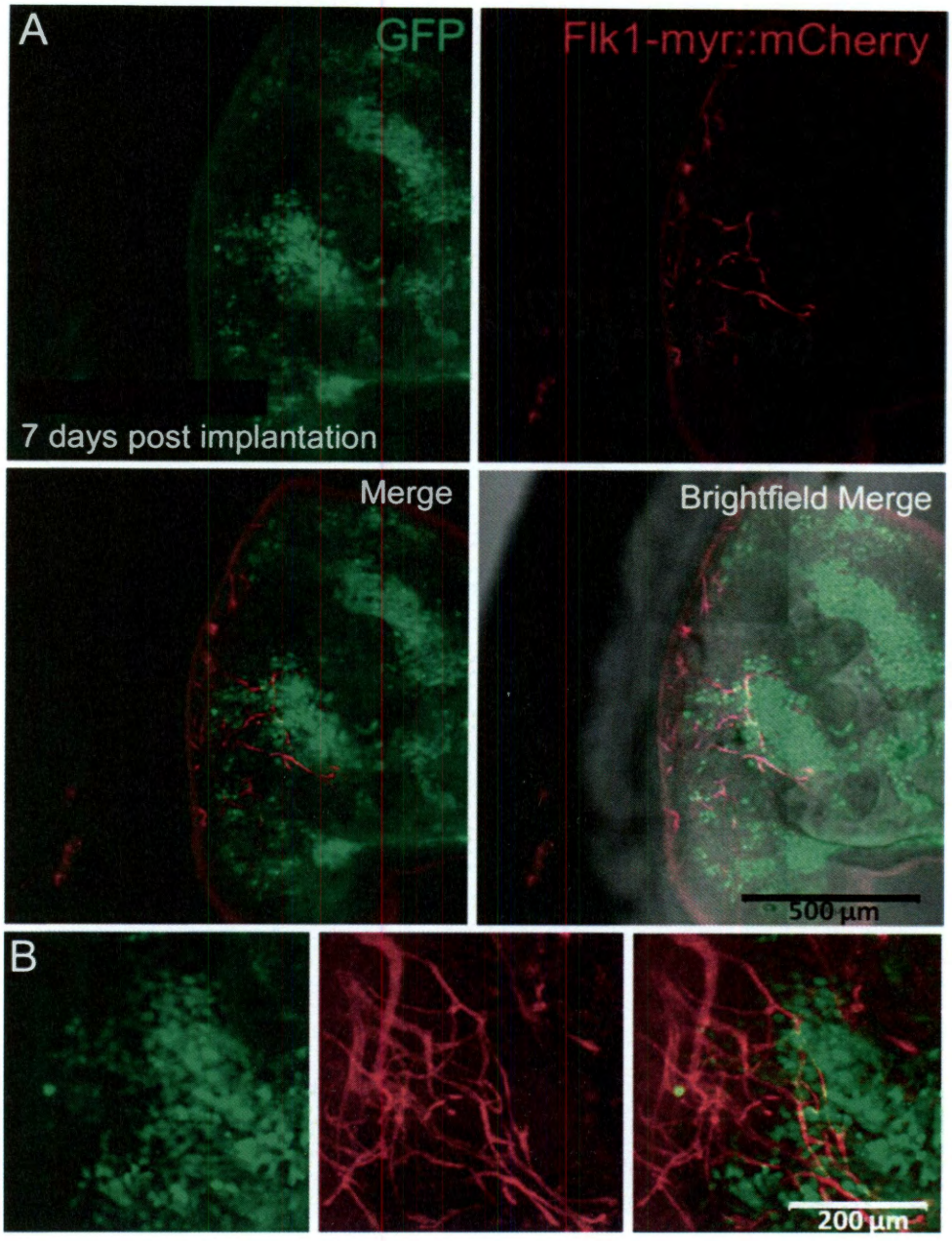

Figure 59. Low magnification (A) and high magnification (B) fluorescent and brightfield overlay images of a hydrogel disk with encapsulated NE-GFP-4C cells 7 days after implantation in the mouse cornea. At this time point, GFP-labeled NSCs (green) were observed to have escaped the dense cell clusters and are spread across the area of the hydrogel. Z-projection of the mCherry channel (red) shows an influx of host vasculature has occurred from the limbic region and is intimately associated with the NE-GFP-4C population.

4.5 Conclusions

Overall, the work presented in this chapter provides preliminary evidence of the pro-angiogenic nature of neural stem cells. The CTX0E03 cell line was confirmed to express VEGF under growth conditions and more strongly when the cells were differentiated in low density conditions. The low density differentiated cultures may also present the possibility of pericyte or smooth muscle lineage commitment based on up-regulation of α-SMA. Smooth muscle and endothelial cell types have both been reported previously from differentiated neural stem cells, suggesting the potential for NSCs to play a direct role in the formation of new vasculature. A more rigorous analysis of the culture generated here, however, is required to fully identify and characterize the low density differentiated population.

Although co-culture interactions between neural stem cells and endothelial cells have been investigated previously in the literature, these studies were primarily limited to 2D substrates or difficult-to-control, natural matrices. It was demonstrated here with a coculture of human NSCs and primary endothelial cells, that the bioactive hydrogel scaffold can provide a suitable 3D environment with precisely controlled biochemical properties for more elegant investigation of these complex, cell-cell interactions. After 7 days *in vitro,* the coculture encapsulations underwent dramatic organization to form an interconnected cell network, while little or no organization occurred for the monoculture of endothelial cells. Further characterization of this network is recommended to determine if any of the structures had luminized, as would be expected in a primitive vascular plexus. Spatial control of the encapsulated cell populations was also demonstrated in a simple, binary hydrogel. For more advanced patterning experiments and control of cell-cell interactions, mask-based or confocal patterning may be employed.[130,131]

The ability to induce vessel growth *in vivo* is ultimately the most relevant test for determining the pro-angiogenic characteristics of a growth factor or cell population. In the preliminary studies presented here, the cornea micropocket angiogenesis assay was therefore used to observe the vascular response to hydrogel-encapsulated neural stem cells in a rodent model. It was found that the hydrogel scaffold successfully supported the delivery and proliferation of GFP-labeled NSCs over a period of 7 days after implantation. Furthermore, a portion of the constructs facilitated both vessel in-growth and outward migration of the neural stem cells from the scaffold. The observation of a vascular response for implanted cell constructs that had not been augmented with any exogenous growth factor provides strong evidence that the NSC themselves are a source of pro-angiogenic signals.

5 Development of a Microencapsulation Technique for NSC Delivery

Much of the work in this section was published in: Franco CL *et al.* "Development and optimization of a dual-photoinitiator, emulsion-based technique for rapid generation of cell-laden hydrogel microspheres." *Acta Biomaterialia*. 2011; 7(9)3267-76.

5.1 Introduction

5.1.1 Neural Stem Cell Therapies

Current clinical trials involving neural stem cell delivery are promising[27,28,40,80,132,133], however cell survival and engraftment is still limited[27,41,134], possibly reducing the potential therapeutic effects. These approaches generally involve the injection of a cell suspension directly into the target location. Cell survival is impacted by both mechanical injury during the injection process, and also the cellular microenvironment of the implantation site, which may not be ideal for maintaining viability due to the extent of tissue disease or injury, or simply because the cells are introduced to a non-native environment. Active clearance of implanted cells by the host immune response is another concern especially when a non-autologous cell source is used.

Encapsulating cell therapies within a supporting matrix can provide valuable protection during delivery, physically restrict cells to the target site, and isolate cells from a potentially hostile immune response. Additionally, this approach provides a means to control the microenvironment to which an implanted cell is initially exposed. Controlling the biochemical environment may be critical for improving the success of NSC therapies since these cells are naturally supported by a highly specialized niche as discussed in detail in Chapter 1.[4,5,47,135,136]

Another consideration for neural tissue engineering is that any kind of cell-scaffold construct must be deliverable via injection in order to limit damage to the surrounding brain tissue.[137] Two main approaches for injectable systems have so far been investigated in the literature. One strategy employs a hydrogel scaffold that, while liquid during injection, forms a suitable matrix once in the body. Thermoresponsive hydrogels are designed to transition from a liquid at RT to a more solid like construct at physiological temperatures.[75,137,138] Following injection into the damaged tissue, the material mixed with cells slowly sets, encapsulating the cells in a soft matrix *in situ*.[138] Thermoresponsive materials used for neural tissue engineering have so far been exclusively naturally derived, and include cellulose-based, chitosan-based, and collagen-hyaluronan based matrices.[75,137,138] Promising compatibility with neural stem cells has been shown *in vitro,* however it has not yet been demonstrated if these systems will succeed in an animal model.[139] In addition, a bulk encapsulation approach such as this may lead to cell death and necrosis at the core of the construct if its dimensions are larger than the oxygen and nutrient diffusion limit.[140] The other approach for brain tissue engineering involves microencapsulation of cells within small particles of a cross-linked matrix prior to implantation.[139] The size and shape of the material is controlled such that injectable delivery can be maintained.

5.1.2 Strategies for Microencapsulation

Historically, cell microencapsulation has been primarily studied as a method for immunoisolation.[141-149] By far the most common technique involves alginate-based materials that are cross-linked by ionic interactions as droplets come into contact with a cationic solution.[146-148,150-152] When the ultimate therapeutic goal is engraftment of the encapsulated cells, however, these alginate systems are not ideal since they do not degrade in a controlled

manner. [140] Additional concerns include batch to batch variability for naturally derived materials and possible toxicity from the polycations used during crosslinking, which may induce an inflammatory response following implantation.[146,149] Several alternative materials for cell encapsulation have also been investigated, including synthetic polymers such as PEG diacrylate and polyvinylalcohol.[146,147,153,154] These can offer benefits such as reduced immunogenicity and greater control over mechanical stability and degradation.[146]

The benefits of providing a physical support when attempting to repair and regenerate neural tissue was demonstrated by Park *et al.* in 2002.[155] The researchers had previously observed that suspensions of NSCs injected into a region of the brain damaged by hypoxic ischemia could engraft and survive only along the edges of the infarct zone.[155] According to their hypothesis, the central area of damage is primarily a liquid-filled cavity and does not maintain enough physical structure to support the cells. When the neural stem cells were seeded onto the surface of small polyglycolic acid (PGA) scaffolds, they could be implanted into the defect by glass micropipette.[155] The polymer provided artificial support, termed a bio-bridge, which provided both implanted and host cells a structure for growth and migration (Figure 60).[155]

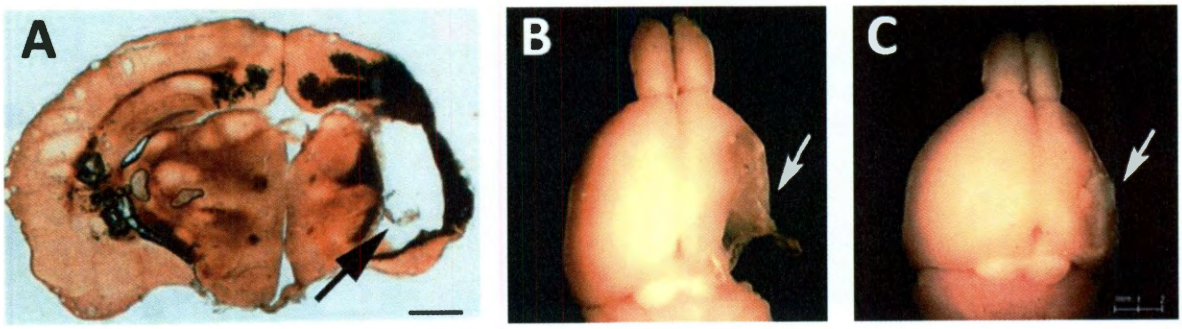

Figure 60. Comparison of different treatment groups in a stroke injured rat brain model.[155] Injection of cell suspension alone (A) showed extensive engraftment (dark staining) at the edges of the infarct region (arrow) but no new tissue formation. Non-treated brain (B) showed no new tissue filling the infarct region (arrow). Implantation of PGA with encapsulated NSCs (C) filled region of infarct and improved survival of engrafted cells. [155] Figure from Park *et al.* 2002.

Histology showed extensive neuronal differentiation from the implanted NSCs, however it was not demonstrated whether the resulting cells were functional or integrated with the existing circuitry.[155] In 2009, Modo *et al.* showed that similar, poly(lactic acid-co-glycolic acid) (PLGA)-based particles could be used as microcarriers for NSC therapy in rats, however functional improvement was not measured.[156] It is important to note that both PGA and PLGA materials degrade hydrolytically into acidic products with potentially detrimental effects on implanted cells and surrounding host tissue. A more biocompatible scaffold, for example poly(ethylene glycol) hydrogels, could provide a better alternative for delivery and support of implanted cells in this type of approach.

5.2 Objectives

As demonstrated in previous sections, the biochemical properties and degradation of PEG-based scaffolds can be precisely controlled to support encapsulated NSCs *in vitro*. The hydrogel material itself, however, had been synthesized in a form unsuitable for injectable delivery. In preparation for therapeutic applications, a simple but highly tunable method was thus developed for emulsion-based generation of PEG microspheres. Rapid crosslinking of suspended polymer droplets was achieved through the use of a unique combination of photoinitiators added to both phases of the system. Compatibility with cell encapsulation was demonstrated with three relevant cell lines *in vitro.* NIH-3T3 fibroblasts, MHP36 neural stem cells, and bEnd.3 brain endothelial cells provided varying morphologies, adhesion preferences, and matrix-metalloproteinase expression to fully explore the potential of the encapsulation system. Finally, through collaboration with researchers at King's College, London, the hydrogel microspheres were demonstrated to successfully deliver a cell-based therapy in a model of ischemic stroke.

5.3 Materials and Methods

All materials were purchased from Sigma unless otherwise noted.

5.3.1 Cell Culture

Conditionally immortalized neural stem cells (MHP36 line[34,157] passage 56 to 62), were generously donated from the lab of Dr. Jack Price. The cells were cultured on fibronectin-coated TCPS flasks, which were prepared by applying 0.07 ml per cm^2 of a 0.01 mg/ml solution of fibronectin to the surface for 15 min at RT. Cells were cultured in DMEM/F12 supplemented with 0.03% BSA, 94 μg/ml apo-transferrin, 15.3 μg/ml putrescine dihydrochloride, 4.7 μg/ml insulin, 380 ng/ml L-thyroxine, 317 ng/ml tri-iodo-L-thyronine, 1.9 mM L-Glutamine, 58 ng/ml progesterone, 38 ng/ml sodium selenite, 9.4 units/ml heparin sodium salt, 10 ng/ml basic-FGF, 1.2 ng/ml interferon, 100 U/ml penicillin, and 100 μg/ml streptomycin. The cells were incubated at 33 °C in a 5% CO_2 environment. Murine brain microvascular endothelial cells (bEnd.3, ATCC, passage 25 to 30) were cultured in High Glucose DMEM (Invitrogen) with 2 mM L-glutamine, 10% FBS, 100 U/ml penicillin, and 100 μg/ml streptomycin at 37 °C in a 5% CO_2 environment. NIH-3T3 fibroblasts (ATCC, passage 128 to 135) were cultured in High Glucose DMEM, with 2mM L-glutamine, 10% bovine calf serum, 100 U/ml penicillin, and 100 μg/ml streptomycin at 37° C in 5% CO_2 environment.

5.3.2 Characterization of Cellular MMP Expression

Relative collagen-specific MMP expression was determined by gelatin zymography of the cell culture supernatants. Cells were seeded in 48 well TCPS plates with 400 μl media per well. Seeding densities were chosen such that the cell cultures remained subconfluent after a 48 h incubation period. MHP36 and 3T3 cells were seeded at 20,000 cells/cm^2, and bEnd.3 cells were

seeded at 5,000 cells/cm^2. Appropriate media and culture conditions (as described above) were used for each cell type. After 48 h incubation, the media was collected and stored at -20 °C, and the cells trypsinized and counted by hemacytometer. Zymography was performed using a 10% gelatin precast Ready Gel (BioRad) according to manufacturer's protocol. Briefly, media samples were diluted 1:1 with loading buffer (125 mM Tris-HCl, pH 6.8, 20% glycerol, 4% SDS, 0.005% Bromophenol Blue) and run at 100 V for 2 h. The gel was then soaked for 30 min each in renaturing buffer (2.5% Triton X-100 in MilliQ H_2O) and then developing buffer (10mM Tris base, 40mM Tris-HCl, 0.2M NaCl, 5mM $CaCl_2$, 0.02% Brij 35) at RT. Fresh developing buffer was then added and the gel incubated at 37 °C overnight with gentle agitation. The gel was stained with Coomassie blue (Sigma) for 1 h at RT and destained with Coomassie destain solution (Methanol:Acetic acid:Water (5:1:4)) for 30 min before imaging (LAS4000 Imager, Fujifilm) and analysis in ImageJ. Band intensity was normalized to the cell count at the 48 h time point.

5.3.3 Development of Emulsion-based Microsphere Synthesis

A consistent protocol for attempting emulsion-based microsphere synthesis was maintained for all studies. In this approach, 20 µl of a hydrogel precursor solution was added to 1 ml of mineral oil in a glass test tube (13 mm by 75 mm), vortexed (Vortex Genie2, VWR) at full speed for 3 s, and exposed to light from a metal halide lamp (Dolan-Jenner) for 25 s. The lamp was modified with heat-absorbing and UV-blocking optical filters (Edmund Optics) to define an excitation range of 365 to 700 nm light. Light exposure was limited to 25 s since microdroplets settle out of solution rapidly and can result in phase separation beyond this time period. Cross-linked hydrogel particles were then separated from the mineral oil by addition of 500 µl of PBS and centrifugation at 300 xg for 2 min. The oil layer was removed by aspiration, and the wash step

was repeated with an additional 500 µl PBS. Finally, the re-suspended microspheres were transferred to a multiwell plate for imaging and further characterization.

The synthesis protocol was first investigated with a single photoinitiator added only to the hydrogel precursor solution (10% 10 kDa PEGDA in HBS). For testing of 2-2-dimethoxy-2-phenyl acetophenone (also known as Irgacure 651, I651) initiated cross-linking, an I651 stock solution (300 mg/ml in NVP) was added at 10 µl/ml to the precursor solution. For testing of eosin Y initiated cross-linking, the precursor solution was supplemented with 3.4 µl/ml NVP, 1.5% TEOA, and 10 µM eosin Y. Microsphere synthesis was attempted according to protocol and the product analyzed for the presence of cross-linked particles. To investigate the effects of a dual combination of photoinitiators, the polymer solution was supplemented with 3.4 µl/ml NVP, 1.5% TEOA, and 10 µM eosin Y, while additionally the oil phase was supplemented with 3 µl/ml of I651 stock solution. Finally, in order to isolate the effect of the oil phase photoinitiator, the synthesis protocol was conducted with 3 µl/ml of I651 stock solution added to the oil phase and no photoinitiator in the precursor solution. All samples were imaged under brightfield microscopy with a ProgRes C5 (Jenoptik) CCD camera mounted to a Zeiss Axiovert 135 inverted microscope. For improved visualization, 0.04% trypan blue solution[158] was added and samples incubated for a minimum of 4 h before imaging on a dissecting microscope affixed with the CCD camera.

The dual photoinitiator combination for microsphere synthesis was further investigated by varying initiator concentrations and adding a cell-compatible surfactant, pluronic F68.[159] Hydrogel precursor solution was formed by mixing 10% 10 kDa PEGDA (refer to Chapter 2 for synthesis of this compound) in HBS containing 3.4 µl/ml NVP and 1.5% TEOA both with and without 0.1% pluronic F68. Eosin Y photoinitiator was added to the solutions at final

concentrations of 0, 5, 10, or 15 μM. Separately, sterile light mineral oil was supplemented with 0, 1, 3, or 5 μl/ml of I651 stock solution. For all combinations of initiator concentrations with and without the surfactant, microspheres were generated and collected in multiwell plates according to the described protocol. To determine particle yield and size distribution, all samples were stained with 0.04% trypan blue and imaged on a dissecting microscope affixed with the ProgRes C5 CCD camera. ImageJ software was used to threshold, watershed, and finally analyze the stained-particle images to produce a particle count per view field and histogram of particle diameters. For analysis of particle diameter distribution, three fields of view (>900 individual microspheres) were analyzed for each group.

5.3.4 Microspheres as Surface Seeded Carriers

The ability of the hydrogel microspheres to function as microcarriers for surface-seeded cell culture was evaluated by incorporating the fibronectin-derived RGDS adhesive peptide sequence. Non-degradable polymer solution (HBS with 10% PEGDA, 1.5% TEOA, 3.4 μl/ml NVP, and 10 μM eosin Y) was prepared both with and without 0.1% pluronic F68. To an aliquot of each solution, PEG-RGDS (refer to Chapter 2 for synthesis of this compound) was added at 3 mM and all solutions were sterilized via filtration through and 0.2 μm membrane. To form bulk hydrogel disks, a 10 μl droplet was sandwiched between sterile glass slides separated by 380 μm polydimethyl siloxane (PDMS) spacers. After exposure to 25 s of white light, the hydrogel disk was transferred to the well of a 24 well plate containing 500 μl sterile PBS. This process was repeated to prepare an N of 3 for each solution. Microspheres were also formed from each of the precursor solutions using the previously described emulsion-based protocol (section 5.3.3) and mineral oil containing 3 μl/ml I651 stock solution. Particles were washed with PBS and transferred to a 24 well plate. The disks and microspheres were incubated overnight at 37 °C

and finally the PBS was replaced with NIH-3T3 culture media. 3T3 fibroblast cells were passaged and seeded onto hydrogels at 3,000 cells/cm^2 for bulk disks or 3,000 cells per µl of microspheres. After 24 h, the cultures were imaged under brightfield microscopy (Zeiss Axiovert 135). Percent cell attachment was quantified across three fields of view for the seeded microspheres.

5.3.5 Microencapsulation and *In Vitro* Cell Culture

NIH-3T3 fibroblasts, MHP36 neural stem cells, and bEnd.3 endothelial cells were each tested independently with the microencapsulation protocol to observe the effect of encapsulation conditions on cell viability. Appropriate media and culture conditions were used for each cell type as described previously in section 5.3.1. For encapsulation, cells were trypsinized and resuspended at a final concentration of 30 x 10^6 cells per ml in sterile-filtered, non-degradable polymer solution (HBS with 10% PEGDA, 1.5% TEOA, 3.4 µl/ml NVP, and 0.1% pluronic F68) containing either 5, 10, or 15 µM eosin Y. Microsphere synthesis, using mineral oil containing either 1, 3, or 5 µl/ml I651 stock solution, was performed according to protocol with the exception that the 500 µl PBS washes were replaced with 1 ml media washes. Resultant microspheres with encapsulated cells were maintained as a suspension culture in multiwell plates for 24 h at 37 °C. To observe viability and distribution of encapsulated cells, samples were incubated for 30 min at RT in PBS containing 2 µM calcein AM and 4 µM ethidium homodimer (Live/Dead Kit, Invitrogen) and imaged by fluorescence microscopy (Zeiss Axiovert 135) or confocal microscopy (Zeiss Live5 DuoScan). For assessment of microencapsulation efficiency, an additional encapsulation of NIH-3T3 cells was similarly performed at 15 x 10^6 cells/ml using the 10 µM eosin Y concentration and 3 µl/ml I651 stock solution. Cells within microspheres were

permeabilized for 5 min in 0.5% Triton X, stained with 4 μM ethidium homodimer, and imaged to quantify total number of encapsulated cells.

For long term encapsulation studies, the nondegradable PEGDA was replaced with MMP-sensitive PEG-PQ-PEG polymer (refer to Chapter 2 for synthesis of this compound) and PEG-RGDS to allow cell spreading and migration within the artificial matrix. The three cell types were resuspended separately at 30 x 10^6 cells/ml in filter-sterilized polymer solution (HBS with 10% PEG-PQ-PEG, 1.5% TEOA, 3.4 μl/ml NVP, and 10 μM eosin Y) containing 3 mM PEG-RGDS and 0.1% pluronic F68. Microspheres were generated using 3 μl/ml I651 stock solution in the mineral oil and purified with media washes according to the described protocol. The resulting samples were cultured in their respective media type for one week with media exchanges every 2 days. After 3 and 7 days, samples were fixed for nuclear and actin staining or immunostaining to allow morphological analysis and phenotypic characterization. Briefly, the cells were fixed for 30 min in 4% PFA, permeabilized for 15 min with 0.5% Triton X-100, and blocked for 2 h with 5% BSA. A portion of the samples was then stained for 2 h at RT in PBS with 5 U/ml rhodamine-phalloidin (Invitrogen) and 2 μM DAPI to allow visualization of actin and nuclei. All steps were performed at RT with reagents diluted in PBS and PBS rinses following each step. For immunostaining, blocked samples were incubated overnight at 4°C in primary antibodies in PBS with 0.5% BSA, rinsed in thoroughly in PBS, incubated with secondary antibodies overnight at 4°C in PBS with 0.5% BSA, rinsed in PBS, and finally stained for 1 h at RT in 2 μM DAPI. Primary antibodies included rabbit anti-nestin (1:200, Abcam) and rat anti-CD31 (1:200, BD Biosciences). Secondary antibodies included Alexa Fluor 488 conjugated donkey anti-rabbit (1:500, Invitrogen), and Alexa Fluor 594 conjugated donkey anti-rat (1:500, Invitrogen). After staining was completed, all samples were imaged by confocal microscopy (Zeiss LIVE 5 DuoScan).

5.3.6 Microspheres for Cell Delivery in a Rodent Model for Stroke

All procedures complied with the UK Animals Scientific Procedures Act (1986) and the Ethical Review Process of the King's College London. After a week of acclimatization, twenty-two Sprague-Dawley rats (250-270g on arrival, Harlan, UK) underwent middle cerebral artery occlusion (MCAo) as previously described.[43] Briefly, a 0.3 mm diameter polypropylene filament (Doccol) was advanced through the internal carotid to the ostium of the MCA in the circle of Willis for a transient 60 min occlusion. At the end of the occlusion period, rats were assessed for forelimb flexion and contralateral circling to confirm ischemia. The filament was then removed to allow reperfusion of the MCA and the neck incision was sutured.

High resolution, T2-weighted MR images (TR=4200ms, TE=10 ms, NE=8, Matrix=192x192, FOV=35x35mm, 50 slices in total by 0.5mm each, Gap=0, Scan Time= 54 min) were taken 10 days following MCAO to allow an accurate assessment of lesion volume and to determine transplantation coordinates. This T2-weighted MRI scan was acquired as a baseline measure as well as 1 week following transplantation to provide a direct measure of the effect of experimental intervention on lesion volume (expressed as% change between baseline and 1 week lesion volumes). Baseline MRI lesion volumes were also used to balance animals into equivalent treatment groups prior to transplantation: MCAo only (n=6), MCAo treated with empty hydrogel beads (n=5), or MCAo treated with microencapsulated bEnd.3 and MHP36 cells (n=5). Animals with no lesion or a purely cortical lesion by MRI were not included in subsequent experiments.

Treatment groups were prepared and implanted two weeks following MCAo. To allow immunohistochemical detection of grafts, cells were incubated *in vitro* with 10 μM 5-bromo-2-deoxyuridine (BrdU) for 3 days prior to microencapsulation and transplantation. Polymer

solution was prepared as 12.5% PEG-PQ-PEG in 10 mM HBS containing 3 mM PEG-RGDS, 10 μM eosin Y, 3.4 μl/ml NVP, and 1.5% v/v TEOA. For the microencapsulated treatment group, MHP36 and bEnd.3 cells were separately passaged and resuspended in the polymer at a final concentration of $50x10^6$ cells/ml. Microspheres were generated by adding 20 μl of polymer only or cell-polymer solution to 1 ml of sterile light mineral oil containing 3 μl of I651 in NVP (300 mg/ml). The mixture was vortexed and exposed to a combination of UV and white light (Dolan-Jenner) for 30 seconds. The resulting microspheres containing each between 5-10 cells were transferred to media by centrifugation and filtered through a 100 μm cell strainer (Millipore). After overnight incubation, microspheres were re-suspended at a concentration of 200 microparticles/μl for MHP36 cells and 1000 microparticles/μl for endothelial cells in 0.1 mM *N*-acetyl-cysteine (NAC, Sigma, UK) in HBSS for implantation. Calcein AM and ethidium homodimer staining (Live/Dead Stain Kit, Invitrogen) was used to determine cell viability (ranging from 70-90% following encapsulation). For each animal, a 20 μl volume of HBSS with 0.1 mM NAC and one of the grafts was injected at a speed of 1 μl/min via stereotactic injection into the center of the lesion as determined by MRI coordinates. Approximately 20,000 MHP36 and 200,000 bEnd.3 cells were transplanted per animal for the microencapsulated treatment group.

One week following transplantation, T2-weighted MR imaging was again performed and animals were sacrificed for histology. Brain tissue was isolated, fixed in 4% PFA overnight, and cryoprotected in 30% sucrose with 0.05% sodium azide prior to cryostat (Lecia) sectioning at a 50 μm thickness. Hematoxylin and eosin (H&E) staining was performed on the tissue sections. Grafted cells were visualized by immunofluorescent staining of the BrdU label. Briefly, sections were exposed to 50% formamide (Fisher Scientific) for 2 h at 65°C, rinsed in Tris-buffered solution (TBS, Sigma), and blocked in 10% goat serum (Vector) in 0.3% TBS-TritonX for 1 h at RT.

Overnight incubation with primary biotinylated antibodies against BrdU (sheep polyclonal or mouse monoclonal anti-BrdU, 1:250, Abcam) was performed at 4°C followed by TBS rinse, repeated blocking step, and finally incubation in secondary antibody (anti-mouse or sheep streptavidin Alexa Fluor 488 conjugated antibody, 1:500, Invitrogen) for 2 h at RT. Stained sections were rinsed in TBS and mounted on coverslips in Vectashield with DAPI (Vector). Additional primary antibodies (polyclonal rabbit anti-nestin (1:100, Abcam) and monoclonal rat anti-CD31 (1:100, Abcam)) and Alexa Fluor-conjugated secondary antibodies (all at 1:500, Invitrogen) were similarly used to distinguish implanted cells.

5.3.7 Statistical Analysis

Significance was determined via unpaired, two-tailed *t*-test when $p < 0.05$. Error bars in figures depict standard deviations for the data sets.

5.4 Results and Discussion

5.4.1 Development and Optimization of the Emulsion-based System

During development of the emulsion based encapsulation technique, cytocompatibility of photoinitiators, cell sensitivity to vortex derived shear forces, and photoinitiator solubility must all be considered. For example, emulsion-based microsphere synthesis requires rapid and complete polymer cross-linking before droplets have time to coalescence or phase separation can occur. It was anticipated that a balance would need to be achieved between higher photoinitiator concentrations required for rapid cross-linking and the cytocompatibility of these concentrations.

For initial investigations, photoinitiator was added solely to the polymer precursor solution. It was found, however, that the emulsion-based approach yielded few or no microspheres with

only a single photoinitiator present at concentrations suitable for cell encapsulation.[160,161] For a hydrophobic photoinitiator with low water solubility such as I651, poor microsphere yield may be due to rapid diffusion of the initiator into the much larger oil phase before polymerization can occur. To limit photoinitiator diffusion, the hydrophilic eosin Y photoinitiator was tested. A small number of particles were generated when eosin Y was used as the sole initiator; however these were neither consistently spherical nor fully cross-linked as shown in Figure 61-A. Specifically, a halo of diffuse material was visible around each bead suggesting lower cross-linking density at the surface.

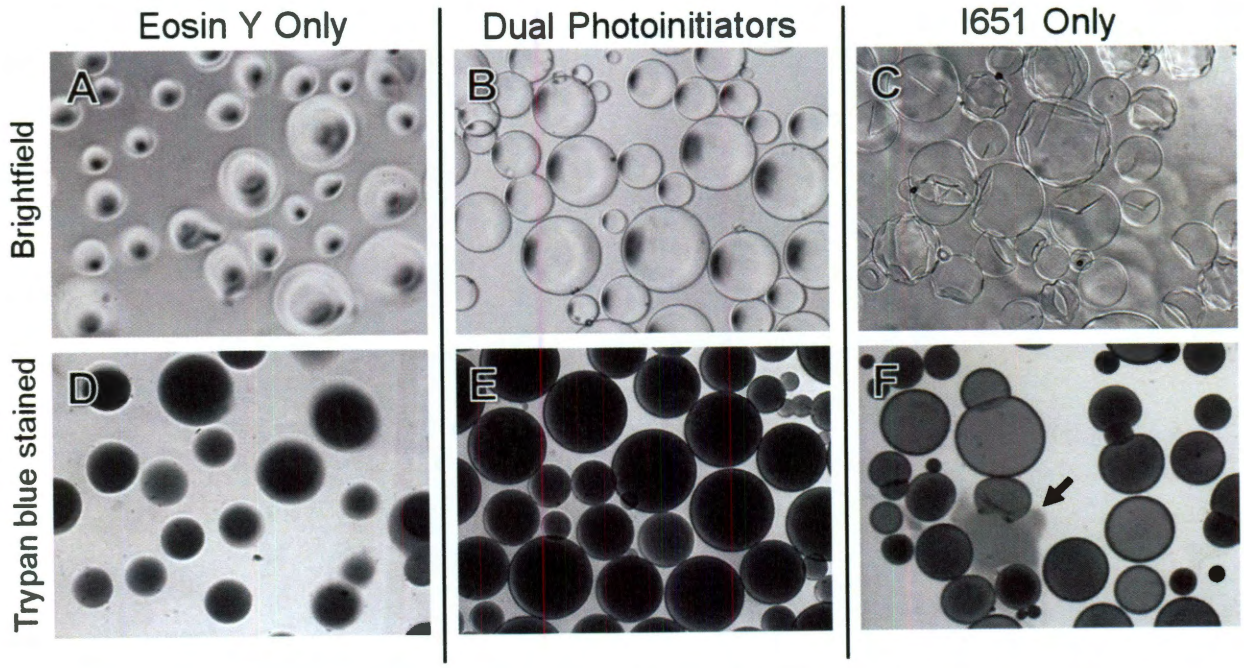

Figure 61. Representative images of microspheres formed with: (A and D) 10 µM eosin Y in polymer phase; (B and E) 10 µM eosin Y in the polymer phase with 3 µl per ml I651 stock solution in the oil phase; and (C and F) 3 µl per ml I651 stock solution in the oil phase only. Arrow indicates particle which had burst and was leaking internal contents. Dual combination of initiators (B and E) provides uniform spherical particles with smooth surface.

Trypan blue, a stain commonly used to assess cell viability, has also been shown in the literature to be useful in staining various biomaterials including PEG-based hydrogels.[158,162,163] For this

work the dye was found to aid in the visualization of the microspheres. In Figure 61-D, the uncross-linked outer halo on the particles was visualized as an area of lighter Trypan blue staining. Based on these observations, a dual-photoinitiator system was conceived that maintained the hydrophilic eosin Y in the aqueous phase but additionally utilized the hydrophobic initiator, I651, in the surrounding oil phase to facilitate cross-linking of the particle surface. A diagram of this unique system is shown in Figure 62.

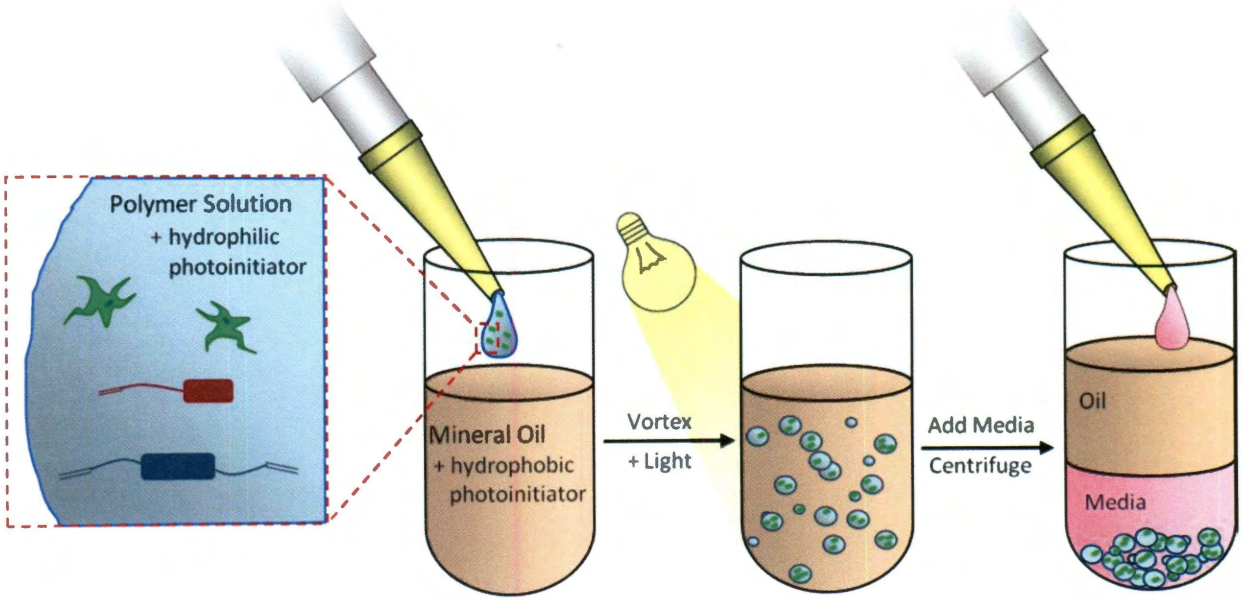

Figure 62. Diagram of vortex-induced emulsion encapsulation method. A polymer precursor solution containing cells (green), adhesive ligands (red), and degradable polymer (blue) is combined with mineral oil in a glass test tube. The solution is vortexed briefly during exposure to a crosslinking light source. A dual-initiator system with a hydrophilic photoinitiator in the aqueous phase and a hydrophobic initiator in the oil phase was found to be ideal for consistent particle formation. Cross-linked microspheres were purified by addition of buffer or media followed by centrifugation and aspiration of the oil layer.

Representative images of the particles formed from the dual-initiator system are shown in Figure 61-B and E. The particles appear highly spherical, have crisp, clear borders, and stain uniformly with the trypan blue dye. Removal of eosin Y from the system was observed to generate particles with a cross-linked shell but seemingly liquid or uncross-linked core as shown

in Figure 61-C. The trypan blue staining of this sample (Figure 61-F) confirmed the idea of a liquid core when some of the particles were compromised under the weight of a coverslip and began leaking (arrow). This indicates that, as predicted, the presence of the photoinitiator in the mineral oil primarily aids in rapid polymerization of the outer shell of the beads. From these results it was concluded that the combination of a hydrophilic initiator in the aqueous phase with a hydrophobic initiator in the oil phase provide dramatically improved particle synthesis and cross-linking.

5.4.2 Controlling Particle Size and Yield

Due to the nature of the vortex-based system, a highly heterogeneous mix of particle sizes is produced. To assess this, trypan blue stained samples made with various initiator concentrations in both the oil and aqueous phases were imaged and analyzed to generate a histogram of the particle diameters. As shown by the blue bars in Figure 63, a combination of 10 μM eosin Y in the polymer phase and 3 μl I651 stock solution in the oil phase produces microspheres ranging from less than 50 μm to over 500 μm in diameter. Larger diameter particles may be more difficult to inject or could be subject to diffusional limitations and reduced cell viability at their core. Therefore, it is desirable to control or limit the size range of microspheres that are produced. This can be accomplished by mechanical filtration of the final particle suspension, or through addition of stabilizing surfactants during synthesis. Pluronic F68 is a PEG-based, cell-compatible surfactant that is frequently used in bioreactors as a shear protectant.[159] It was found that addition of a low concentration (0.1% pluronic F68) to the polymer solution significantly reduced the average particle size (Figure 63, red bars).

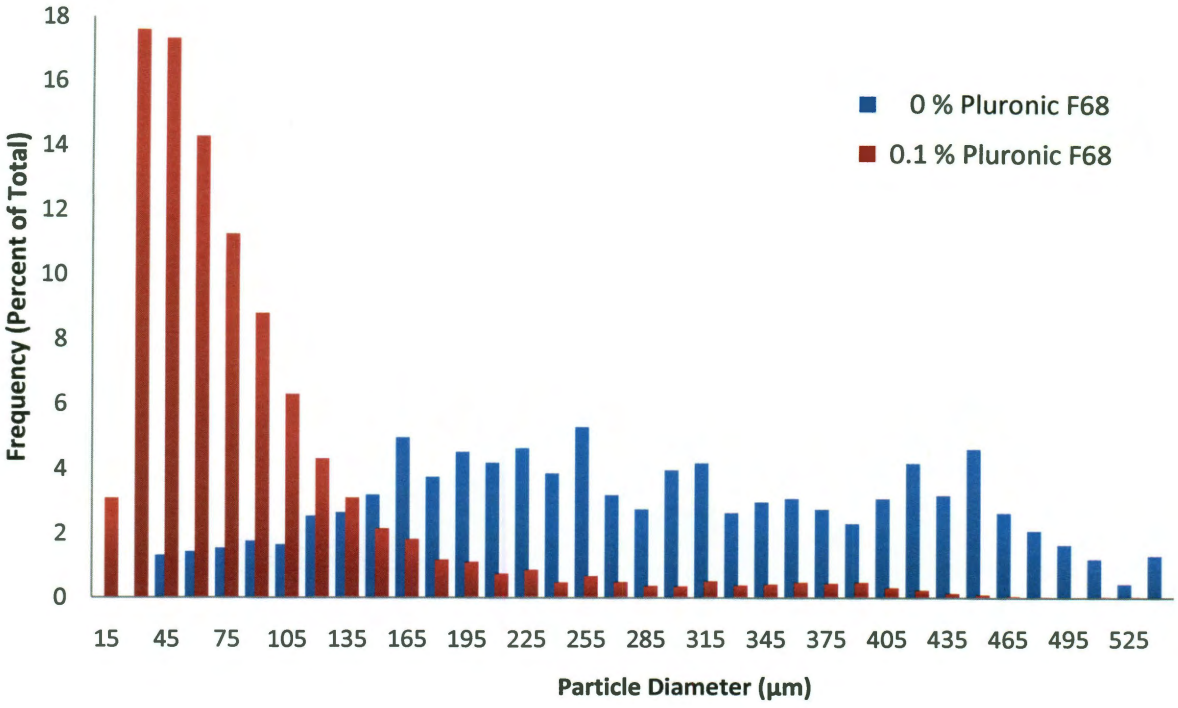

Figure 63. Comparison of particle size distribution for microspheres formed with 10 µM eosin Y in the polymer phase and 3 µl I651 stock solution in the oil phase with and without 0.1% pluronic F68. The presence of the surfactant shifts the particle diameters to the left such that average size was reduced from 280 to 95 µm diameter.

In addition to reducing particle diameter, the surfactant also significantly increased the number of microspheres produced for all encapsulations in which the oil phase photoinitiator was present. See Figure 64 for quantification of particle yield without (A) and with (B) the surfactant included. Both of these observations are likely caused by the stabilizing effect of the surfactant on the emulsion, which first allows smaller microspheres to be formed within the same shear environment, and then reduces the likelihood that particles will coalesce before cross-linking can occur. Figure 64 additionally shows that with surfactant present, yield generally increased as the photoinitiator concentration in either the polymer or oil phase was increased. This follows expectations since higher concentrations would lead to faster cross-linking and less time for polymer droplets to settle out of solution.

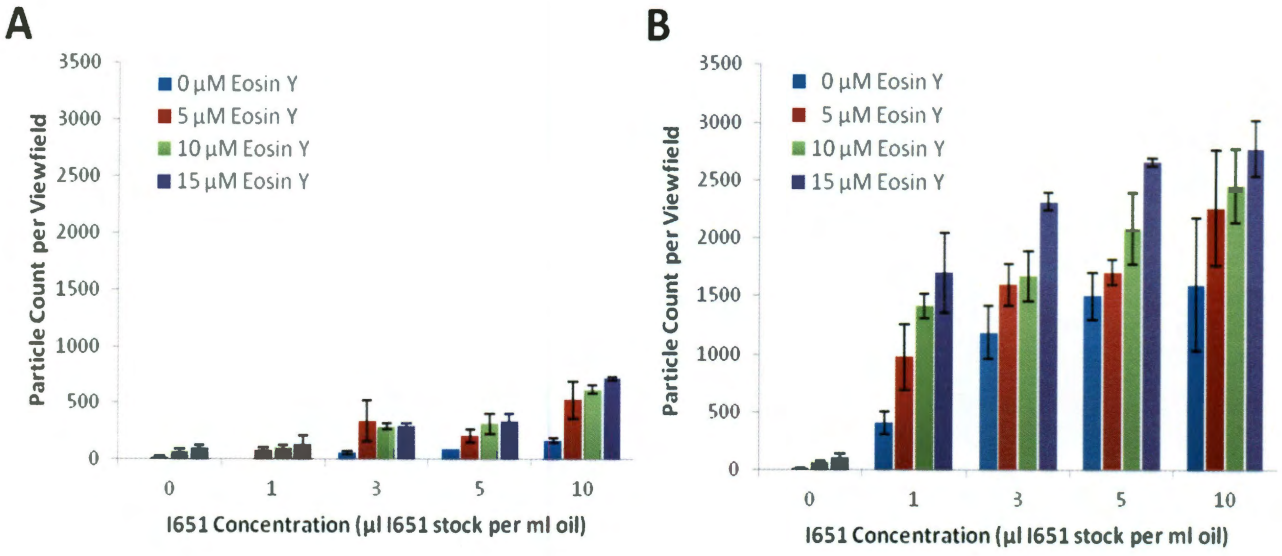

Figure 64. Quantification of particle yield across a range of eosin Y and I651 concentrations both (A) without and (B) with 0.1% pluronic F68 added to the polymer phase. In general, increasing particle yield was observed with increasing photoinitiator concentrations. In addition, a significant increase in particle yield occurred upon addition of 0.1% pluronic F68 surfactant for all conditions in which I651 was present.

5.4.3 Hydrogel Microspheres as Surface Seeded Carriers

To determine if the microsphere formulation provides an equivalent matrix to traditionally formed hydrogels, the particles were first evaluated with surface seeded cultures of the fibroblast control cell line. Unmodified PEGDA hydrogels naturally resist protein adsorption and therefore do not support cell attachment.[63,164,165] Incorporation of adhesive peptide sequences into the matrix, however, can provide attachment sites and allow seeded cells to spread on the material.[63,66,68-71,164-167] The fibronectin-derived RGDS peptide sequence is known to bind cell surface integrins, stimulating adhesion and spreading on synthetic scaffolds such as PEG-based hydrogels.[63,164,166,167] In this work, the RGDS peptide was covalently linked to an acrylated PEG spacer so that it could be cross-linked into the hydrogel matrix. Bulk hydrogel disks and hydrogel

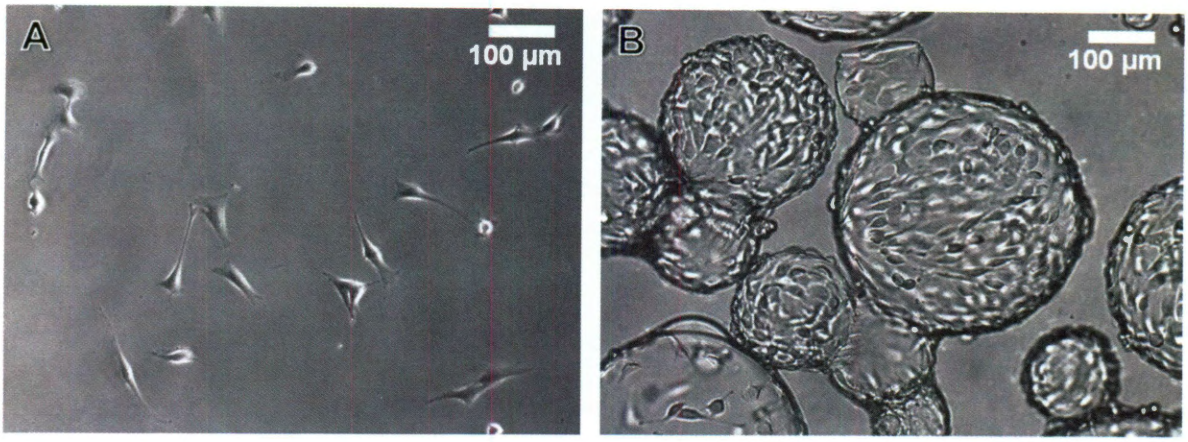

Figure 65. NIH-3T3 fibroblasts seeded on the surface of (A) a bulk hydrogel disk and (B) hydrogel microspheres containing 3 mM PEG-RGDS adhesive ligand. Microsphere formulation was observed to maintain bioactivity comparable with that of the traditionally formed hydrogel. Cells seeded on hydrogel surface or beads with 0 mM PEG-RGDS remained rounded in suspension and did not associate with the polymer surface (not shown).

microspheres were generated from non-degradable precursor material containing 0 or 3 mM PEG-RGDS. NIH-3T3 fibroblasts were then seeded and incubated for 24 h to allow time for the cells to interact with the scaffold. As seen in Figure 65, both the bulk and microsphere form of the RGDS-containing hydrogel behaved similarly by supporting cell attachment and spreading. No cell attachment was observed for samples which did not contain RGDS. Quantification of these images confirmed 0% of cells attached to microspheres lacking PEG-RGDS, while 83% of cells were adherent on microspheres with 3 mM PEG-RGDS incorporated. These results confirm that the emulsion-based synthesis did not affect the bioactivity of the scaffold, and shows the feasibility of using this technique for the generation of microcarriers.

5.4.4 Microencapsulation Cytocompatibility and Efficiency

Photoinitiator sensitivity is known to vary across cell types.[161] Therefore, by optimizing the encapsulation system across multiple single cell line, it was expected that the chosen concentrations woud be more useful for a wider range of applications. Encapsulations were

performed across all combinations of a high, medium, and low concentration of I651 and eosin Y. Calcein AM and ethidium homodimer staining then allowed direct observation of cell viability and distribution. Ultimately, the ideal conditions will minimize cytotoxicity while maximizing microsphere yield.

As previously shown in Figure 64, higher eosin Y and I651 concentrations generate a larger number of microspheres. Figure 66 however, reveals significantly reduced viability in nearly all cases when I651 initiator concentration in the oil phase was increased. Although the lowest

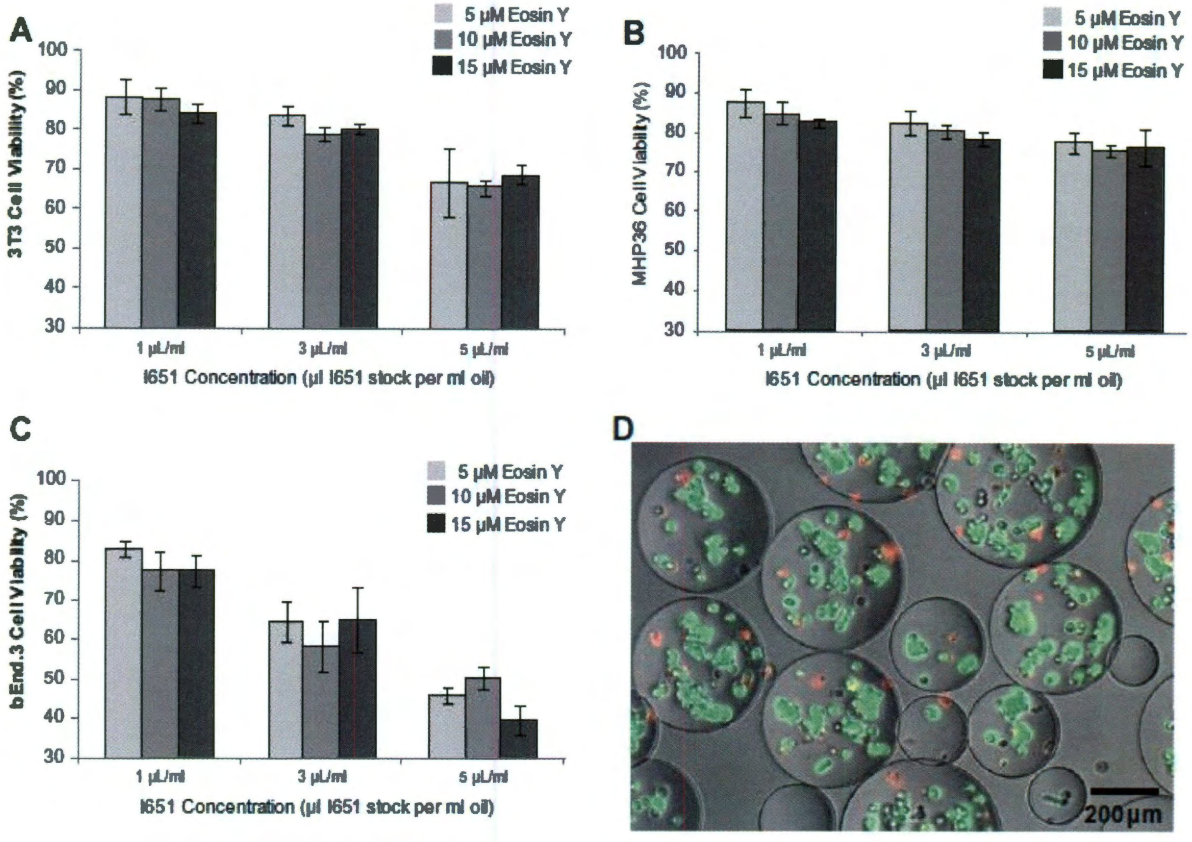

Figure 66. Viability analysis for (A) NIH-3T3, (B) MHP36 and (C) bEnd.3 cell lines following microencapsulation. Eosin Y photoinitiator concentration in the polymer phase was varied from 5 to 15 µM, while I651 stock solution added to the oil phase was varied from 1 to 5 µl per ml. A representative brightfield and fluorescence overlay of microencapsulated MHP36 cells stained with calcein AM (green, live) and ethidium homodimer (red, dead) is shown in (D). Variations in photoinitiator sensitivity can be observed across the three cell lines.

I651 concentration (1 µl stock solution per ml oil) produced the highest cell viability, it generally resulted in the formation of fewer, larger microspheres or misshapen particles. Higher concentrations of eosin Y generally did not impact cell viability for the cell lines tested, however it may be expected that other cell types for which the encapsulation might be used could be more sensitive. For these reasons, an intermediate level of 10 µM eosin Y in the polymer phase and 3 µl/ml I651 stock solution in the oil phase was chosen as the standard conditions for cell encapsulation in subsequent experiments. In Figure 66-D, a representative image is shown of MHP36 cells that had been encapsulated under these conditions and then labeled with calcein AM and ethidium homodimer. The results indicated that the cells are well dispersed within the spheres and quantification confirmed viability of greater than 80%. Finally, the efficiency of the encapsulation technique was assessed with NIH/3T3 cells using the standard cell encapsulation conditions. For these conditions, microencapsulation efficiency was quantified at 85% of the starting cell number.

5.4.5 Characterization of Cellular MMP Expression

In contrast to a 2D environment, a cell's ability to spread or migrate following encapsulation within the 3D hydrogel matrix will be influenced not only by integrin activation, but additionally its ability to degrade the material through secretion of proteolytic enzymes [168,169]. This is a result of the small pore sizes which physically restrict cell spreading when a nondegradable polymer is used [169]. MMP-2 and 9 expression levels were therefore characterized across the three cell lines, since encapsulation will ultimately be tested with an MMP-sensitive hydrogel material. Gelatin zymography was used to determine the relative amounts of collagen-specific MMP expressed by the three cell lines. For this assay, protease activity appears as clear bands against a dark background corresponding to MMP-2 at 62 kDa and MMP-9 and at 92 kDa. Figure 67-A

and 6-B show the zymogram results and quantified band intensity adjusted according to the final cell number for each cell type and normalized to 3T3 MMP-2 expression. MMP-2 and 9 expression was clearly identified in the endothelial and fibroblast cell cultures.

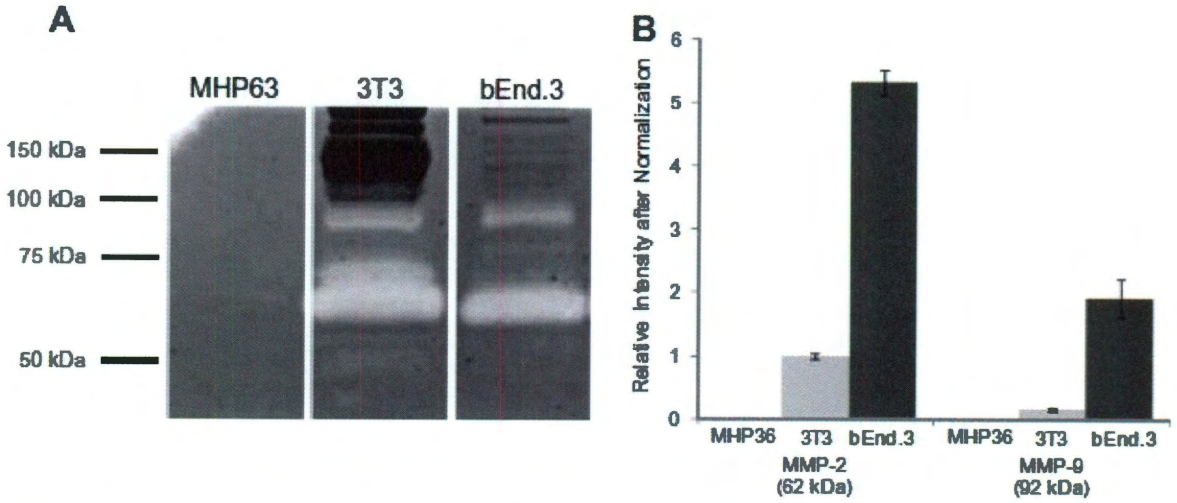

Figure 67. Gelatin zymogram and (B) quantified expression after normalization, showing varying levels of MMP expression across three cell lines: MHP36, negligible expression; 3T3, low expression; bEnd.3, high expression.

The bEnd.3 cell line, known for its enhanced proteolytic activity [170], showed over 5 times higher expression compared to the 3T3 cells. MHP36 neural stem cells, in contrast, had no detectable collagenase activity using this assay. This data shows that the chosen cell lines provide a broad range of collagenase activity and will likely vary in their response when encapsulated within the MMP-sensitive hydrogel used in this work.

5.4.6 *In Vitro* Analysis of Microencapsulated Cultures

For cell spreading to occur following 3D encapsulation within PEG hydrogels, the surrounding matrix must both support cell adhesion and be capable of degrading to make room for the advancing filopodia.[168] Thus, for long term microencapsulated culture, the MMP-sensitive PEG-PQ-PEG polymer, in combination with PEG-RGDS additive, was used to provide a convincing

extracellular mimic in which encapsulated cells can spread and migrate in 3D.[69,70] Individual microencapsulated cultures of these three cell lines were assessed by DAPI and rhodamine-phalloidin staining after 7 days for visualization of actin and nuclei (Figure 68, D-F). The autofluorescence from residual eosin Y photoinitiator was additionally used to visualize the location of the hydrogel material surrounding the cells (Figure 68, A-C).

As expected, the cell lines varied in their observed ability to degrade and spread in the hydrogel. For MHP36 cells, the combination of negligible collagenase expression and a high rate of proliferation contributed to the formation of neurosphere-like clusters of cells over time. It was further indicated that these cell clusters were displacing rather than degrading the surrounding matrix based on observations of stretching and distortion of the hydrogel in the eosin Y fluorescence channel (Figure 68-A). In encapsulated 3T3 cultures, phalloidin staining revealed fine process extensions on most cells and in some cases clear spreading of cells within the matrix. This response was expected based on their moderate level of MMP expression as observed by zymography. The bEnd.3 cell line, in contrast, showed dramatic process extension by all encapsulated cells and extensive spreading within the 3D scaffold, which is consistent with their high expression levels of MMP-2 and 9. By maintaining viable cultures of all three cell lines to the 7 day time point, we have demonstrated the ability of the degradable hydrogel microspheres to provide a conducive, 3D culture environment for a variety of cell types.

Microspheres were also found to be compatible with traditional immunohistochemical analysis of encapsulated cells. As shown in Figure 69-A and B, monocultures of MHP36 or bEnd.3 were fixed and stained for cell-specific markers following 3 days of *in vitro* culture. MHP36 cells were

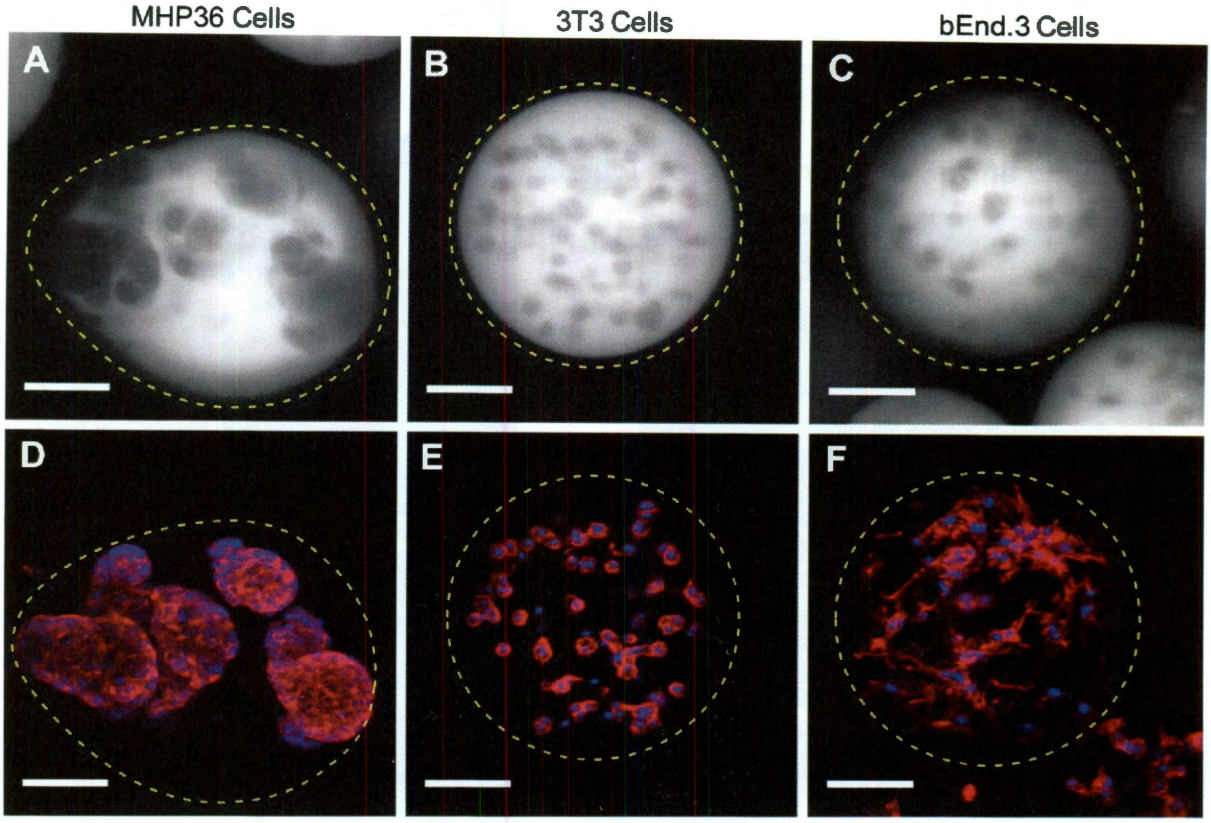

Figure 68. Representative confocal projections of (A and D) MHP36, (B and E) 3T3 and (C and F) b.End3 microencapsulated cultures at the 7-day time point, showing relative cell spreading and process extension in the 3D matrix. (A)–(C) show autofluorescence signal from the hydrogel matrix, while (D)–(F) show DAPI (nuclei, blue) and phalloidin (actin, red) staining. Cell spreading within the collagenase degradable hydrogel was more extensive for cells with higher MMP expression levels. Scale bar represents 100 μm.

found to strongly express the NSC marker nestin, and to be negative for the endothelial marker, CD31. bEnd.3 cells, in contrast, showed robust CD31 expression, and in addition expressed lower amounts of nestin protein. Following co-encapsulation of the two cell types within a single microsphere culture, these differences in marker expression could be utilized to distinguish the two cell types. In Figure 69-C, one can identify proliferative MHP36 clusters (white arrows) based on nestin positive staining, as well as larger, CD31 positive bEnd.3 cells. Demonstrating the compatibility of the microspheres with traditional cell characterization techniques is an important step towards developing the system for further *in vitro* and *in vivo* studies.

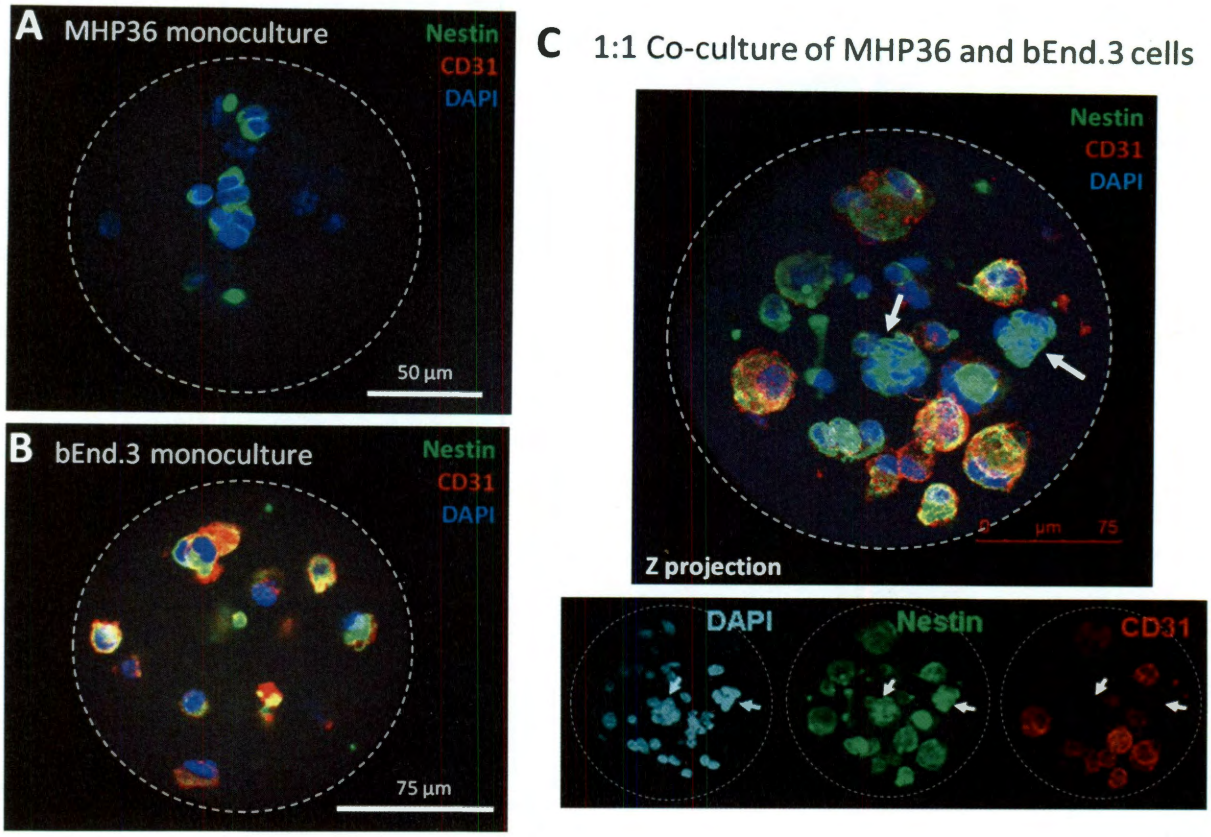

Figure 69. Immunofluorescent staining of MHP36 and bEnd.3 cells encapsulated within the microsphere system following 3 days in culture. Monoculture of MHP36 cells was found to be strongly positive for the NSC marker, nestin (a) while brain endothelial cells showed CD31 as well as moderate nestin expression (b). Differential marker expression allowed identification of MHP36 cell clusters (C, arrows) following co-encapsulation and culture with the bEnd.3 cells.

5.4.7 Delivery of Encapsulated Cells in a Model of Ischemic Stroke

Collaborators at the King's College, London, have previously reported on the ability of MHP36 cell transplantation to promote functional recovery in a rodent model of ischemic stroke.[43] Low cell survival and engraftment, however, suggest the possibility for further improving the therapeutic effect of this treatment. Microencapsulation of the cell therapy within a hydrogel matrix may be one solution to provide both physical protection and a more supportive microenvironment following delivery. In a preliminary study, the ability of the microspheres to deliver viable encapsulated cells to the lesion site was evaluated. Transplantation was

performed with a combination of MHP36 cells and bEnd.3 endothelial cells separately encapsulated within the microspheres. Cooperative signaling between endothelial and neural stem cells has been previously reported to promote both neurogenic and angiogenic responses in the brain and *in vitro.* Promoting revascularization at the lesion site in addition to neural differentiation may be one avenue to regenerate the lost tissue. Towards this end, viable delivery of both cell types was evaluated within this proof-of-concept study.

A diagram of the experimental timeline is presented in Figure 70-A. Ten days following MCAo, animals were evaluated with T2-weighted MR imaging to determine the extent and location of ischemic tissue damage. Two weeks after MCAo, encapsulated cell therapy or control treatments (hydrogel only or vehicle only) were administered by stereotactic injection to the

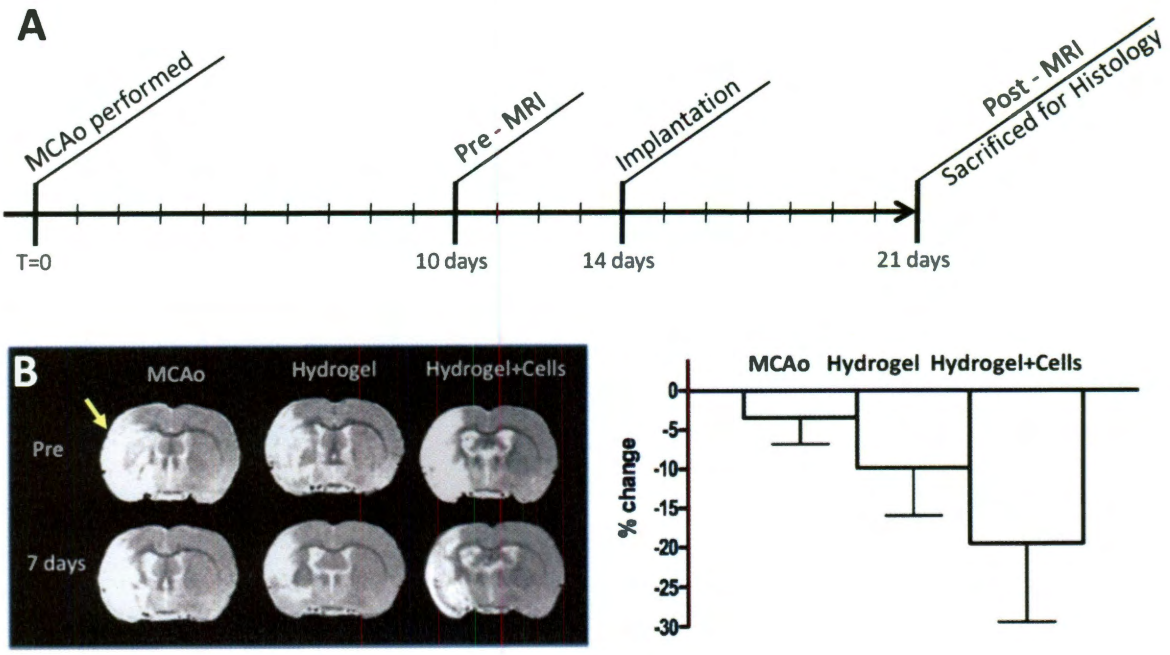

Figure 70. Investigation of encapsulated MHP36 therapy in a rodent model for stroke. (a) Diagram of study time-line. (b) T-2 weighted MRI images showing area of ischemic damage (arrow) and quantification of lesion volume changes one week following treatment.

central coordinates of the lesion. One week following treatment, animals were re-evaluated by MRI and sacrificed for histology. Comparison of baseline and post-MR images allowed evaluation of the percent change in lesion volume one week following therapy (Figure 70-B). Limited group sizes were such that none of the differences between treatment groups showed statistical significance, however a 4-fold reduction in the size of affected tissue was observed when encapsulated cells were administered compared to vehicle-only treatment group. It is recommended for future studies that larger group sizes and multiple time points be employed in order to fully investigate this promising trend.

During histological analysis of the sectioned tissues, hematoxylin and eosin was found to provide clear contrast between the implanted hydrogel and surrounding brain. As shown in Figure 71, polymer was successfully delivered and retained in the lesion site and injection tract for the hydrogel-only control group. Similar, reddish brown staining was not present in the vehicle only control tissue. At this time-point, microspheres of the material were not

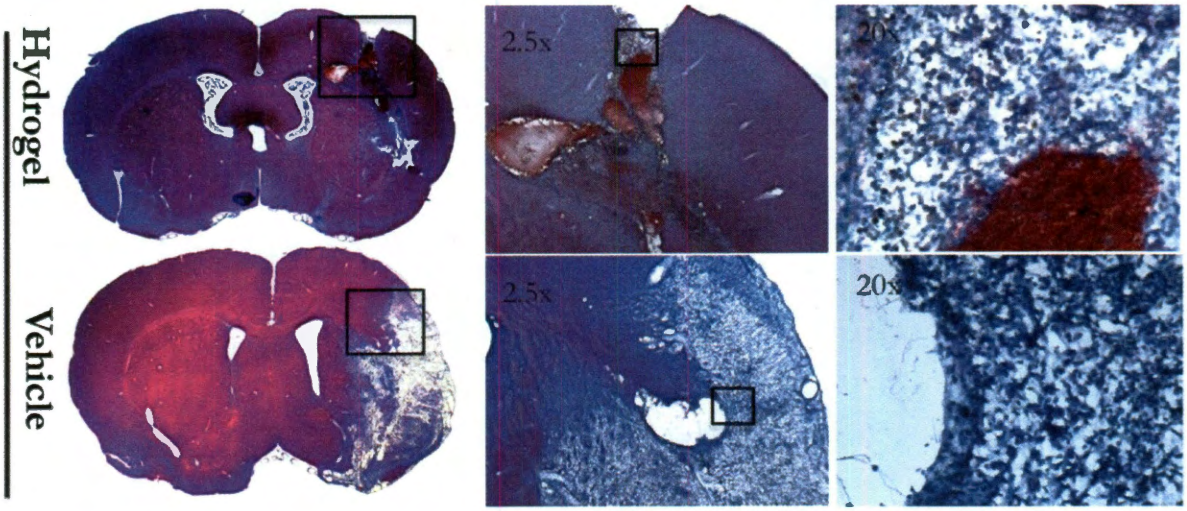

Figure 71. Hematoxylin and Eosin staining of fixed tissue sections clearly identified hydrogel material (reddish brown) within the lesion cavity and injection tract of the hydrogel-only group. Vehicle-only control did not show a similar staining pattern.

distinguishable, possibly suggesting degradation of the scaffold following implantation.

The successful delivery and support of viable MHP36 and bEnd.3 cells out to one week *in vivo* was additionally observed through immunohistochemical staining. As shown in Figure 72, BrdU positive MHP36 and bEnd.3 cells could both be clearly identified within the lesion site. The two delivered cell types were delineated by contrasting CD31 expression. Infiltration of host vascular cells (BrdU-, CD31+) suggests possible angiogenic response, however further studies are required to confirm and investigate these findings. Overall, this study provided excellent proof-of-concept that a cell-based therapy could be micro-encapsulated and delivered via injection into the injured rodent brain. Larger group sizes and additional controls will ultimately be required for future experiments in order to determine the effects of encapsulation on behavioral improvement in the rodent model.

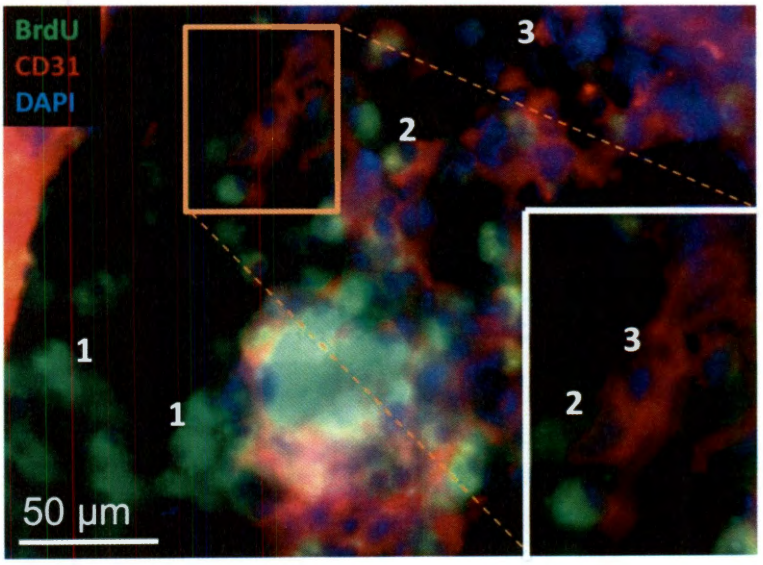

Figure 72. Immunofluorescent image at the site of the implanted cell therapy. MHP36 cells are identified by BrdU+, CD31- staining pattern (1), while implanted endothelial cells are distinguished by BrdU+, CD31+ staining (2). Host vascular cells were also observed to infiltrate the area based on BrdU-, CD31+ staining (3).

5.5 Conclusion

This work presents a novel method for simple, rapid, microencapsulation of cells using universally available laboratory equipment. In comparison to the commonly used calcium-

alginate microencapsulation system, the method presented here allows for more fine-tuned control over the physical and biochemical properties of the material. Furthermore, since the system employs a bulk encapsulation approach it is potentially scalable with few additional modifications. One drawback to the vortex-based emulsion generation is the heterogeneous mix of particle sizes that is produced. Although surfactant addition and filtration can be used to select a desired particle size range, further improvement of the technique could be accomplished through the use of a more controlled shear environment during emulsion generation.

The work herein has demonstrated that this system can be applied to a variety of cell types and that the material can be modified for both cell adhesion and enzyme-mediated degradation. Although the integrin-binding RGDS peptide and the collagenase-sensitive PQ peptide were employed in these studies, the system is highly modular, and thus any combination of adhesive and protease cleavable components could be utilized in order to tune the polymer scaffold for a specific application. As shown in previous sections, whole proteins can additionally be tethered to the matrix. It is thus theorized that growth factor or cytokine integration into the microspheres could provide more sophisticated control over the behavior of the encapsulated cells or could alternatively be used as a method for local drug delivery following *in vivo* implantation.

To prepare for future, therapeutic applications, these microspheres were lastly evaluated as carriers to deliver a cell-based therapy in a rodent model for stroke. Histological analysis at a one week time point confirmed successful delivery and prolonged survival of both encapsulated cell types. Furthermore, MR imaging of the stroke-damaged brain before and after treatment revealed a trend of decreasing lesion volume following delivery of the microencapsulated cell

therapy as compared to control groups. Further investigations are needed, however to determine whether the hydrogel carriers provide a statistically significant benefit over the traditional approach of injecting a free cell suspension.

Overall, the flexibility and ease of microsphere synthesis as presented in this work indicates potential both for *in vitro* studies and *in vivo* cell delivery. It is expected that this approach will serve as an additional, highly useful tool for the rapid generation and study of tissue engineered constructs for a wide variety of applications.

6 Summary of Conclusions and Implications

6.1 Development of a Synthetic Niche for NSC Investigations *In Vitro*

A bioactive, PEG-based scaffold is presented here as an ideal system for the study of neural stem cell behavior *in vitro*. The cyclic RGD-modified surface was confirmed to support equivalent NSC proliferation and differentiation to that of the traditional laminin-coated TCPS substrate. Substitution of a whole ECM protein, such as laminin, with a small peptide provides several advantages including reduced cost, reduction of batch-to-batch variability, and greater control over ligand concentration and presentation to the cells. Another significant benefit of the hydrogel system is the ability to support true, three-dimensional cultures. Replacing PEGDA with polymer chains containing a protease-cleavable peptide permitted cell-mediated degradation and remodeling following encapsulation. In this environment, the neural stem cells were capable of both self renewal and differentiation and were observed to organize into complex, interconnecting 3D networks. In contrast to naturally derived 3D culture substrates such as matrigel, the PEG-based scaffold provides greater control over which bioactive factors are presented to the cells. Though not tested here, broad control over the mechanical properties of the hydrogel could also be achieved with minimal impact on biochemical characteristics by simply varying the molecular weight or weight percent of the polymer in solution.

6.2 Control of NSC Behavior with Tethered Factors

In addition to adhesive and degradable sequences, it was also shown that whole proteins such as growth factors could be covalently linked to the hydrogel. *In vivo,* growth factors are often sequestered by components of the extracellular matrix. Sequestering of factors can permit localized signaling and is especially important since a single growth factor may have very

different downstream effects depending on the cell type or tissue it reaches. Two common growth factors in the CNS were investigated here as tethered signals in the synthetic scaffold, fibroblast growth factor and nerve growth factor. With these immobilized proteins, the ability of the scaffold to influence the proliferation and neuronal differentiation of surface seeded cultures was demonstrated. In addition to the two signals shown here, a vast array of proteins with possible influence over neural stem cell fate have been identified. Systematic investigation of these proteins against a neutral background, such as that provided by the hydrogel scaffold, could greatly enhance the general knowledge in this field.

6.3 Investigation of the Angiogenic Potential of NSCs

Neighboring cells in the niche are another source for both soluble and direct signaling to the NSCs. These interactions are often highly complex and bi-directional as presented herein with the interplay between neural stem cells and the endothelial cells of the vasculature. In a preliminary study, this work demonstrated that the hydrogel matrix can permit observation of this coculture interaction in a well-defined, *in vitro* setting. Evidence of angiogenic signaling from the neural stem cells to the endothelial cells was observed both in the coculture, and in a more relevant, *in vivo* setting through the use of the cornea micropocket assay. Evidence was also shown of a more direct role for NSCs in angiogenesis via the possibility of differentiation along vascular lineages. Future studies employing time-lapse imaging would provide critical data towards unraveling this complex system.

6.4 Microencapsulation Approach for Injectable Cell Constructs

For the final portion of this thesis work, the hydrogel scaffold was produced in a form that could be delivered via minimally invasive injection. Generation of hydrogel microspheres was

achieved using a dual combination of photoinitiators to rapidly crosslink the polymer droplets within a water-in-oil emulsion. Extensive optimization of this process was conducted to improve microsphere yield, provide control over particle diameter, and to maximize cell viability at the end of the process. Overall the technique provides multiple key advantages over previously published microencapsulation systems. For example, the use of common laboratory equipment means this method is simple and affordable to set up. In addition, because the microspheres are produced in bulk, large quantities can be generated rapidly and the overall method is much easier to scale-up compared to droplet or microfluidic approaches. Based on the data shown here, a variety of cell types can tolerate the emulsion-based microencapsulation process and can be studied *in vitro* as encapsulated suspensions. Finally, the microspheres were shown to successfully support the delivery of neural stem cells *in vivo.*

6.5 Future Directions

By screening of a variety of hydrogel configurations using the techniques presented here, specific combinations of physical and biochemical characteristics could be identified that promote a desired cellular behavior, such as the differentiation of NSCs along a neuronal lineage. Identifying which matrix, protein, and cellular components drive a particular fate may in turn provide valuable clues as to the role these components likely play in the *in vivo* neural stem cell niche. In addition, the ideal polymer compositions for particular applications could be investigated for clinical use in the field of neural tissue engineering. For example, in the next generation of tissue engineered therapeutics for stroke treatment, an optimized hydrogel material could be employed to support and direct the microencapsulated neural stem therapy, driving the formation of new neurons to restore and repair the damaged tissue.

The potential of the hydrogel microsphere formulation on its own to improve *in vivo* delivery is already being shown beyond the applications described in this work. Olabisi *et al.* in 2010 employed the method to provide immunoprotection and physically restrict a cell-based drug delivery system in a model of heterotopic ossification.[171] For this study, the microencapsulated cells showed improved survival and provided nearly twice the bone-forming capacity as compared to an injection of a free cell suspension.[171] Other applications for the micro-encapsulation technique could include delivery of stem cells to repair non-neuronal tissues such as damaged heart muscle from myocardial infarction, or delivery and protection of pancreatic islet cells for insulin therapy.

Overall, the versatility of the hydrogel material combined with this rapid, scalable technique for microencapsulation provides a powerful tool for the generation of customized, cell-based therapeutics for nearly any tissue engineering application.

7 References

1. Center for Disease Control and Prevention. National Center for Health Statistics. 2011. Available at: http://www.cdc.gov/.

2. Weissman IL. Stem cells: units of development, units of regeneration, and units in evolution. *Cell*. 2000;100(1):157-68.

3. Gage FH. Mammalian neural stem cells. *Science*. 2000;287(5457):1433-8.

4. Nystul TG, Spradling AC. Breaking out of the mold: diversity within adult stem cells and their niches. *Curr Opin Genet Dev*. 2006;16(5):463-8.

5. Li L, Xie T. Stem cell niche: structure and function. *Annu Rev Cell Dev Biol*. 2005;21:605-31.

6. Watts C, McConkey H, Anderson L, Caldwell M. Anatomical perspectives on adult neural stem cells. *J Anat*. 2005;207(3):197-208.

7. Taupin P, Gage FH. Adult neurogenesis and neural stem cells of the central nervous system in mammals. *J Neurosci Res*. 2002;69(6):745-9.

8. Goldman SA, Nottebohm F. Neuronal production, migration, and differentiation in a vocal control nucleus of the adult female canary brain. *Proc Natl Acad Sci U S A*. 1983;80(8):2390-4.

9. Lois C, Alvarez-Buylla A. Proliferating subventricular zone cells in the adult mammalian forebrain can differentiate into neurons and glia. *Proc Natl Acad Sci U S A*. 1993;90(5):2074-7.

10. Reynolds BA, Weiss S. Generation of neurons and astrocytes from isolated cells of the adult mammalian central nervous system. *Science*. 1992;255(5052):1707-10.

11. Basak O, Taylor V. Stem cells of the adult mammalian brain and their niche. *Cell Mol Life Sci*. 2009;66(6):1057-72.

12. Brazel CY, Limke TL, Osborne JK, et al. Sox2 expression defines a heterogeneous population of neurosphere-forming cells in the adult murine brain. *Aging Cell*. 2005;4(4):197-207.

13. Gage FH, Ray J, Fisher LJ. Isolation, characterization, and use of stem cells from the CNS. *Annu Rev Neurosci*. 1995;18:159-92.

14. Wiese C, Rolletschek A, Kania G, et al. Nestin expression--a property of multi-lineage progenitor cells? *Cell Mol Life Sci.* 2004;61(19-20):2510-22.

15. Geuna S, Borrione P, Fornaro M, Giacobini-Robecchi MG. Adult stem cells and neurogenesis: historical roots and state of the art. *Anat Rec.* 2001;265(3):132-41.

16. Temple S. The development of neural stem cells. *Nature.* 2001;414(6859):112-7.

17. Johansson CB, Momma S, Clarke DL, et al. Identification of a neural stem cell in the adult mammalian central nervous system. *Cell.* 1999;96(1):25-34.

18. Doetsch F. The glial identity of neural stem cells. *Nat Neurosci.* 2003;6(11): 1127-34.

19. Alvarez-Buylla A, García-Verdugo JM, Tramontin a D. A unified hypothesis on the lineage of neural stem cells. *Nat Rev Neurosci.* 2001;2(4):287-93.

20. Merkle FT, Alvarez-Buylla A. Neural stem cells in mammalian development. *Curr Opin Cell Biol.* 2006;18(6):704-9.

21. Hsu Y-C, Lee D-C, Chiu I-M. Neural stem cells, neural progenitors, and neurotrophic factors. *Cell Transplant.* 2007;16(2):133-50.

22. Mirzadeh Z, Merkle FT, Soriano-Navarro M, Garcia-Verdugo JM, Alvarez-Buylla A. Neural stem cells confer unique pinwheel architecture to the ventricular surface in neurogenic regions of the adult brain. *Cell Stem Cell.* 2008;3(3):265-78.

23. Ihrie R a, Alvarez-Buylla A. Lake-front property: a unique germinal niche by the lateral ventricles of the adult brain. *Neuron.* 2011;70(4):674-86.

24. Kriegstein A, Alvarez-Buylla A. The glial nature of embryonic and adult neural stem cells. *Annu Rev Neurosci.* 2009;32:149-84.

25. Merkle FT, Tramontin AD, García-Verdugo JM, Alvarez-Buylla A. Radial glia give rise to adult neural stem cells in the subventricular zone. *Proc Natl Acad Sci U S A.* 2004;101(50):17528-32.

26. Sylvester KG, Longaker MT. Stem cells: review and update. *Arch Surg.* 2004; 139(1):93-9.

27. Lindvall O, Kokaia Z. Stem cells for the treatment of neurological disorders. *Nature.* 2006;441(7097):1094-6.

28. Abe K. Therapeutic potential of neurotrophic factors and neural stem cells against ischemic brain injury. *J Cereb Blood Flow Metab.* 2000;20(10):1393-408.

29. Zandonella C. Stem-cell therapies: the first wave. *Nature*. 2005;435(7044):877-8.

30. Fuchs E, Segre JA. Stem cells: a new lease on life. *Cell*. 2000;100(1):143-55.

31. Svendsen CN, Smith AG. New prospects for human stem-cell therapy in the nervous system. *Trends Neurosci*. 1999;22(8):357-64.

32. Imitola J. Prospects for neural stem cell-based therapies for neurological diseases. *Neurotherapeutics*. 2007;4(4):701-14.

33. Trounson A, Thakar RG, Lomax G, Gibbons D. Clinical trials for stem cell therapies. *BMC Med*. 2011;9(1):52.

34. Gray JA, Hodges H, Sinden J. Prospects for the clinical application of neural transplantation with the use of conditionally immortalized neuroepithelial stem cells. *Philos Trans R Soc Lond B Biol Sci*. 1999;354(1388):1407-21.

35. ReNeuron Group. 2011. Available at: http://www.reneuron.com/.

36. Goldman S. Stem and progenitor cell-based therapy of the human central nervous system. *Nat Biotechnol*. 2005;23(7):862-71.

37. Delcroix GJ-R, Schiller PC, Benoit J-P, Montero-Menei CN. Adult cell therapy for brain neuronal damages and the role of tissue engineering. *Biomaterials*. 2010;31(8):2105-20.

38. Riess P, Zhang C, Saatman KE, et al. Transplanted neural stem cells survive, differentiate, and improve neurological motor function after experimental traumatic brain injury. *Neurosurgery*. 2002;51(4):1043-52; discussion 1052-4.

39. Kim SU, Vellis J de. Stem cell-based cell therapy in neurological diseases: a review. *J Neurosci Res*. 2009;87(10):2183-200.

40. Burns TC, Verfaillie CM, Low WC. Stem cells for ischemic brain injury: a critical review. *J Comp Neurol*. 2009;515(1):125-44.

41. Locatelli F, Bersano A, Ballabio E, et al. Stem cell therapy in stroke. *Cell Mol Life Sci*. 2009;66(5):757-72.

42. Kim SU. Genetically engineered human neural stem cells for brain repair in neurological diseases. *Brain Dev*. 2007;29(4):193-201.

43. Modo M, Rezaie P, Heuschling P, et al. Transplantation of neural stem cells in a rat model of stroke: assessment of short-term graft survival and acute host immunological response. *Brain Res*. 2002;958(1):70-82.

44. Picinich SC, Mishra PJ, Mishra PJ, Glod J, Banerjee D. The therapeutic potential of mesenchymal stem cells. Cell- & tissue-based therapy. *Expert Opin Biol Ther.* 2007;7(7):965-73.

45. Wurmser AE, Palmer TD, Gage FH. Neuroscience. Cellular interactions in the stem cell niche. *Science.* 2004;304(5675):1253-5.

46. Dusheck J. It's the ecology, stupid! *Nature.* 2002;418(6898):578-9.

47. Fuchs E, Tumbar T, Guasch G. Socializing with the neighbors: stem cells and their niche. *Cell.* 2004;116(6):769-78.

48. Riquelme P a, Drapeau E, Doetsch F. Brain micro-ecologies: neural stem cell niches in the adult mammalian brain. *Philos Trans R Soc Lond B Biol Sci.* 2008;363(1489):123-37.

49. Lutolf MP, Hubbell JA. Synthetic biomaterials as instructive extracellular microenvironments for morphogenesis in tissue engineering. *Nat Biotechnol.* 2005;23(1):47-55.

50. Blau HM, Brazelton TR, Weimann JM. The evolving concept of a stem cell: entity or function? *Cell.* 2001;105(7):829-41.

51. Mercier F, Kitasako JT, Hatton GI. Anatomy of the brain neurogenic zones revisited: fractones and the fibroblast/macrophage network. *J Comp Neurol.* 2002;451(2):170-88.

52. Kuhn HG, Winkler J, Kempermann G, Thal LJ, Gage FH. Epidermal growth factor and fibroblast growth factor-2 have different effects on neural progenitors in the adult rat brain. *J Neurosci.* 1997;17(15):5820-9.

53. Garcion E, Halilagic A, Faissner A, Ffrench-Constant C. Generation of an environmental niche for neural stem cell development by the extracellular matrix molecule tenascin C. *Development.* 2004;131(14):3423-32.

54. Teixeira AI, Duckworth JK, Hermanson O. Getting the right stuff: controlling neural stem cell state and fate in vivo and in vitro with biomaterials. *Cell Res.* 2007;17(1):56-61.

55. Thonhoff JR, Lou DI, Jordan PM, Zhao X, Wu P. Compatibility of human fetal neural stem cells with hydrogel biomaterials in vitro. *Brain Res.* 2008;1187:42-51.

56. Schmidt CE, Leach JB. Neural tissue engineering: strategies for repair and regeneration. *Annu Rev Biomed Eng.* 2003;5:293-347.

57. Bjugstad KB, Redmond DE, Lampe KJ, et al. Biocompatibility of PEG-based hydrogels in primate brain. *Cell Transplant*. 2008;17(4):409-15.

58. Mahoney MJ, Anseth KS. Three-dimensional growth and function of neural tissue in degradable polyethylene glycol hydrogels. *Biomaterials*. 2006;27(10):2265-74.

59. Weber LM, Lopez CG, Anseth KS. Effects of PEG hydrogel crosslinking density on protein diffusion and encapsulated islet survival and function. *J Biomed Mater Res A*. 2009;90(3):720-9.

60. Peppas NA, Hilt JZ, Khademhosseini A, Langer R. Hydrogels in Biology and Medicine: From Molecular Principles to Bionanotechnology. *Advanced Materials*. 2006;18(11):1345-60.

61. Roberts MJ, Bentley MD, Harris JM. Chemistry for peptide and protein PEGylation. *Adv Drug Deliv Rev*. 2002;54(4):459-476.

62. Veronese FM. Peptide and protein PEGylation: a review of problems and solutions. *Biomaterials*. 2001;22(5):405-17.

63. Hern DL, Hubbell JA. Incorporation of adhesion peptides into nonadhesive hydrogels useful for tissue resurfacing. *J Biomed Mater Res*. 1998;39(2):266-76.

64. DeLong SA, Gobin AS, West JL. Covalent immobilization of RGDS on hydrogel surfaces to direct cell alignment and migration. *J Control Release*. 2005;109(1-3):139-48.

65. Gunn JW, Turner SD, Mann BK. Adhesive and mechanical properties of hydrogels influence neurite extension. *J Biomed Mater Res A*. 2005;72(1):91-7.

66. Gobin AS, West JL. Effects of epidermal growth factor on fibroblast migration through biomimetic hydrogels. *Biotechnol Prog*. 2003;19(6):1781-5.

67. DeLong S a, Moon JJ, West JL. Covalently immobilized gradients of bFGF on hydrogel scaffolds for directed cell migration. *Biomaterials*. 2005;26(16):3227-34.

68. Leslie-Barbick JE, Moon JJ, West JL. Covalently-immobilized vascular endothelial growth factor promotes endothelial cell tubulogenesis in poly(ethylene glycol) diacrylate hydrogels. *J Biomater Sci Polym Ed*. 2009;20(12):1763-79.

69. West JL, Hubbell JA. Polymeric Biomaterials with Degradation Sites for Proteases Involved in Cell Migration. *Macromolecules*. 1999;32(1):241-4.

70. Gobin AS, West JL. Cell migration through defined, synthetic ECM analogs. *FASEB J*. 2002;16(7):751-3.

71. Moon JJ, Saik JE, Poché RA, et al. Biomimetic hydrogels with pro-angiogenic properties. *Biomaterials*. 2010;31(14):3840-7.

72. Conover JC, Notti RQ. The neural stem cell niche. *Cell Tissue Res*. 2008;331(1): 211-24.

73. Yamada KM. Adhesive recognition sequences. *J Biol Chem*. 1991; 266(20):12809-12.

74. Kerever A, Schnack J, Vellinga D, et al. Novel extracellular matrix structures in the neural stem cell niche capture the neurogenic factor fibroblast growth factor 2 from the extracellular milieu. *Stem Cells*. 2007;25(9):2146-57.

75. Brännvall K, Bergman K, Wallenquist U, et al. Enhanced neuronal differentiation in a three-dimensional collagen-hyaluronan matrix. *J Neurosci Res*. 2007;85(10): 2138-46.

76. Ortinau S, Schmich J, Block S, et al. Effect of 3D-scaffold formation on differentiation and survival in human neural progenitor cells. *Biomed Eng Online*. 2010;9(1):70.

77. Bhang SH, Lim JS, Choi CY, Kwon YK, Kim B-S. The behavior of neural stem cells on biodegradable synthetic polymers. *J Biomater Sci Polym Ed*. 2007;18(2):223-39.

78. Saha K, Irwin EF, Kozhukh J, Schaffer DV, Healy KE. Biomimetic interfacial interpenetrating polymer networks control neural stem cell behavior. *J Biomed Mater Res A*. 2007;81(1):240-9.

79. Ranieri JP, Bellamkonda R, Bekos EJ, et al. Neuronal cell attachment to fluorinated ethylene propylene films with covalently immobilized laminin oligopeptides YIGSR and IKVAV. II. *J Biomed Mater Res*. 1995;29(6):779-85.

80. Pollock K, Stroemer P, Patel S, et al. A conditionally immortal clonal stem cell line from human cortical neuroepithelium for the treatment of ischemic stroke. *Exp Neurol*. 2006;199(1):143-55.

81. Saha K, Keung AJ, Irwin EF, et al. Substrate modulus directs neural stem cell behavior. *Biophys J*. 2008;95(9):4426-38.

82. Little LE, Dane KY, Daugherty PS, Healy KE, Schaffer DV. Exploiting bacterial peptide display technology to engineer biomaterials for neural stem cell culture. *Biomaterials*. 2011;32(6):1484-94.

83. Humphries JD, Byron A, Humphries MJ. Integrin ligands at a glance. *J Cell Sci.* 2006;119(Pt 19):3901-3.

84. Schaffner P, Dard MM. Structure and function of RGD peptides involved in bone biology. *Cell Mol Life Sci.* 2003;60(1):119-32.

85. Bogdanowich-Knipp SJ, Chakrabarti S, Williams TD, Dillman RK, Siahaan TJ. Solution stability of linear vs. cyclic RGD peptides. *J Pept Res.* 1999;53(5):530-41.

86. Stroemer P, Patel S, Hope A, et al. The neural stem cell line CTX0E03 promotes behavioral recovery and endogenous neurogenesis after experimental stroke in a dose-dependent fashion. *Neurorehabil Neural Repair.* 2009;23(9):895-909.

87. Stevanato L, Corteling RL, Stroemer P, et al. c-MycERTAM transgene silencing in a genetically modified human neural stem cell line implanted into MCAo rodent brain. *BMC Neurosci.* 2009;10:86.

88. Lutolf MP, Lauer-Fields JL, Schmoekel HG, et al. Synthetic matrix metalloproteinase-sensitive hydrogels for the conduction of tissue regeneration: engineering cell-invasion characteristics. *Proc Natl Acad Sci U S A.* 2003;100(9):5413-8.

89. Hall PE, Lathia JD, Miller NGA, Caldwell MA, Ffrench-Constant C. Integrins are markers of human neural stem cells. *Stem Cells.* 2006;24(9):2078-84.

90. Prowse ABJ, Chong F, Gray PP, Munro TP. Stem cell integrins: Implications for ex-vivo culture and cellular therapies. *Stem Cell Res.* 2010.

91. Suzuki Y, Yanagisawa M, Yagi H, Nakatani Y, Yu RK. Involvement of beta1-integrin up-regulation in basic fibroblast growth factor- and epidermal growth factor-induced proliferation of mouse neuroepithelial cells. *J Biol Chem.* 2010;285(24):18443-51.

92. Campos LS. Beta1 integrins and neural stem cells: making sense of the extracellular environment. *Bioessays.* 2005;27(7):698-707.

93. Pruszak J, Ludwig W, Blak A, Alavian K, Isacson O. CD15, CD24, and CD29 define a surface biomarker code for neural lineage differentiation of stem cells. *Stem Cells.* 2009;27(12):2928-40.

94. Flanagan LA, Rebaza LM, Derzic S, Schwartz PH, Monuki ES. Regulation of human neural precursor cells by laminin and integrins. *J Neurosci Res.* 2006;83(5):845-56.

95. Kumagai H, Tajima M, Ueno Y, Giga-Hama Y, Ohba M. Effect of cyclic RGD peptide on cell adhesion and tumor metastasis. *Biochem Biophys Res Commun.* 1991;177(1):74-82.

96. Aumailley M, Gurrath M, Müller G, et al. Arg-Gly-Asp constrained within cyclic pentapeptides. Strong and selective inhibitors of cell adhesion to vitronectin and laminin fragment P1. *FEBS Lett.* 1991;291(1):50-4.

97. Xiao Y, Truskey GA. Effect of receptor-ligand affinity on the strength of endothelial cell adhesion. *Biophys J.* 1996;71(5):2869-84.

98. Pfaff M, Tangemann K, Müller B, et al. Selective recognition of cyclic RGD peptides of NMR defined conformation by alpha IIb beta 3, alpha V beta 3, and alpha 5 beta 1 integrins. *J Biol Chem.* 1994;269(32):20233-8.

99. Yue X-S, Murakami Y, Tamai T, et al. A fusion protein N-cadherin-Fc as an artificial extracellular matrix surface for maintenance of stem cell features. *Biomaterials.* 2010;31(20):5287-96.

100. Roth V. Exponential Regression Fit for Doubling Time Calculation. 2006.

101. Hatten ME, Mason CA. Mechanisms of glial-guided neuronal migration in vitro and in vivo. *Experientia.* 1990;46(9):907-16.

102. Carpenter MK, Cui X, Hu ZY, et al. In vitro expansion of a multipotent population of human neural progenitor cells. *Exp Neurol.* 1999;158(2):265-78.

103. Nieder C, Andratschke N, Astner ST. Experimental concepts for toxicity prevention and tissue restoration after central nervous system irradiation. *Radiat Oncol.* 2007;2:23.

104. Li Q, Ford MC, Lavik EB, Madri JA. Modeling the neurovascular niche: VEGF- and BDNF-mediated cross-talk between neural stem cells and endothelial cells: an in vitro study. *J Neurosci Res.* 2006;84(8):1656-68.

105. Heese K, Low JW, Inoue N. Nerve growth factor, neural stem cells and Alzheimer's disease. *Neurosignals.* 2006;15(1):1-12.

106. Wong LS, Khan F, Micklefield J. Selective covalent protein immobilization: strategies and applications. *Chem Rev.* 2009;109(9):4025-53.

107. Jabbari E. Bioconjugation of hydrogels for tissue engineering. *Curr Opin Biotechnol.* 2011.

108. Belcheva N, Woodrow-Mumford K, Mahoney MJ, Saltzman WM. Synthesis and biological activity of polyethylene glycol-mouse nerve growth factor conjugate. *Bioconjug Chem.* 2000;10(6):932-7.

109. Aizawa Y, Leipzig N, Zahir T, Shoichet M. The effect of immobilized platelet derived growth factor AA on neural stem/progenitor cell differentiation on cell-adhesive hydrogels. *Biomaterials.* 2008;29(35):4676-83.

110. Kolb HC, Finn MG, Sharpless KB. Click Chemistry: Diverse Chemical Function from a Few Good Reactions. *Angew Chem Int Ed Engl.* 2001;40(11):2004-2021.

111. Rostovtsev VV, Green LG, Fokin VV, Sharpless KB. A stepwise huisgen cycloaddition process: copper(I)-catalyzed regioselective "ligation" of azides and terminal alkynes. *Angew Chem Int Ed Engl.* 2002;41(14):2596-9.

112. Moses JE, Moorhouse AD. The growing applications of click chemistry. *Chem Soc Rev.* 2007;36(8):1249-62.

113. Wehrman T, He X, Raab B, et al. Structural and mechanistic insights into nerve growth factor interactions with the TrkA and p75 receptors. *Neuron.* 2007;53(1): 25-38.

114. Bradshaw RA, Murray-Rust J, Ibáñez CF, et al. Nerve growth factor: structure-function relationships. *Protein Sci.* 1994;3(11):1901-13.

115. Veronese FM. Peptide and protein PEGylation: a review of problems and solutions. *Biomaterials.* 2001;22(5):405-17.

116. Song H, Stevens CF, Gage FH. Astroglia induce neurogenesis from adult neural stem cells. *Nature.* 2002;417(6884):39-44.

117. Chenn A, Walsh CA. Regulation of cerebral cortical size by control of cell cycle exit in neural precursors. *Science.* 2002;297(5580):365-9.

118. Thored P, Wood J, Arvidsson A, et al. Long-term neuroblast migration along blood vessels in an area with transient angiogenesis and increased vascularization after stroke. *Stroke.* 2007;38(11):3032-3039.

119. Palmer TD, Willhoite AR, Gage FH. Vascular niche for adult hippocampal neurogenesis. *J Comp Neurol.* 2000;425(4):479-94.

120. Ruiz de Almodovar C, Lambrechts D, Mazzone M, Carmeliet P. Role and therapeutic potential of VEGF in the nervous system. *Physiol Rev.* 2009;89(2): 607-48.

121. Bovetti S, Hsieh Y-C, Bovolin P, et al. Blood vessels form a scaffold for neuroblast migration in the adult olfactory bulb. *J Neurosci*. 2007;27(22):5976-80.

122. Shen Q, Goderie SK, Jin L, et al. Endothelial cells stimulate self-renewal and expand neurogenesis of neural stem cells. *Science*. 2004;304(5675):1338-40.

123. Tsai RY, McKay RD. Cell contact regulates fate choice by cortical stem cells. *J Neurosci*. 2000;20(10):3725-35.

124. Oishi K, Ogawa Y, Gamoh S, Uchida MK. Contractile responses of smooth muscle cells differentiated from rat neural stem cells. *J Physiol*. 2002;540(Pt 1):139-52.

125. Larina IV, Shen W, Kelly OG, et al. A membrane associated mCherry fluorescent reporter line for studying vascular remodeling and cardiac function during murine embryonic development. *Anat Rec (Hoboken)*. 2009;292(3):333-41.

126. Poché RA, Saik JE, West JL, Dickinson ME. The mouse cornea as a transplantation site for live imaging of engineered tissue constructs. *Cold Spring Harb Protoc*. 2010;2010(4):pdb.prot5416.

127. Ford MC, Bertram JP, Hynes SR, et al. A macroporous hydrogel for the coculture of neural progenitor and endothelial cells to form functional vascular networks in vivo. *Proc Natl Acad Sci U S A*. 2006;103(8):2512-7.

128. Teng H, Zhang ZG, Wang L, et al. Coupling of angiogenesis and neurogenesis in cultured endothelial cells and neural progenitor cells after stroke. *J Cereb Blood Flow Metab*. 2008;28(4):764-71.

129. Rogers MS, Birsner AE, D'Amato RJ. The mouse cornea micropocket angiogenesis assay. *Nat Protoc*. 2007;2(10):2545-50.

130. Khetan S, Burdick J. Cellular encapsulation in 3D hydrogels for tissue engineering. *J Vis Exp*. 2009;(32).

131. Leslie-Barbick JE, Shen C, Chen C, West JL. Micron-scale spatially patterned, covalently immobilized vascular endothelial growth factor on hydrogels accelerates endothelial tubulogenesis and increases cellular angiogenic responses. *Tissue Eng Part A*. 2011;17(1-2):221-9.

132. Miljan EA, Sinden JD. Stem cell treatment of ischemic brain injury. *Curr Opin Mol Ther*. 2009;11(4):394-403.

133. Hicks A, Jolkkonen J. Challenges and possibilities of intravascular cell therapy in stroke. *Acta Neurobiol Exp (Wars)*. 2009;69(1):1-11.

134. Kondziolka D, Wechsler L, Achim C. Neural transplantation for stroke. *J Clin Neurosci*. 2002;9(3):225-30.

135. Watt FM, Hogan BL. Out of Eden: stem cells and their niches. *Science*. 2000;287(5457):1427-30.

136. Spradling A, Drummond-Barbosa D, Kai T. Stem cells find their niche. *Nature*. 2001;414(6859):98-104.

137. Stabenfeldt SE, García AJ, LaPlaca MC. Thermoreversible laminin-functionalized hydrogel for neural tissue engineering. *J Biomed Mater Res A*. 2006;77(4):718-25.

138. Crompton KE, Goud JD, Bellamkonda RV, et al. Polylysine-functionalised thermoresponsive chitosan hydrogel for neural tissue engineering. *Biomaterials*. 2007;28(3):441-9.

139. Steindler DA. Neural stem cells, scaffolds, and chaperones. *Nat Biotechnol*. 2002;20(11):1091-3.

140. Nicodemus GD, Bryant SJ. Cell encapsulation in biodegradable hydrogels for tissue engineering applications. *Tissue Eng Part B Rev*. 2008;14(2):149-65.

141. Sambanis A. Encapsulated islets in diabetes treatment. *Diabetes Technol Ther*. 2003;5(4):665-8.

142. Hussain MA, Theise ND. Stem-cell therapy for diabetes mellitus. *Lancet*. 2004;364(9429):203-5.

143. Vos P de, Hamel AF, Tatarkiewicz K. Considerations for successful transplantation of encapsulated pancreatic islets. *Diabetologia*. 2002;45(2):159-73.

144. Efrat S. Cell therapy approaches for the treatment of diabetes. *Curr Opin Investig Drugs*. 2001;2(5):639-42.

145. Sambanis A. Engineering challenges in the development of an encapsulated cell system for treatment of type 1 diabetes. *Diabetes Technol Ther*. 2000;2(1):81-9.

146. Orive G, Hernández RM, Rodríguez Gascón A, et al. History, challenges and perspectives of cell microencapsulation. *Trends Biotechnol*. 2004;22(2):87-92.

147. Murua A, Portero A, Orive G, et al. Cell microencapsulation technology: towards clinical application. *J Control Release*. 2008;132(2):76-83.

148. Jen AC, Wake MC, Mikos AG. Review: Hydrogels for cell immobilization. *Biotechnol Bioeng*. 1996;50(4):357-64.

149. Orive G, Hernández RM, Gascón AR, et al. Cell encapsulation: promise and progress. *Nat Med.* 2003;9(1):104-7.

150. Lim F, Sun AM. Microencapsulated islets as bioartificial endocrine pancreas. *Science.* 1980;210(4472):908-10.

151. Smidsrød O, Skjåk-Braek G. Alginate as immobilization matrix for cells. *Trends Biotechnol.* 1990;8(3):71-8.

152. Martinsen A, Skjåk-Braek G, Smidsrød O. Alginate as immobilization material: I. Correlation between chemical and physical properties of alginate gel beads. *Biotechnol Bioeng.* 1989;33(1):79-89.

153. Haque T, Chen H, Ouyang W, et al. Superior cell delivery features of poly(ethylene glycol) incorporated alginate, chitosan, and poly-L-lysine microcapsules. *Mol Pharm.* 2004;2(1):29-36.

154. Hunt NC, Grover LM. Cell encapsulation using biopolymer gels for regenerative medicine. *Biotechnol Lett.* 2010;32(6):733-42.

155. Park KI, Teng YD, Snyder EY. The injured brain interacts reciprocally with neural stem cells supported by scaffolds to reconstitute lost tissue. *Nat Biotechnol.* 2002;20(11):1111-7.

156. Bible E, Chau DYS, Alexander MR, et al. The support of neural stem cells transplanted into stroke-induced brain cavities by PLGA particles. *Biomaterials.* 2009;30(16):2985-94.

157. Sinden JD, Rashid-Doubell F, Kershaw TR, et al. Recovery of spatial learning by grafts of a conditionally immortalized hippocampal neuroepithelial cell line into the ischaemia-lesioned hippocampus. *Neuroscience.* 1997;81(3):599-608.

158. Yeh J, Ling Y, Karp JM, et al. Micromolding of shape-controlled, harvestable cell-laden hydrogels. *Biomaterials.* 2006;27(31):5391-8.

159. Michaels JD, Papoutsakis ET. Polyvinyl alcohol and polyethylene glycol as protectants against fluid-mechanical injury of freely-suspended animal cells (CRL 8018). *J Biotechnol.* 1991;19(2-3):241-57.

160. Bryant SJ, Nuttelman CR, Anseth KS. Cytocompatibility of UV and visible light photoinitiating systems on cultured NIH/3T3 fibroblasts in vitro. *J Biomater Sci Polym Ed.* 2000;11(5):439-57.

161. Williams CG, Malik AN, Kim TK, Manson PN, Elisseeff JH. Variable cytocompatibility of six cell lines with photoinitiators used for polymerizing hydrogels and cell encapsulation. *Biomaterials*. 2005;26(11):1211-8.

162. Obara K, Ishihara M, Ishizuka T, et al. Photocrosslinkable chitosan hydrogel containing fibroblast growth factor-2 stimulates wound healing in healing-impaired db/db mice. *Biomaterials*. 2003;24(20):3437-44.

163. Ishihara M, Obara K, Ishizuka T, et al. Controlled release of fibroblast growth factors and heparin from photocrosslinked chitosan hydrogels and subsequent effect on in vivo vascularization. *J Biomed Mater Res A*. 2003;64(3):551-9.

164. DeLong S a, Gobin AS, West JL. Covalent immobilization of RGDS on hydrogel surfaces to direct cell alignment and migration. *J Control Release*. 2005;109(1-3):139-48.

165. Hubbell JA. Biomaterials in tissue engineering. *Biotechnology (N Y)*. 1995;13(6): 565-76.

166. Burdick JA, Anseth KS. Photoencapsulation of osteoblasts in injectable RGD-modified PEG hydrogels for bone tissue engineering. *Biomaterials*. 2002; 23(22):4315-23.

167. Mann BK, Gobin AS, Tsai AT, Schmedlen RH, West JL. Smooth muscle cell growth in photopolymerized hydrogels with cell adhesive and proteolytically degradable domains: synthetic ECM analogs for tissue engineering. *Biomaterials*. 2001;22(22):3045-51.

168. Dikovsky D, Bianco-Peled H, Seliktar D. Defining the role of matrix compliance and proteolysis in three-dimensional cell spreading and remodeling. *Biophys J*. 2008;94(7):2914-25.

169. Raeber GP, Lutolf MP, Hubbell JA. Molecularly engineered PEG hydrogels: a novel model system for proteolytically mediated cell migration. *Biophys J*. 2005;89(2):1374-88.

170. Montesano R, Pepper MS, Möhle-Steinlein U, et al. Increased proteolytic activity is responsible for the aberrant morphogenetic behavior of endothelial cells expressing the middle T oncogene. *Cell*. 1990;62(3):435-45.

171. Olabisi RM, Lazard ZW, Franco CL, et al. Hydrogel microsphere encapsulation of a cell-based gene therapy system increases cell survival of injected cells, transgene expression, and bone volume in a model of heterotopic ossification. *Tissue Eng Part A*. 2010;16(12):3727-36.